Aus dem Max-Delbrück-Centrum für Molekulare Medizin

DISSERTATION

Two glial cell types make structural and functional contact to the calyx of Held in the mouse medial nucleus of the trapezoid body

zur Erlangung des akademischen Grades
Doctor of Philosophy in Medical Neurosciences
(PhD in Medical Neurosciences)

vorgelegt der Medizinischen Fakultät
Charité – Universitätsmedizin Berlin

von

Jochen Müller

aus Kassel

Gutachter: 1. Prof. Dr. Helmut Kettenmann

2. Prof. Dr. Uwe Heinemann

3. Prof. Dr. Hans-Joachim Pflüger

Datum der Promotion: 01.09.2008

Table of contents

List of figures

Abbreviations

Two-Photon Laser Scanning Microscope / Microscopy (2PM)

4-Aminopyridine (4-AP)

Artificial cerebrospinal fluid (aCSF)

Active Zone (AZ)

alpha-amino-3-hydroxy-5-methyl-4-isoxazole propionic acid (AMPA)

alpha-amino-3-hydroxy-5-methyl-4-isoxazole propionic acid receptor (AMPAR)

D-2-amino-5-phosphonopentanoate (APV)

Anterior Ventral Cochlear Nucleus (aVCN)

D-Aspartate (D-Asp)

Adenosine triphosphate (ATP)

Bicucculine (Bic)

Brain-derived neurotrophic factor (BNDF)

Bovine serum albumine (BSA)

Cornus Ammonis 1-3 (CA1-3)

Calyx of Held (CoH)

Current clamp (CC)

Charged couple device (CCD)

Confocal Laser Scanning Microscope/Microscopy (CLSM)

6-cyano-7-nitroquinoxaline-2, 3-dione (CNQX)

Central nervous system (CNS)

Cyclothiazide (CTZ)

Carbocyanin (Cy3)

Diaminobenzidine (DAB)

Differential interference contrast (DIC)

1,19-dioctadecyl-6,69-di (4-sulfophenyl)-3,3,39,39-tetramethylindocarbocyanine (DiI)

Excitatory amino acid transporter (EAAT)

Enhanced green fluorescent protein (eGFP)

glycol-bis(2-aminoethylether)-N,N,N',N'-tetraacetic acid (EGTA)

Electron microscope / microscopy (EM)

Evoked postsynaptic current (ePSC)

Excitatory postsynaptic current (EPSC)

Excitatory postsynaptic potential (EPSP)

Fluorescence (F)

Baseline Fluorescence (F_0)

Fluorescence relative to baseline Fluorescence (F/F_0)

γ -Aminobutyric acid (GABA)

γ -Aminobutyric acid receptor (GABAR)

Glutamate aspartate transporter (GLAST)

Glial fibrillary acidic protein (GFAP)

Glutamate transporter type-1 (GLT-1)

Globular bushy cells (GBC)

Glutamate (Glu)

Glutamate transporters (GluT)

Glycine (Gly)

Glycine receptor (GlyR)

Green fluorescent protein (GFP)

1-(4-Aminophenyl)-4-methyl-7,8-methylenedioxy-5H-2,3-benzodiazepine hydrochloride (GYKI 52466) (GYKI)

4-(2-hydroxyethyl)-1-piperazineethanesulfonic acid (HEPES)

Holding potential (HP)

Horseradish peroxidase (HRP)

Ionized calcium-binding adaptor molecule 1 (Iba-1)

Current-Voltage (IV)

Inhibitory postsynaptic current (IPSC)

Inhibitory postsynaptic potential (IPSP)

Infrared (IR)

Infrared differential interference contrast (IR-DIC)

Intracellular Ca^{2+} concentration ($[Ca^{2+}]_i$)

Ionotropic glutamate receptor (iGluR)

Kainic acid / kainate (KA)

Kainic acid / kainate receptor (KAR)

Lateral superior olive (LSO)

Lucifer Yellow (LY)

Lidocaine N-ethyl bromide (QX-314)

Medial nucleus of the trapezoid body (MNTB)

Medial superior olive (MSO)

Membrane potential (MP)

Metabotropic glutamate receptor (mGluR)

Miniature postsynaptic current (mPSC)

Mitochondria (mit)

(+)-5-methyl-10,11-dihydro-5H-dibenzo[a,d]cyclohepten-5,10-imine maleate (MK801)

Myelin oligodendrocyte glycoprotein (MOG)

Na+ voltage-gated channels (Na_v)

Neuron-Glial 2 (NG2)

Neuron specific nuclear protein (NeuN)

Normal goat serum (NGS)

N-methyl-D-aspartate (NMDA)

N-methyl-D-aspartate receptor (NMDAR)

Number of vesicles (n)

Number of vesicle release sites (N)

Oligodendroglia progenitor cell (OPC)

Probability (p)

Passive cell (PC)

Phosphate buffered saline (PBS)

Phosphate buffer (PB)

Paraformaldehyde (PFA)

Peripheral nervous system (PNS)

Postsynaptic current (PSC)

Principal neuron (PN)

Puncta adherenzia (PA)

Quantal size (q)

Readily releasable pool of vesicles (RRP)

Rhodamine-2 (Rhod-2)

Room temperature (RT)

Ruthenium Red (RuR)

Spontaneous postsynaptic current (sPSC)

2-(3-Carboxypropyl)-3-amino-6-(4 methoxyphenyl)pyridazinium bromide, SR95531, Gabazine (GBZ)

Standard deviation of the mean (S.D.M.)

Standard error of the mean (S.E.M.)

Superior olivary complex (SOC)

Strychnine (Str)

Sulforhodamine 101 (S101)

Threo- ß-Benzoylaspartic Acid (TBOA)

Tetrodotoxin (TTX)

Triton-X 100 (TX100)

Voltage clamp (VC)

Voltage-gated Ca2+ channels (VGCCs)

1. Introduction

1.1. Synaptic transmission in chemical synapses

Neuronal communication is mediated via synapses, which are, according to the mechanisms of the signal transmission, classified into two types: chemical and electrical. In the chemical synapses, transmission is mediated by fusion of small membrane bound organelles, the synaptic vesicles, with the presynaptic plasma membrane and release of the vesicular content, the transmitter, into the synaptic cleft (Figure 1A). This process of transmitter release occurs at specialized contact sites between pre- and postsynaptic plasma membranes. The synaptic vesicles, containing neurotransmitter, are found to be docked to and clustered around the presynaptic density, called active zone (Figure 1A, B). The active zone contains Ca^{2+} channels and the molecular machinery, which controls fusion of the vesicles with the plasma membrane (Figure 1A). The postsynaptic membrane on the other hand contains neurotransmitter receptors and ligand-gated ion channels (Figure 1B and 2D, E) concentrated in the so-called postsynaptic density. An action potential (AP) arriving at the presynaptic terminal initiates transmission by depolarisation of the presynapse, leading to opening of voltage-gated Ca^{2+} channels. The influx of Ca^{2+} ions leads to a rapid increase in the intracellular Ca^{2+} concentration ($[Ca^{2+}]_i$) that activates certain molecular machinery, the SNARE complex, which causes vesicles to fuse with the plasma membrane (Südhof, 2004). By fusing with the plasma membrane, synaptic vesicles release their neurotransmitter content into the synaptic cleft and thereby activate ligand-gated ion channels on the postsynaptic membrane (Figure 1B).

The synapses in the central nervous system (CNS) can be either excitatory or inhibitory, based on the postsynaptic effect. The primary type of excitatory synapse in the CNS is glutamatergic. The involved glutamate receptors are pharmacologically classified based on specific ligand binding as α-amino-3- hydroxy-5-methyl-4-isoxazoleproprionic acid (AMPA), kainic acid (KA) or N-methyl-D-aspartate (NMDA)

receptors. Activation of these receptors will generate excitatory postsynaptic currents (EPSCs) depolarizing the postsynaptic neuron. Rapid inhibition in the CNS is mediated mainly by GABAergic or glycinergic synapses, the activation of which leads to inhibitory postsynaptic currents (IPSCs) that either hyperpolarize or stabilize the postsynaptic membrane potential.

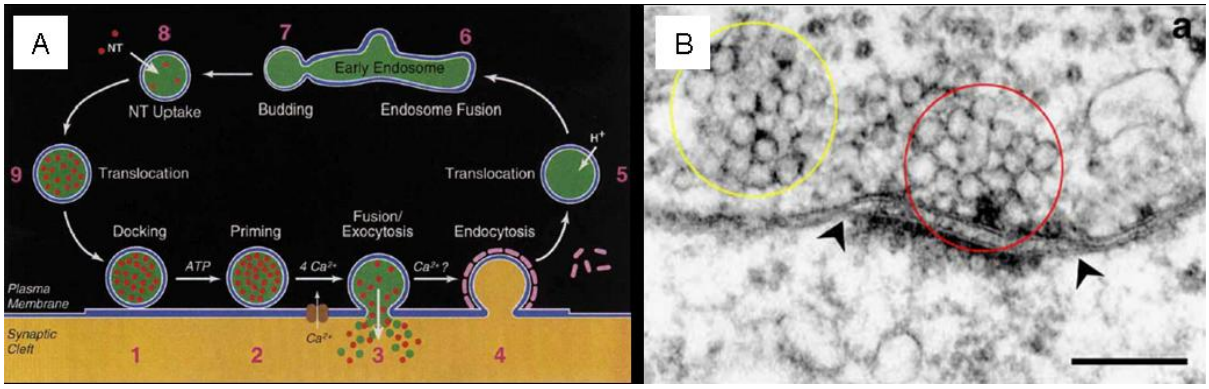

Figure 1. The vesicle cycle
(A) Vesicle cycle in the presynapse as suggested by Südhof (1995)
(B) Membrane specializations and organization of synaptic vesicles at the calyx of Held. A high magnification electron microscopy image through a synaptic contact at the active (apposition) zone between the presynaptic calyx of Held (top) and the postsynaptic principal neuron (bottom). Note the typical widening of the synaptic cleft between the perforated pre- and postsynaptic densities (dark black structures between arrowheads). Note also the two pools of synaptic vesicles resembling the readily releasable and recycling pool (within red circle) and the reserve pool (within yellow circle). Bar 0.2 µm. Taken from (Rollenhagen and Lübke, 2006).

1.2. Morphological differences of CNS synapses

Chemical synapses are classified into groups according to the contact site of the presynaptic element. Figure 2 depicts the most common arrangements, namely axo-dendritic synapses, in which the axon of the presynaptic neuron contacts the dendritic structures, the spines (figure 2A, D), axo-axonic synapses, in which the presynaptic axon makes contact to an axon of the postsynaptic neuron (figure 2B) and axo-somatic synapses, in which the presynapse directly contacts the soma of the postsynaptic neuron (figure 2C, E). A specialisation of the latter type is the calyx-type synapse (figure 2E). The word calyx is latin, meaning cup-like structure. In these synapses the presynaptic ending spreads out and covers more than half of the postsynaptic soma like a cup, forming a single gigantic synaptic structure, which is

why they are referred to as giant synapses. There are two synapses of this type in the brainstem. The endbulbs of Held in the anterior ventral cochlear nucleus (aVCN) and the calyces of Held in the medial nucleus of the trapezoid body (MNTB). In fact, the calyx of Held is the biggest synapse in the mammalian nervous system.

Less common than the above mentioned synapses are dendro-somatic and dendro-dendritic synapses, in which presynaptic dendrites establish contact to the soma or dendrites of the postsynaptic neuron.

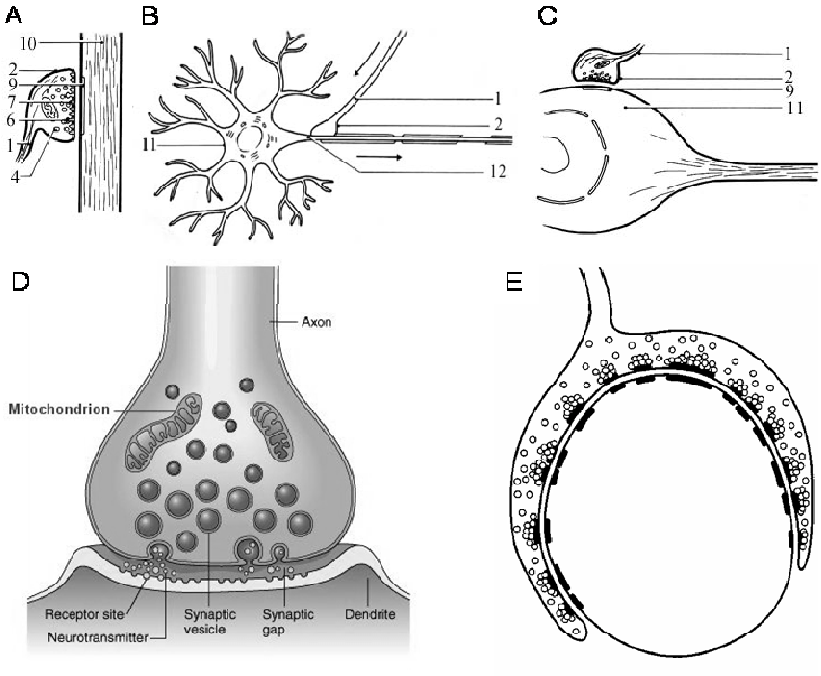

Figure 2. Synaptic morphology
(A) Axo-dendritic synapse. The presynaptic axon contacts a dendrite of a postsynaptic cell.
(B) Axo-axonic synapse. The presynaptic axon contacts an axon of a postsynaptic cell.
(C) Axo-somatic synapse. The presynaptic cell estabslishes contact directly onto the soma of the postsynaptic neuron. 1. Presynaptic axon 2. Bouton terminal 4. Presynaptic vesicles 6. Presynaptic vesicle discharging 7. Presynaptic membrane 9. Postsynaptic membrane 10. Postsynaptic dendrite 11. Postsynaptic cell body 12. Postsynaptic axon. (A) to (C) are modified from http://www.sci.port.ac.uk/rad/anatomy
(D) Schematic visualization of the functional aspects of synaptic transmission at the example of an axo-dendritic synapse. The dendrite of the postsynapse has a specialised structure, the spine, in which the postsynaptic structures are concentrated. For details refer to the text. Taken from http://universe/review.ca/I10/40/synapse
(E) Schematic drawing of a calyx-type somatic terminal. The circles depict synaptic vesicles and the strong lines synaptic specialisations, the pre- and postsynaptic densities. Taken from Walmsley et al. (1998).

1.3. The calyx of Held synapse

The calyx of Held (CoH) is a giant synapse (Figure 2E and 3) and forms part of the auditory circuit involved in sound localization at the level of the superior olivary complex (SOC) (Figure 3A, for review, see (von Gersdorff and Borst, 2002;

Schneggenburger and Forsythe, 2006)). The CoH is an excitatory glutamatergic synapse arising from globular bushy cells (GBCs), which receive direct excitatory input from the auditory nerve fibres in the anterior ventral cochlear nucleus (aVCN) and project their axons onto the principal neurons in the contralateral medial nucleus of the trapezoid body (MNTB). The principal neurons are interneurons, providing an inhibitory projection to other nuclei of the SOC such as the lateral superior olive (LSO) where for the first time inputs from both ears converge (Figure 3A).

Each MNTB neuron receives input from a single CoH (Figure 3B, C) (von Gersdorff and Borst, 2002). The CoH consists of multiple, thick “fingers” that grasp the postsynaptic cell. These terminals contain multiple active zones (Figure 2C, ~ 600 in rats of postnatal day nine (P9) (Sätzler et al., 2002) and ~ 400 in P9 mice (Youssoufian et al., 2005)), where synaptic vesicles cluster, facing the postsynaptic density. However, the individual active zones themselves are found to be similar to those in other synapses in the central nervous system. The unusual morphology and the multiple sites of synaptic vesicle fusion ensure fast, reliable synaptic transmission, such that incoming presynaptic action potentials (APs) trigger postsynaptic EPSPs, which reliably exceed the threshold for postsynaptic AP generation, even at high input frequencies. The glutamate, released from the presynaptic cell, generates dual component postsynaptic currents. The fast component results from activation of AMPA/KA receptors (AMPA/KAR), while the slow component is generated by activation of NMDA receptors (NMDAR). The CoH synapse represents a very useful model system to study synaptic transmission and its modulation, because both the presynaptic terminal and the postsynaptic neuron are electrophysiologically accessible (Barnes-Davies and Forsythe, 1995) (Figure 3B, C).

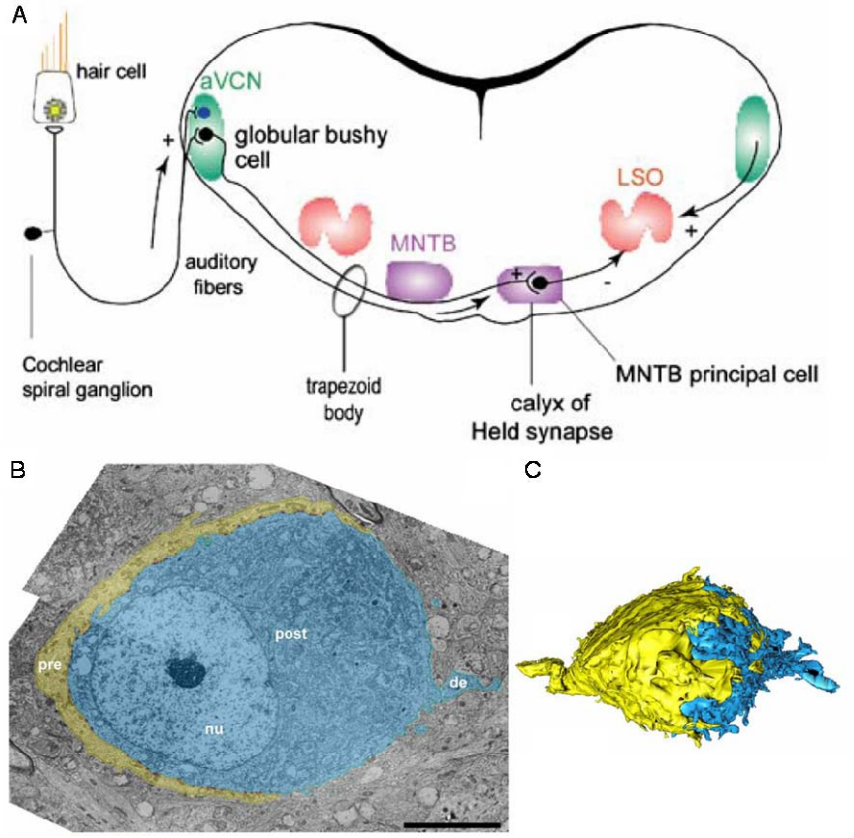

Figure 3. The calyx of Held synapse in the auditory brainstem circuit
(A) Representation in the coronal plane of the brainstem auditory pathway and the calyx of Held synapse, which forms part of the auditory circuit at the level of the superiory olivary complex (SOC). Bushy cells in the anterior ventral cochlear nucleus (aVCN) receive excitatory input from the auditory nerve fibres. The calyx of Held arises from globular bushy cells in the aVCN onto a principal cell in the contralateral medial nucleus of the trapezoid body (MNTB). The principal cells provide an inhibitory projection to other nuclei of the SOC such as the lateral superior olive (LSO). The calyx of Held is thus a tertiary auditory synapse that rapidly relays afferent activity, providing the LSO and other nuclei with (inhibitory) information with regard to sound arriving at the contralateral ear. Taken from Schneggenburger and Forsythe (2006).
(B) Electron micrograph of the calyx of Held from a P9 rat (yellow “pre” presynaptic calyx, blue “post” postsynaptic MNTB principal neuron, “nu” nucleus, “de” dendrite). Bar 5µm. Taken from Rollenhagen et. al. (2006).
(C) Computer assisted three-dimensional volume reconstruction of the calyx of Held-principal neuron synapse in the MNTB. The nerve terminal forms a cup-like structure with finger-like stalks that cover about 40% of the surface of the principal neuron. The final part that gives rise to the giant end terminal is seen left in yellow. Note the numerous spine-like protrusions on the surface of the principal neuron and the axon initial segment right in blue. Taken from Rollenhagen et. al. (2006).

1.4. The development of the auditory brainstem network

The auditory brainstem neuronal circuitry shows a highly ordered organization. In rats the afferent fibres that later give rise to the future calyces, start to grow out of the aVCN at embryonic day 14 (E14, 8 days before birth) and the most advanced

ones already cross the midline at E15 (Figure 4A). Kandler and Friauf (Kandler and Friauf, 1993) showed that the first contacts onto the principal cells of the MNTB are already established between P0 (postnatal day 0, the day of birth) and P3 (Figure 4B). To trace the synapse development, the authors used carbocyanine dye DiI or biocytin labelling of axonal fibres in *in vitro* fixed-slice preparations. They found further axonal growth and synaptic maturation to occur within the next week. By P10, almost all calyces had a morphology that resembled a mature calyx and by P14 they were almost indistinguishable from those of adults (Figure 4B). Different functional changes take place at the calyx of Held synapse along with the morphological modifications. In the Figure 4 (lower panel, left) a postsynaptic response is shown that was obtained from a P0 rat by the local axon stimulation (see Methods). Usually, evoked EPSCs at this age were only in the order of a few hundred pA, fluctuated extensively in amplitude and occurred in marked asynchrony. However, with development of the animals EPSCs increased in amplitude, became synchronous and phase-locked (Figure 4B). At the same time maturation of the synapse was accompanied by several other fine-tuning processes taking place both pre- and postsynaptically: among them being a change from AMPA/KA/NMDA to mainly AMPA/KAR–mediated EPSCs (Forsythe, 1994; Barnes-Davies and Forsythe, 1995; Joshi and Wang, 2002; Koike-Tani et al., 2005); an increase in the size of a readily-released pool (RRP) of vesicles with parallel reduction in release probability (Taschenberger and von Gersdorff, 2000; Ishikawa et al., 2002; Joshi and Wang, 2002; Fedchyshyn and Wang, 2005).

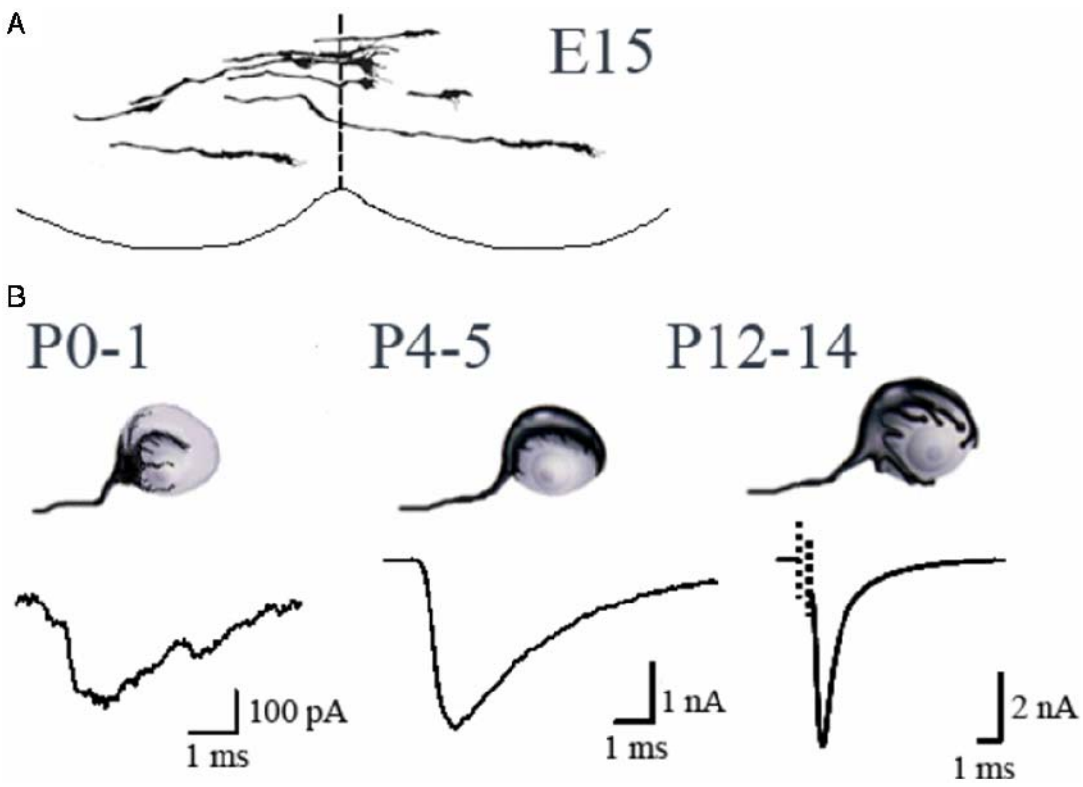

Figure 4. Schematic representation of the calyx of Held maturation
(A) At embryonic day E15 axon growth cones travel to the contralateral side, where they will form first contacts with principal neurons before birth.
(B) Once the synapse is established, further maturation occurs, during which the calyx changes its shape from cup-like to a highly branched structure. At the same time synaptic responses increase in amplitude, become synchronized and fast to provide the phase-locked high fidelity transmission. Taken from (Korogod, 2006)

1.5. Properties of glial cells

The cellular composition of the adult vertebrate nervous system consists of neurons and neuroglia (Kandel, 1995). The neuroglial cells are currently subdivided into four (Kettenmann and Ransom, 2005), according to newer studies into five (Peters, 2004; Butt et al., 2005), major categories. In the CNS there are astrocytes, oligodendrocytes and microglia. In the peripheral nervous system (PNS) the Schwann-cells represent the pendant of the oligodendrocytes of the CNS. Recent studies depict the NG2 cells as an independent glial cell type in the CNS, being the above mentioned fifth cell type.

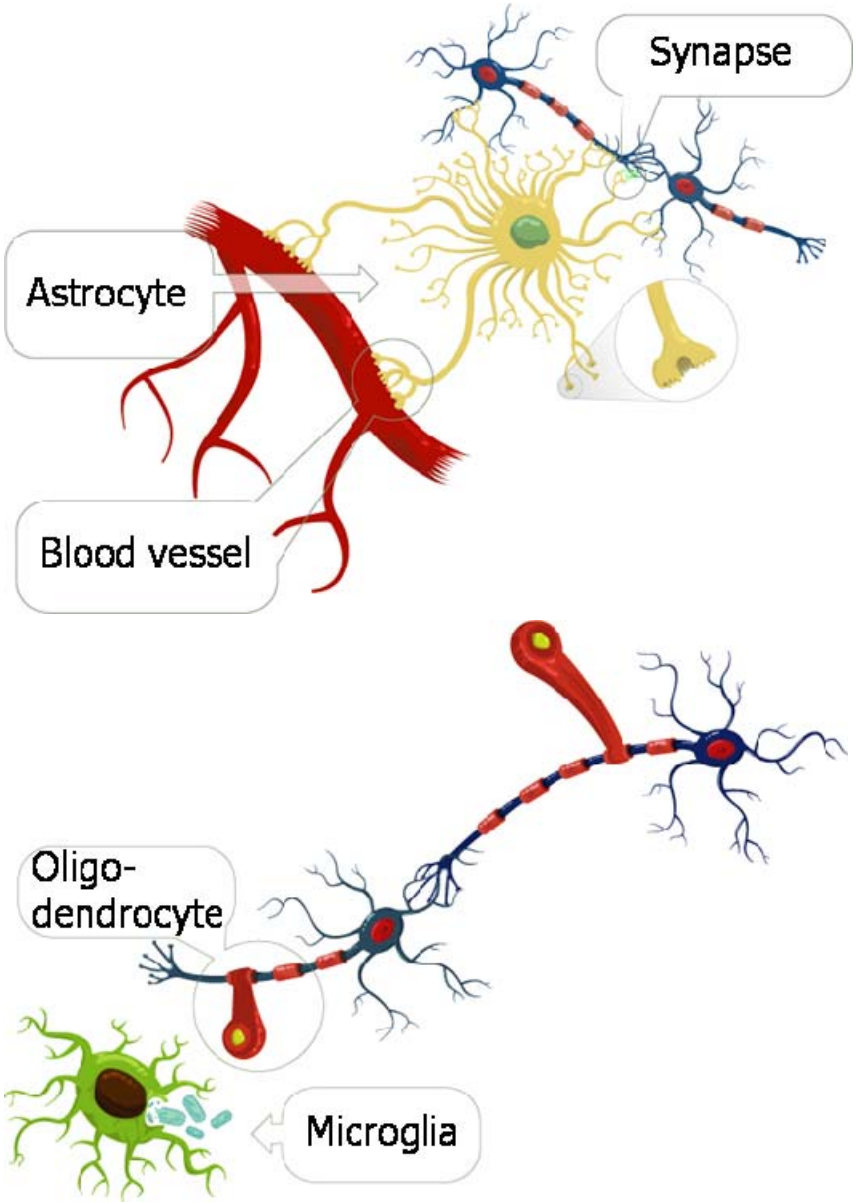

Figure 5. Neuroglial cell types
Astrocytes (yellow) contact blood vessels (dark red) with specialised structures, the end-feet, and neurons, taking up the glucose from the blood and save energy in form of glycogen. They are the only cell type in the nervous system that can produce glycogen. They also convert glucose encymaticaly to lactate, providing this as an energy source to the neuons (dark blue). They also enwrap synapses, thereby limiting cross-talk between the synapses. The oligodendrocytes (light red) enwrap parts of the axon, providing the myelin sheat, which enables fast saltatory signal conduction. The microglia (green) are the immuncompetent cells of the brain, providing the majority of antigens in the nervous system. They can also phagocyte cells, such as dead neurons or bacteria (light blue). Figure modified from http://learn.genetics.utah.edu/units/addiction/reward/images/

According to the classical view of the nervous system, the numerically superior glial cells have inferior roles in that they provide an ideal environment for neuronal cell function. Rudolf Virchow first discribed these cells in 1858 as filling, giving them the greek name for putty or glue, glia (Virchow, 1858).

However, after 150 years the view has changed. We now know that the versatility of glial cells for the function of the nervous system was long and dramatically underestimated. Glial cells have a variety of functions in the nervous system. The microglial cells (figure 5) are the only cell population of the CNS of mesodermal origin and represent the immun-competent cells of the CNS. All other glial cell types are supposed to be of neuro-ectodermal origin. The myelinsheat-forming Schwann cells of the PNS and oligodendroglial cells of the CNS enwrap the axons to speed up the saltatory conduction velocity. However, the astrocytes and also the “new” glial cell type, the chondroitin sulfate proteoglycan NG2 expressing cells serve different functions. Astrocytes provide support and nutrition, maintain homeostasis, react upon pathological insults (astrogliosis) and participate actively in neuronal signal transduction (Horner and Palmer, 2003; Nedergaard et al., 2003; Newman, 2003; Ransom et al., 2003; Slezak and Pfrieger, 2003). The role of the NG2 cells is at the moment rather controversly discussed. Being first described as an immature cell (Levine and Nishiyama, 1996) it was shown on the one hand that they do have some immature or precursor cell properties, being able to differentiate into oligodendrocytes, astrocytes and neurons (Belachew et al., 2003; Zhu et al., 2008). But NG2 cells are also present in mature animals, participating actively in signal transduction, even receiving direct synaptic input (Bergles et al., 2000; Jabs et al., 2005; Lin et al., 2005; Kukley et al., 2007; Ziskin et al., 2007). Additionally immature cells such as progenitor cells would not be expected to have such a complex morphology as NG2 positive cells do have, as observed in light microscopic preparations, especially the highly ramified nature of their processes (Nishiyama et al 2002). For this reason the authors suggest the cells should be called “polydendrocytes”. Butt et al (2002) also suggest the NG2 positive cells in the adult brain to be a mature neuroglial cell type, proposing them to be called “synantocytes”, because Bergles et al (2000) have shown that vesicles filled axon terminals from pyramidal cells in the hipopcampus form synaptic junctions with the processes of NG2 positive cells. The concrete role of this cell in the nervous system has still to be elucidated.

1.6. Glial cells participate in synaptic transmission

Glial cells, in particular astrocytes and their fine processes are considered to be part of the synaptic complex. They have been shown to play an important role in synaptic behaviour (Lin and Bergles, 2004; Newman, 2005) forming the so-called tripartite synapse (Araque et al., 1999). They not only act as physical barriers to diffusion but also by their specific uptake and removal of neurotransmitters by various types of transporters (Danbolt, 2001). Tight enwrapping of synapses by astrocytic processes restricts spill-over of transmitter outside the synaptic cleft, thereby limiting intercellular crosstalk mediated by volume transmission (Oliet et al., 2004).

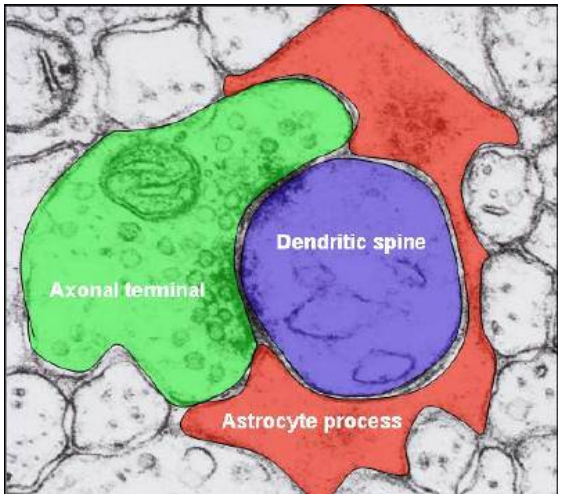

Figure 6. The tripartite synapse
The axon terminal (green) contacts a dendritic spine (blue). The synaptic area is completely enwrapped by an astrocytic process (red). The three elements from a functional unit, the tripartite synapse. Taken from (Volterra et al., 2002).

The classical type of astrocyte expresses glutamate transporters, and neuronal glutamatergic synaptic activity induces currents due to the glutamate uptake activity (Bergles and Jahr, 1997; Matthias et al., 2003). Astrocytes are characterised by the expression of glial fibrillary acidic protein (GFAP), which has been used as a marker protein for astroglia. Astrocytes show non-inactivating membrane currents with no voltage activated component when repetitively clamped to depolarizing and hyperpolarizing membrane potentials and are therefore also referred to as “passive cells”.

At a given synapse the astrocytes can functionally but also morphologically interact in quite diverse ways. However, not all synapses in the CNS are ensheathed with glial processes. The range varies from 29% of the synapses in the visual cortex

being associated with astrocytes (Spacek, 1985), to 57% in the hippocampus (Ventura and Harris, 1999) and up to 67% of parallel fiber-Purkinje cell and 94% climbing fiber-Purkinje cell synapses, respectively, in the cerebellum (Spacek, 1985; Grosche et al., 1999; Xu-Friedman et al., 2001). Also in a given synaptic specialization like the axo-somatic synapse, the glial contacts can vary to a great extent in number as well as in contact site. Figure 7 depicts six different morphological interactions of astrocytes with axo-somatic synapses. Interestingly, at the endbulbs of Held in the aVCN, of which the postsynaptic cells give rise to the calyces of Held in the MNTB, velate astroglial processes not only completely surround the endbulbs of Held but also separate, by finger-like glial extensions, the acive zones included in the calyx (Figure 7F)

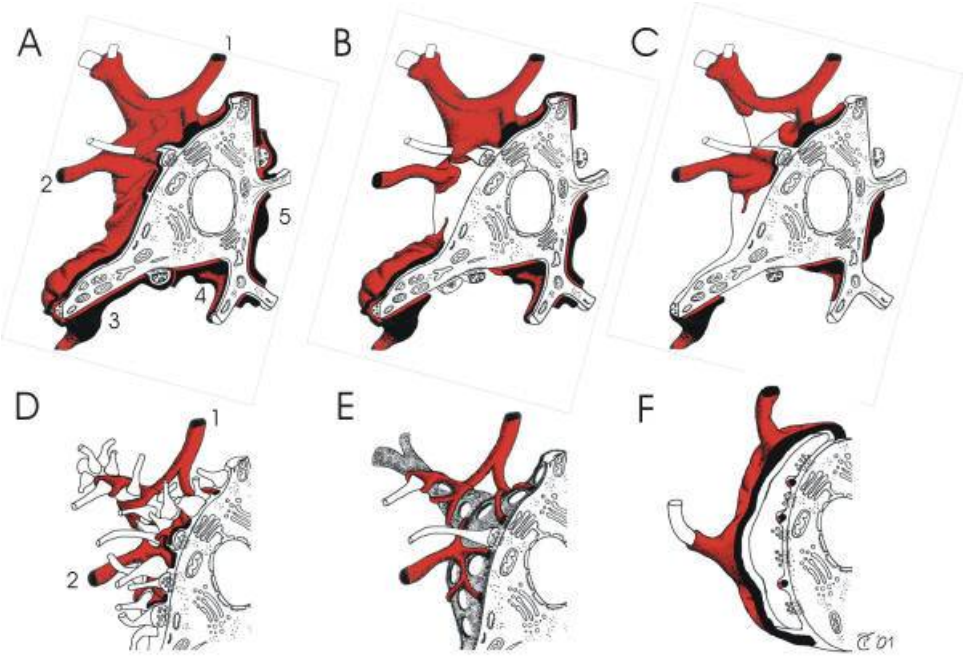

Figure 7. Morphological interaction of astrocytes with axo-somatic synapses
Only a minority of neuronal somata attracts astroglial processes. Constant (mean) numbers of processes that contact neuronal somata (1-5 in A-C and 1 and 2 in D-F) indicate random contact relations. In contrast to this, lamellipodia and filopodia that establish contact with neuronal somata show considerable variation in contact size. This is uncorrelated to the number and distribution of axo-somatix synapses.
(A) The neuronal cell body surface, including the axo-somatic synapses may be completely covered by astrocytic lamellae.
(B) The neuronal cell body surface is contacted, but the axo-somatic synapses are excluded.
(C) The neuronal cell body and the axo-somatic synapses are randomly contacted.
(D) The neuronal soma may be studded with axon terminals but the astroglial contacts remain few (e.g. on some motoneurons).
(E) Neurons carrying so-called perineuronal nets can be contacted by thin astroglial processes branching between synapses, but they tend to stay away from them.
(F) At the Held's bouton giant synapse in the anterior ventral cochlear nucleus, the presynapse covers part of the neuronal cell body. The whole structure is completely surrounded by perisynaptic glia even extending between its active zones. Taken from (Volterra et al., 2002).

A second type of glial cell receives synaptic-like input from both glutamatergic and GABAergic terminals (Bergles et al., 2000; Matthias et al., 2003; Lin and Bergles, 2004; Lin and Bergles, 2004; Jabs et al., 2005; Lin et al., 2005; Kukley et al., 2007; Ziskin et al., 2007). At the ultrastructural level, synaptic-like structures have been reported to terminate on this type of glial cell (Jabs et al., 2005; Kukley et al., 2007; Ziskin et al., 2007). The chondroitin sulfate proteoglycan NG2 was described as a marker for this cell type (Levine and Nishiyama, 1996). However, the cellular and molecular identity of this cell type is still rather controversially discussed (for review see (Paukert and Bergles, 2006)). This is reflected by a diverse terminology for those cells found in the literature. They have been termed receptor astrocyte (Matthias et al., 2003; Jabs et al., 2005), oligodendrocyte precursor cell (Bergles et al., 2000), polydendrocyte or synantocyte (Butt et al., 2002), but mostly NG2-expressing, NG2-positive or simply NG2 cells (Nishiyama et al., 1999; Berry et al., 2002; Chittajallu et al., 2004; Karram et al., 2005; Paukert and Bergles, 2006). Currently, however, it is still unknown whether synapses on this glial cell type are distinct contacts or if both a NG2 cell and a neuron can receive input from the same presynaptic terminal.

1.7. Astrocytes respond to synaptic activity

A couple of studies in the intact tissue provide evidence that astrocytes respond to various neurotransmitters (for review see (Porter and McCarthy, 1997)). In acute slice preparations (*in situ*) it was shown that astrocytes from different brain regions do react to neuronal activity (Dani et al., 1992; Porter and McCarthy, 1996; Fellin and Carmignoto, 2004; Schipke and Kettenmann, 2004; Newman, 2005; Perea and Araque, 2005). However, as the main pathway of astrocytic communication is via Ca^{2+} signals, the work in slices focuses on the investigation of astrocytic Ca^{2+} signals occurring during or shortly after neuronal stimulation (Dani et al., 1992; Porter and McCarthy, 1996). Over 15 years ago, first evidence for Ca^{2+} signalling in astrocytes induced by neuronal activity in an intact network came from work using organotypically cultured slices of rat hippocampus. Triggering neuronal activity by

stimulation of neuronal afferents led to a delayed Ca^{2+} signal in astrocytes. This signal was than travelling in a wave-like manner in between astrocytes (Dani et al., 1992).

A number of recent studies have made clear that neuronal activity elicits responses in astrocytes, namely increases in intracellular Ca^{2+} concentration or the induction of membrane currents and that this is a general phenomenon. The hippocampus has been a favourite structure to study such neuron-glia interactions. Stimulation of Schaffer collaterals triggers Ca^{2+} increases in astrocytes located in the striatum radiatum of the CA1 region (Porter and McCarthy, 1996). Interneurons trigger Ca^{2+} increase in astrocytes mediated by $GABA_B$ receptors (Kang et al., 1998) and there is even evidence for a direct synaptic input to glial cells (Bergles et al., 2000; Kukley et al., 2007; Ziskin et al., 2007). A cholin-mediated neuron to astrocyte signaling has been recently reported by Araque and coworkers (Araque et al., 2002). In acute slices from rat hippocampus, the stratum oriens/alveus, which contains cholinergic afferents, was stimulated and whole-cell membrane currents and intracellular Ca^{2+} levels of astrocytes in the hippocampal stratum oriens were recorded. Nerve-fibre stimulation evoked a long-lasting inward current and increased the Ca^{2+} levels in astrocytes (Araque et al., 2002).

Another important preparation studied for neuron glia interaction is the cerebellum. Single-pulse stimulation of parallel fibres triggers a local increase in Ca^{2+} in Bergmann glia processes, while the signal can also be recorded in the soma with a stronger stimulation (Grosche et al., 1999). This form of neuron astrocyte interaction is mediated by nitric oxide (Matyash et al., 2001). Stimulation of climbing fibres also triggers a response in Bergmann glia brought along by an adrenoreceptor-mediated mechanism (Kulik et al., 1999). Neuronal activity also elicited large currents in glia due to electrogenic glutamate uptake (Bergles and Jahr, 1997). This mechanism of signalling, the uptake of glutamate by astrocytes via glutamate transporters, is the best characterized form of neuron to astrocyte signalling. Astrocytes play a very important role in glutamatergic signal transmission, as synaptic transmission at these synapses is only terminated by removal of glutamate from the synaptic cleft. Thus, it is not surprising that this function of astrocytes, the glial glutamate transport, can

also modulate short-term synaptic plasticity (Turecek and Trussell, 2000). Astrocytic glutamate transporter currents can even be used to monitor synaptic function and plasticity (Bergles and Jahr, 1998).

1.8. Astrocytes influence synaptic transmission

There are a number of studies, which demonstrate that astrocytes are important for synaptic transmission in the cerebellum (Iino et al., 2001), in the retina (Newman and Zahs, 1998) and in the hippocampus (Kang et al., 1998). Also spontaneously, naturally occurring glial Ca^{2+} oscillations trigger the activation of neurons via NMDA receptor activation (Parri et al., 2001). In the hippocampus Ca^{2+} increases in astrocytes trigger synchronous, spontaneous synaptic activity in closely apposed neurons (Fellin et al., 2004).

Generally, astrocytes are capable of releasing a number of substances that can influence neuronal signal transmission, the most prominent one being glutamate. Glutamate release from astrocytes occurs after increase in intracellular Ca^{2+} in astrocytes (for review see (Montana et al., 2006)). In addition to that, the glial coverage of the synapse regulates the amount of glutamate released from the neuron acting on metabotropic receptors on the presynapse. This is an important way by which astrocytes modulate the release of neurotransmitters from presynaptic terminals (Oliet et al., 2001; Oliet et al., 2004).

It has been shown that astrocytes can directly influence neuronal activity as shown by an increase in spontaneous neuronal synaptic activity (Kang et al., 1998; Brockhaus and Deitmer, 2002). In the retina Newman and Zahs (Newman and Zahs, 1998) could show that glial activation modulates ganglion cell spike activity that is driven by light stimulation. The spectrum of glial influence varies from presynaptic activation of metabotropic receptors influencing transmitter release rates (Oliet et al., 2001; Oliet et al., 2004), transporter mediated regulation of mGluR-mediated excitation of interneurons (Huang et al., 2004), influencing the spontaneous activity of presynaptic interneurons (Brockhaus and Deitmer, 2002), synchronisation of neuronal activity (Angulo et al., 2004), input specific activation of astrocytes, which in

turn elicit NMDAR-mediated currents (Perea and Araque, 2005), control of synaptic strength (Jourdain et al., 2007) and, as mentioned before, regulation of synaptic activity by activity levels of glial neurotransmitter transporters (Huang et al., 2004).

1.9. Glial cells in the MNTB

Even though Hans Held himself, the eponym for the calyx of Held (Held, 1893) published a large article about the neuroglia back in 1903 (Held, 1903), it took nearly a whole century for the first publication to occur even mentioning neuroglia in the MNTB (Elezgarai et al., 2001). This and other morphological studies revealed that glial processes contact the pre- and postsynaptic membranes and express both glutamate receptors and transporters (Elezgarai et al., 2001; Satzler et al., 2002; Renden et al., 2005). However, so far no results have been published on the functional relevance of neuroglial cells in this particular brain region. Thus, the aim of the present study was to characterize the types of glial cells functionally associated with the CoH terminal and study mechanisms by which they are involved in signal transduction at the CoH-principal neuron synapse in the MNTB.

2. Experimental Procedures

2.1. Preparation of brain stem slices

All experiments were performed according to the guidelines of the German animal protection law. For the experiments, 8 to 10 day old out-bred NMRI mice (Charles River, Berlin) or transgenic GFAP-eGFP mice (Nolte et al., 2001) were used. For slice preparation, mice were decapitated and their brains were immediately transferred to ice cold bicarbonate-buffered artificial cerebrospinal fluid (aCSF) gassed with carbogene (5 % CO_2 and 95 % O_2). The aCSF contained (in mM): 134 NaCl, 2.5 KCl, 1.3 $MgCl_2$, 2 $CaCl_2$, 1.25 K_2HPO_4, 26 $NaHCO_3$, 10 glucose, equilibrated with carbogene to pH 7.4. The brainstem and the cerebellum were cut from the cortex in a 30° angle by hand (Figure 8A). This assured a preservation of the afferent fibres from the aVCN to the MNTB. The brainstem and the cerebellum were then glued to the chamber of the vibratom for slicing procedure. The stage, filled with ice cold aCSF, was cooled with a cooling element stored in a freezer at -20°C for at least two hours prior to the slicing procedure. Four to six transverse slices (160-180 µm) were cut sequentially in the rostral direction from the level of the seventh brain nerve using a tissue slicer (Microm HM 650 V, Walldorf, Germany) set to the lowest cutting speed and the highest amplitude and frequency. This assured the least damage to the afferent fibers during the slicing procedure (R. Schneggenburger, personal communication). The brainstem slices were gently transferred to a holding chamber and kept in aCSF at room temperature, for at least 45 min until they were used for recording.

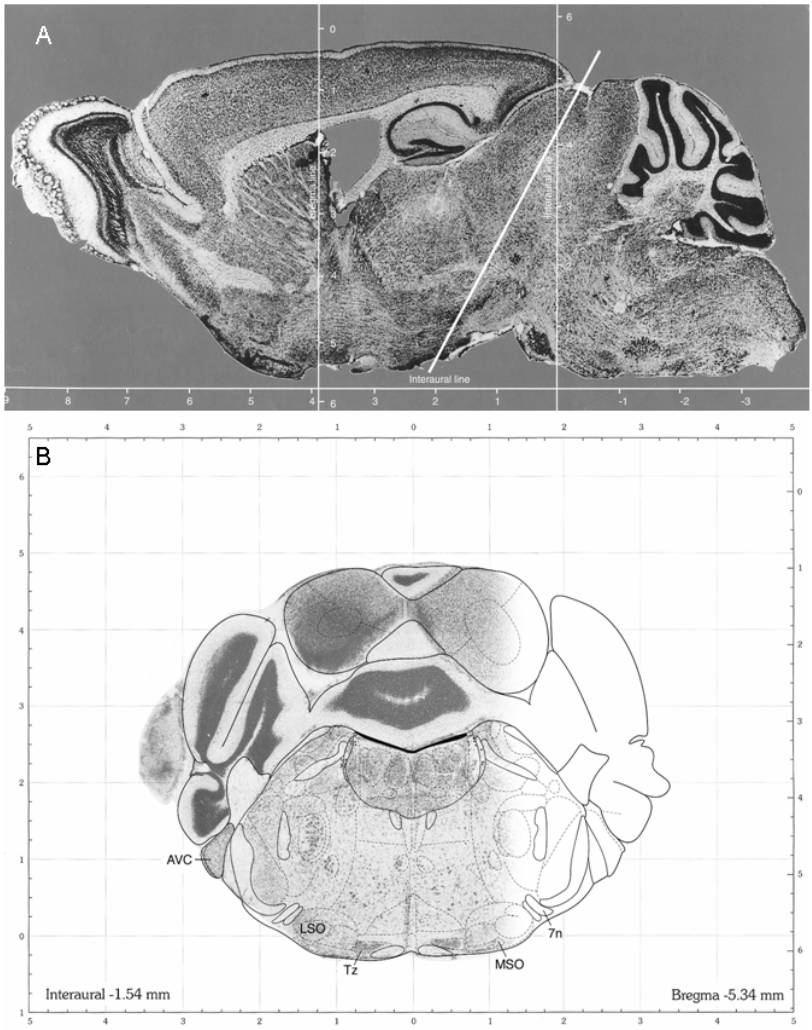

Figure 8. Slice preparation and location of the MNTB
(A) Lateral view of the adult mouse brain, rostral to caudal from left to right. The white bar shows the position of the transverse cut.
(B) Overlay of a schematic map and a fotocollage of a transverse slice, containing the region of interest. The important nuclei are labelled with abbreviations. AVC, anterior ventral cochlear nucleus, LSO, lateral superior olive, MSO medial superior olive, Tz, medial nucleus of the trapezoid body. All pictures modified from "The mouse brain atlas", (Franklin and Paxinos, 1997).

2.2. Identification of glial cells in the MNTB

The experiments were done using an Olympus BX51WI upright microscope equipped with 10x and 40x water immersion objectives (numerical aperture 0.25 and 0.8, for LMPlan IR10x and LUMPlan FI/IR W 40x objective, respectively) and equipped with bright field and infrared video differential interference contrast optics (IR-DIC, Olympus Germany, Hamburg, Germany). The MNTB was recognized due to the size of the principal neurons (~20 µm, figure 12). The confirmation of the brain slice for the correct region was obtained from the web page of the Mouse Brain Library: http://www.mbl.org and the mouse brain atlas ((Franklin and Paxinos, 1997), figure 8). When starting the project, experiments were only performed in GFAP-eGFP mice (Nolte et al., 2001) until it became evident that the eGFP expressing

cells are solely of the passive type (see results part, figure 12, 13). By that time it was then possible, due to the training, to visibly identify the passive cells in standard water immersion optics and approach them with a patch micropipette. After doing experiments for some time in wildtype NMRI mice it was then also possible to visibly identify complex glial cells and distinguish them from the passive glial cells, due to the smaller soma size of the complex glial cells (see results part, figure 13, 15).
Images of passive and complex glial cells as well as principal neurons were obtained with a CCD camera (Sensicam, PCO AG, Kelheim, Germany) mounted on the microscope.
Identification of GFAP-eGFP fluorescent cells was performed with an excitation of 480 ± 20 nm by a HG lamp (U-ULH, Olympus, Hamburg, Germany, excitation filter D 480/40 M, Chroma Technology, Rockingham, VT, USA) mounted via a fibre system (TILL Photonics, Gräfelfing, Germany) to the microscope. The emitted light was collected at 510 ± 40 nm (D 510/80 M, Chroma Technology, Rockingham, VT, USA). Images of GFAP-eGFP fluorescent cells were obtained with two Photon laser scanning microscopy (see Methods part Two-Photon Microscopy at the recording site).

2.3. Calcium recordings

Slices were incubated with the Ca^{2+} indicator dye Fluo-4-acetoxymethylester (10 µM Fluo-4-AM, Molecular Probes, Eugene, OR, USA) in aCSF at 37°C under 95% O_2 and 5% CO_2 for 45 min directly after the preparation procedure. The slices were gently transfered to a storage beaker where they were allowed to recover at room temperature for at least 30 min before recording.
Imaging of Ca^{2+}-signals was done with a fast Odyssey scanning system (Odyssey XL, Noran Instruments, Prairie Technologies, Middleton, WI, USA). Fluo-4 was excited with an Argon 488 nm single line laser (ALC 60, American Laser Corporation, USA; Laserlight, Berlin, Germany) coupled into the Odysses via a fibre system (KineFLEX – P2 S 488 nm, Point source, Southampton, England). Signals were read out with Intervision software, running on an UNIX-based image workspace

station (Indy Workstation, Silicon Graphics, Sunnyvale, CA, USA). Fluorescence signals were detected offline with Image Pro 5.0 (Image Pro Plus 5.0, Media Cybernetics, Bethesda, MD, USA).

The first ten pictures yielded baseline fluorescence (F_0). The response was expressed as change of Fluorescence (F) at the peak of response in relation to baseline fluorescence (F/F_0). To estimate the amount of inhibition of a Ca^{2+}-response after application of an antagonist, the responses were normalized to the control response and expressed as % change.

2.4. Electrophysiological recordings

Membrane currents were recorded with the patch clamp technique in the whole-cell recording configuration (Hamill et al., 1981) (figure 9). For details see figure legend of figure 9, which was modified with few words from Hamill et al (1981). Current signals were amplified with a double EPC 9 (EPC9/2, HEKA Elektronik, Lambrecht, Pfalz, Germany; membrane potential not corrected for liquid junction potentials), filtered at 3 kHz, sampled at 10 kHz, recorded by the TIDA software (TIDA Version 5.20, HEKA Elektronic, Lambrecht, Pfalz, Germany) and stored in a personal computer. Resting membrane potentials (MP) of recorded cells were identified with a TIDA routine. Membrane capacitance (C_m) values of recorded cells were calculated based on the equation $C_m = \tau / R_a$ where τ is the decay time constant of the transient current elicited by a depolarizing 10 mV pulse from a holding potential of -70 mV and R_a the access resistance (series resistance R_s). R_s was calculated by the Ohmic law ($R_s = U / I_{trans}$).

For experiments with midline stimulation a bipolar concentric electrode (MCE-100, Rhodes medical Instruments Woodland Hill, California, USA) was placed gently on the midline of the brainstem slice (Figure 10) and 100 µs current pulses between 100 µA and 1 mA were injected. The recorded cells were at least 300 µm away of the stimulation site to reduce stimulus artifacts and to assure that the cells were not directly stimulated (Schneggenburger et al., 1999).

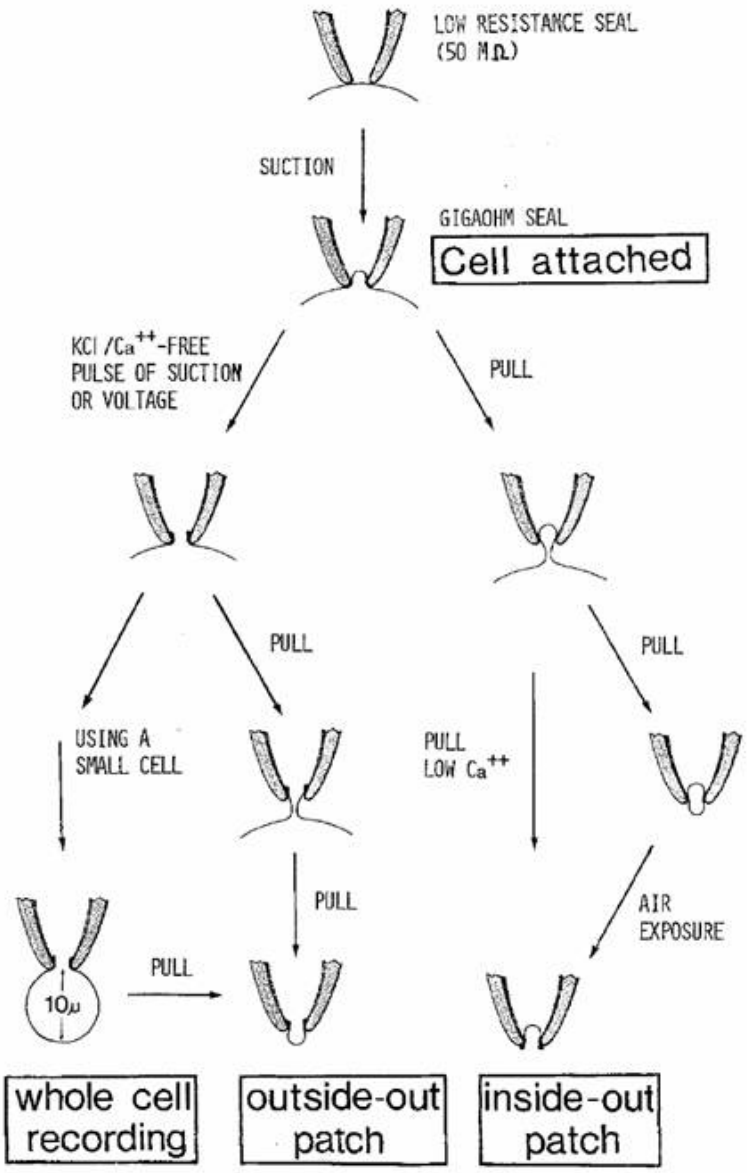

Figure 9. Schematic representation of the procedures, which lead to recording configuration
The four recording configurations, described in (Hamill et al., 1981) are "cell-attached", "whole-cell recording", "outside out patch" and "inside-out patch". The upper most frame depicts the configuration of a pipette in simple mechanical contact with a cell. This displays the configuration as has been used in the past for single channel recording (Neher et al.1978). Upon slight suction on the back of the patch micropipette the seal between membrane and pipette increase in resistance by 2 or 3 orders of magnitude. This leads what is called a cell-attached patch. The improved seal allows a 10-fold reduction in background noise. This stage is the starting point for all possible following steps, like manipulation to isolate membrane patches, which lead to two different cell-free recording configurations "outside-out patch" and "inside-out patch". Alternatively, voltage clamp currents can be recorded from the cell "whole cell recording". The figure legend modified from: Hamill, O. P. et. al. (1981).

Patch micropipettes with a resistance of 3-5 MΩ (for the neurons) or 5-8 MΩ (for the glial cells) resulting in an uncompensated series resistance (R_s) of 10-20 MΩ for neurons and 20-50 MΩ for glial cells at the beginning of recording. Recordings with a

R_s > 30 MΩ (neurons) and > 60 MΩ (glial cells) were discarded from further analysis. The actual value of the R_s was measured during the recording (repetitively every 10 sec in case of the recording of spontaneous activity and in case of the midline stimulation experiments before and after afferent fibre stimulation repetitively every ten seconds) by applying 10 ms pulses of 10 mV (from -70 to -60 mV). Patch micropipettes were pulled from thin walled borosilicate glass (o.d. 1.5 mm, i.d. 0.87 mm; Hilgenberg, Malsfeld, Germany) using a P2000 laser based micropipette puller (Sutter Instruments, Novato, USA). Micropipette solution used for neuronal recording (solution A) contained (in mM): 97.5 potassium gluconate, 32.5 CsCl, 5 EGTA, 10 HEPES, 1 $MgCl_2$, 30 TEA-Cl, 3 lidocaine N-ethyl bromide (QX314). For glial recording (solution B), the internal solution contained (in mM): 120 potassium gluconate, 10 KCl, 1 $MgCl_2$, 10 HEPES, 0.1 EGTA, 0.025 $CaCl_2$, 1 K_2ATP, 4 glucose, 0.2 Na_2 GTP. For experiments with repetitive stimulation and spontaneous activity in the glial cells an internal solution (solution C) was used containing (in mM): 130 KCl, 1 $MgCl_2$, 10 HEPES, 0.1 EGTA, 0.025 $CaCl_2$, 1 K_2ATP, 4 glucose, 0.2 Na_2 GTP. The pH was adjusted to 7.2 with CsOH for solution A and KOH for solution B and C. The final osmolarities of the internal solutions were ≈ 280 mmol/kg and of the aCSF was ≈ 320 mmol/kg as determined with a VAPRO 5520 vapor pressure osmometer (Wescor, Inc, Logan, Utah 84321 USA).

All experiments were performed at room temperature (20-22°C). Chemicals were obtained from Sigma (Deisenhofen, Germany) or Tocris (Avonmouth, UK) if not otherwise indicated.

Slices were superfused with aCSF and substances were applied by changing the perfusate. In order to test the response of complex cells to agonists of neurotransmitters receptors, the indirect neuronal effect was minimized by adding tetrodotoxin (TTX, 1 µM) to the aCSF. During KA application 10 µM MK801, 50 µM D-APV (to block NMDAR), 1 µM strychnine and 10 µM SR95531 (Gabazine) (to block inhibitory input) were added to the bath solution.

The analyses of the synaptic currents and the decay time constants τ were performed with PeakCount software (Version 3.0.0) developed by Christian

Henneberger at the Institute of Neurophysiology of the Charité, Berlin, Germany, using a first derivative threshold detection algorithm.

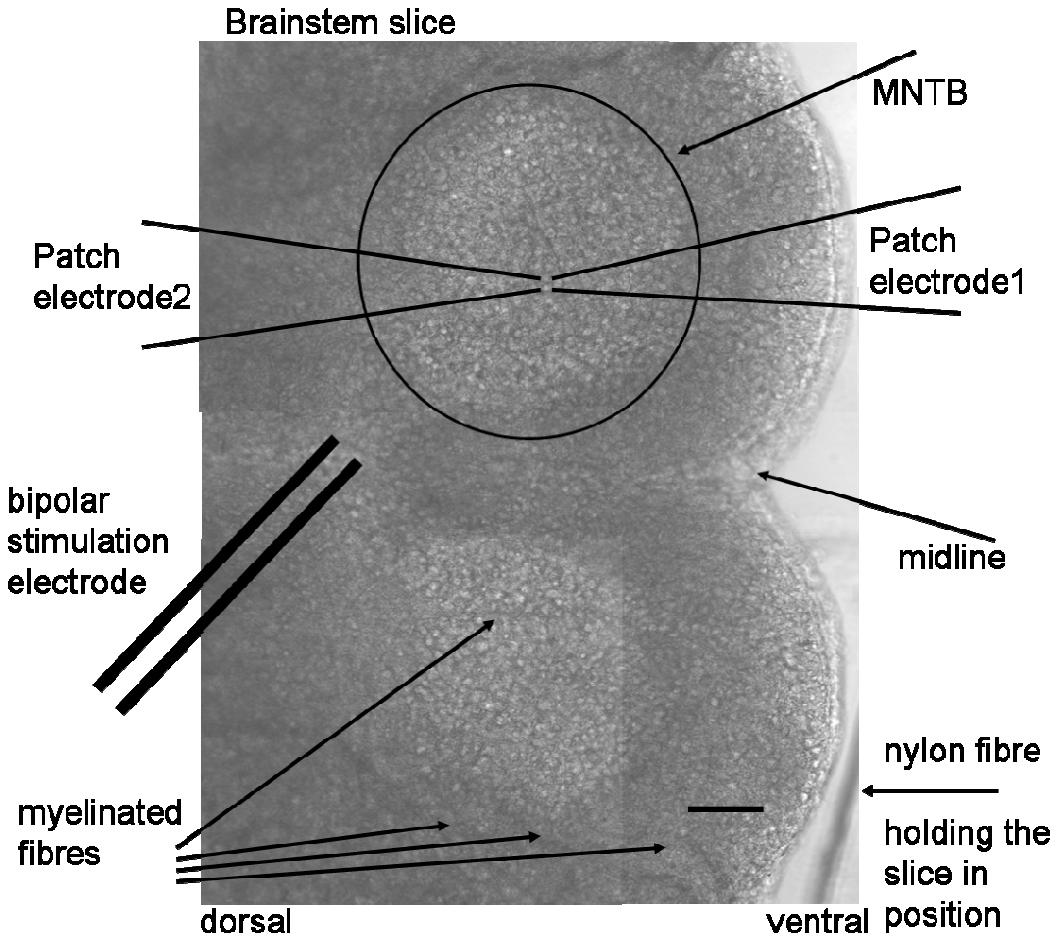

Figure 10. Experimental settings for experiments including electrical presynaptic fibre stimulation
The MNTB is clearly identifiable due to the size of the principal neuron somata. The bipolar concentric stimulation electrode was placed on the midline where the fibers from the aVCN cross to the contralateral side, giving rise the calyces of Held. Scale bar 100µm.

2.5. Electrophysiological identification of the recorded cell type

To unequivocally identify the recorded cell type the cell was clamped for 50 ms to a series of de- and hyperpolarizing potentials in steps of 10 mV ranging from -140 to +40 mV from a holding potential of -70 mV (Figure 11). This yielded the current profile of the recorded cell, which are characteristic for each cell type (Matthias et al., 2003).

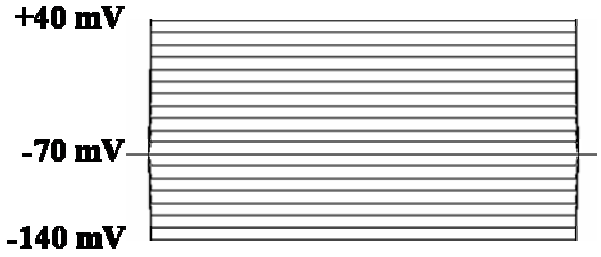

Figure 11. Stimulation protocol for recording current profiles
The cell was clamped to a holding potential of -70 mV. A series of voltage jumps, 10 mV each, was applied for 50 ms up to -160 and +40 mV. The recorded currents were plotted over another.

2.6. Estimating the probability of failure of synaptic transmission at the calyx and the number of release sites towards the glial cell

The question is addressed wether complex glial cells contact more than one neuron. Events were recorded in parallel from complex glial cells and principal neurons. There were events in the neuron alone, in the complex glial cell alone and coincident events. When the complex glial cell contacts only this one neuron, an event in the glial cell alone, without corresponding event in the neuron, would indicate a failure of synaptic transmission from the calyx to the neuron (given that the observed events are all caused by incoming presynaptic spikes, as assumed under 100 µM 4-AP). Thus, when the probability of transmission failure at the calyx is lower than the probability of observing isolated events in the complex glial cell, it can be concluded that the complex glial cell receives input from more than one calyx.

This analysis is based on the release-site model and the quantal theory of synapse function (Vere-Jones, 1966; Katz, 1969). It starts from the assumption that the calyx synapse has *N* independent release sites that are activated by a presynaptic action potential with probability *p.* At each release site, activation leads to the release of a single quantum of transmitter, evoking a membrane current with the quantal amplitude *q* in the postsynaptic membrane. The mean amplitude *I* of the postsynaptic current is thus

$$I = Npq$$

and one can therefore calculate the probability *p* of activation of an individual release site from *I*, *N*, and *q* via

$$p = \frac{I}{Nq}.$$

As the probability that an individual release site is not activated by a presynaptic spike is $1 - p$, the probability P_f of failure of synaptic transmission is

$$P_f = (1 - p)^N.$$

Similarly, if the probability P_f of failure of synaptic transmission, and the probability *p* of activation of an individual release site are known, one can estimate the number *N* of release sites by:

$$N = \frac{\log P_f}{\log(1 - p)}.$$

2.7. Dye coupling experiments

During recording, cells were filled with Lucifer Yellow (LY, 0.1%) and Biocytin (0.5%) by dialysing the cytoplasm with the patch pipette solution. To avoid destruction of the cell as the pipette was pulled off after recording, the seal was destroyed by a large hyperpolarization (clamping the cell for 5 ms to -270 mV from a holding potential of -70 mV). Following recording, LY fluorescence was examined in a two-photon laser scanning microscope and afterwards slices were fixed in 4% paraformaldehyde in 0.1 M phosphate buffer and stored there until biocytin detection. Biocytin detection was performed as described by D'Ambrosio et al. (D'Ambrosio et al., 1998) with few modifications; briefly, sections were incubated with the Elite ABC kit (Vector, Burlingame, CA) for 48 hrs. The diaminobenzidine reaction was stopped after exactly 60 min, $NiCl_2$ was used for intensification. Slices were embedded in Aqua Polymount (Polysciences, Inc., USA) and inspected in a Zeiss Axioskop microscope with a 40x objective (Carl Zeiss, Jena**,** Germany). Images were taken with a digital camera (Axiocam, Zeiss) and appropriate software (Axiovision, Zeiss).

2.8. Immunohistochemistry

GFAP-eGFP transgenic mice (P8 - P10) were deeply anesthetized with Sodium-Pentobarbital (100 mg/kg body weight, Sanofi, Paris, France) and perfused intracardially with a solution of 4% paraformaldehyde in 0.1M phosphate buffer (PB, pH 7.4). Brains were dissected out and postfixed for 2 h at 4°C. After several washes in PB, brains were incubated overnight in 30% sucrose in PB. The next day, they were quickly frozen in Isopentan, cooled roughly to -20 to -30 °C by dry ice. The cooling procedure of Isopentan was performed so short to ensure that the Isopentan was still cold but not solid. Cryosections (20 µm thick) were mounted on gelatin-coated slides and allowed to dry for 30 min at room temperature. Sections were permeabilized with 0.1% Triton X-100 (TX100) in PB for 20 min and incubated in blocking solution (BS; 0.5% BSA, 4% normal goat serum (NGS), 0.01% TX100 in PB) for 1 h at room temperature. Rabbit polyclonal antibodies to GFAP (DAKO, Hamburg, Germany) were diluted 1:1000 (in PB/1% BSA/1% NGS, 0.01% TX-100). Anti-NeuN neuronal cell marker (Chemicon, Hofheim, Germany) was diluted 1:200; monoclonal antibodies to myelin-oligo-glycoprotein (MOG; kindly provided by Chris Linington) were used at a dilution of 1:100; rabbit anti-mouse antibodies to microglia (Iba-1 1:500; Wako, Neuss, Germany). Sections were incubated with the primary antibodies for 24 h at 4°C. Primary antibodies were visualized by application of Alexa-568 goat anti-rabbit IgG or Alexa-594 goat anti-mouse IgG (1:2000; Molecular Probes, Eugene, OR). Secondary antibodies were incubated for at least 2 h at room temperature. After three washes, sections were mounted with Aqua–Polymount (Polyscience Inc., USA) and inspected in the confocal laser scanning microscope (CLSM) equipped with a 488 nm argon ion laser (Molecular Dynamics, Sunnyvale CA) mounted on an upright microscope (Axioskop, Zeiss). eGFP fluorescence was excited at 457 nm (beam splitter 510 nm) and detected with a 530 nm bandpass filter. Red fluorescence of Alexa or Cy3 was excited at 517 nm (beam splitter 535 nm) and detected with a 570 nm long-pass filter. CLSM images were stored and processed on an Indigo workstation using the program Imagespace (http://imagespace.sourceforge.net/) and superimposed by Adobe Photoshop

(Adobe, San Jose, CA, USA). Specificity of immunoreactivity was controlled by incubation of tissue sections in (secondary) antibody dilution buffer instead of primary antibodies. In the controls, the immunocytochemical reactions in the CNS were usually negative. However, unspecific labelling of the meninges and connective tissue appeared in some cases.

2.9. Immunostaining for AN2 (NG2) of Lucifer Yellow filled cells

During recording, cells were filled with Lucifer Yellow (LY, 0.1%) by dialysing the cytoplasm with the patch pipette solution. To avoid destruction of the cell as the pipette was pulled off after recording, the seal was destroyed by a large hyperpolarization (clamping the cell for 5 ms to -270 mV from a holding potential of -70 mV). Subsequently, slices were fixed for 30 min with 4% paraformaldehyde (PA) and then permeabilized with 0.5% Triton X-100 in phosphate-buffered saline (PB), followed by treatment with PB containing 0.5% Triton X-100, 1% bovine serum albumin (BSA) and 20% normal goat serum (NGS). Slices were incubated overnight at 4^{o}C with monoclonal antibodies against AN2 (1:50, antibodies were gift from the group of J. Trotter). CY3-conjugated secondary antibodies were applied for 2 hours at room temperature (RT). Slices were thoroughly rinsed, mounted on coverslips with Aqua Polymount and analyzed with a conventional epifluorescence light microscop (Axiophot, Zeiss) or a confocal laser scanning microscope (CLSM) as mentioned above.

2.10. Two-Photon microscopy at the recording site

A two-photon laser scanning Olympus BX51WI microscope with a 40x water immersion objective lens was used to detect fluorescent signals (TILL Photonics, Gräfelfing, Germany). A Mira 900 laser (Coherent, Santa Clara, CA, USA) tuned to 860 nm was used for excitation. Image acquisition was controlled by Olympus software Fluoview FV300 (Olympus America, Melville, NY). In the transfluorescence

pathway, a 585 nm dichroic mirror was used to separate green and red fluorescence. D510/80M and HQ600LP filters were placed in the "green" and "red" pathways, respectively, to eliminate transmitted or reflected excitation light (Chroma Technology, Rockingham, VT, USA). For intracellular loading of cells, either LY (0.1 %) or Alexa Fluor-594 (0.01 %) were used to outline the cell structures.

The microscope was modified so that the electrophysiological experiments could be performed in parallel to the two-photon microscopy. To shield the recording site against background noise, the custom-build Faraday cage was mounted on the table including only the microscope and the micromanipulators (Mini25, Luigs and Neumann, Ratingen Germany, for the patch electrodes and MHE-3, Narishige, Tokyo, Japan for the stimulation electrode). A microscope table was custom-build to fit into the microscope and the cage and to carry the recording chamber as well as all three manipulators. So the stimulation electrode could be placed onto the brainstem slice and moved without damaging the tissue afterwards. The recording chamber was custom-build to ensure no movement of the slice due to mechanical disturbance of the perfusion system. To achieve that the entry as well as the exit of the bath solution were arranged in a U-turn-shape, thereby limiting direct perfusion waves. In this recording configuration it was possible to record from slices for over an hour without any movement of the area under investigation. All the modifications were done by Rainer Kröber together with Jochen Müller.

2.11. Electron microscopy

Complex cells were identified by their current pattern and dialyzed via the patch electrode containing additional biocytin (0.5%) and LY (0.1%). Biocytin filling was judged to be complete when the LY fluorescence was visible in fine distal processes. Usually, the cells were completely stained after 15 min and the electrode was pulled off after the seal was damaged by a large hyperpolarizing current injection to avoid destruction of the cell membrane. Any extracellular biocytin deposits were readily washed out in PBS. Biocytin–stained slices were fixed with 4% paraformaldehyde (PFA) and 1% glutaraldehyde (GA) for 3 hours and rinsed with PBS for another 30

min. The tissue was incubated in 1.5 mg 3,3´- diaminobenzidine tetrahydrochloride (diaminobenzidine, Sigma, St. Louis, MO) and 1 mg $NiCl_2$ per 1 ml PBS. The diaminobenzidine reaction was stopped when dark brown reaction became visible. The slices were then washed several times and postfixed for 30 min in buffered 1% osmium tetroxide solution. They were dehydrated through graded concentrations of ethanol, preembedded with propylene oxide, and flat- embedded in Epon (Plano, Marburg, Germany). Ultrathin sections were contrasted with uranyl acetate and lead citrate and examined in a Zeiss electron microscope at 80 kV (TYPE; Zeiss, Jena, Germany). Electron micrographs were taken at low magnification (x 1,250) to have overview of the neuropil and then at high magnification (x 10,000) to show ultrastructural specifications.

2.12. Statistical analysis

Statistical analyses were performed using Origin 7.0 software. The results are expressed as mean ± standard deviation (S.D.M.) if not otherwise stated. When experiments included control and more than one test group, data were statistically evaluated with the Tukey test, a probe for analysis of variance (ANOVA). Student´s *t* test was used for analysis in experiments with two groups (control and test).

3. Results

3.1. The CoH synapse is in contact with two types of glial cells

Two types of glial cells in close association with the CoH synapse could be identified and distinguished from each other by their different appearance due to enhanced green fluorescence protein (eGFP) fluorescence in glial fibrillary acidic protein (GFAP)-eGFP transgenic mice (Figure 12) (Nolte et al., 2001). One type was highly fluorescent, whereas the other one was not or only weakly fluorescent. By dialyzing the two cell types with Alexa Fluo 594 or with Lucifer Yellow (LY) via the patch-pipette, the cell population with high fluorescence intensity was found to be characterized by numerous ramified processes, whereas the other population with low or no fluorescence displayed only a few processes with little, if any branching (Figure 13B). The cell somata of eGFP-labelled cells could be in very close contact to the CoH synapse (Figure 12, 13) and a given cell contacted several principal neurons with its processes. Moreover, principal neurons were always associated with a net of eGFP-labelled processes (Figure 12). A similar interaction was found for the non-fluorescent cells. A given non-fluorescent cell had processes projecting to several CoH terminals (arrows in Figure 16).

Whole cell recordings from both cell types revealed that the highly fluorescent cells had a resting membrane potential (MP) of –70 $\pm$ 3 mV, a membrane resistance (R_m) of 27 $\pm$ 8 MΩ, and a membrane capacitance (C_m) of 22.9 $\pm$ 16.4 pF (n = 25). The non-fluorescent cells had a MP of -77 $\pm$ 8 mV, a higher R_m of 159 $\pm$ 39 MΩ and a lower C_m of 14.4 $\pm$ 5.4 pF (n = 25). All the values are uncorrected for liquid junction potentials (3 – 5 mV on average) and series resistance. The two cell types were also distinct in their membrane current pattern. The fluorescent cells showed passive membrane currents when de- or hyperpolarized between –160 to +40 mV for 50 ms (see methods part, Figure 11) resulting in a linear current voltage relationship (n = 25, Figure 13A). In the non-fluorescent cell type, depolarizing voltage steps elicited currents with a delayed activation, sometimes preceded by small transient inward

currents at potentials more positive than -20 mV. In response to hyperpolarizing voltage steps only small currents were observed resulting in an outward rectification of the current voltage relationship (n = 25, Figure 13A). The peak currents at +40 mV were 1.96 ± 1.20 and 1.16 ± 0.27 nA for the fluorescent and non-fluorescent cells, respectively. In the following, these cell populations will be referred to as passive and complex glial cells, respectively, similar to those cell types previously described in the hippocampus (Steinhäuser et al., 1992; Matthias et al., 2003).

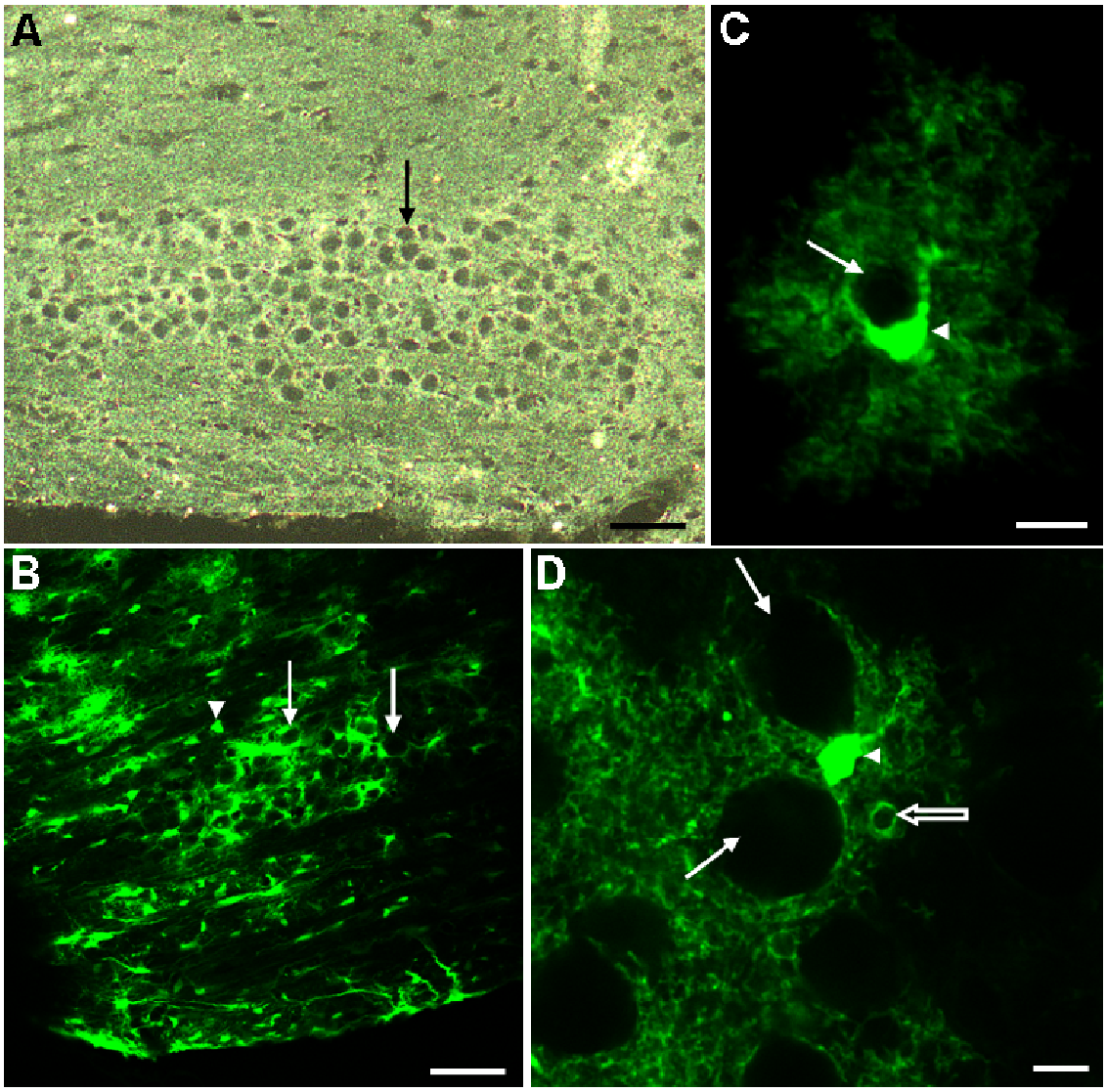

Figure 12. The MNTB area in bright field and two-Photon laser scanning microscopy

(A) Bright field overview image of the MNTB area. Note the clear identifiable borders of the MNTB and the large soma size of the principal neurons (arrow). Scale bar 70 µm.
(B) Two-Photon laser scanning microscopy image of the MNTB brain region from the brainstem of a P9 GFAP-eGFP transgenic mouse. Passive glial cells appear highly fluorescent (arrowhead). A close net of astrocytic processes surrounds every neuronal cell body (arrows), separating them from one another. Note the remarkable orientation of the neuronal fibre tract crossing the MNTB area from the upper right to the lower left side. Single focal plane, scale bar 50 µm.
(C) Two-Photon laser scanning microscopy image of a single astrocyte (arrowhead) in the MNTB of a GFAP-eGFP mouse. Note the complete surrounding of the principal neuron (arrow) with astrocytic processes. The image is an overlay of four consecutive sections, taken one µm apart from each other. Scale bar 10 µm.
(D) Two-Photon laser scanning microscopy image of a single astrocyte (arrowhead) in the MNTB of a GFAP-eGFP mouse. In contrast to the astrocyte shown in C, the astrocytic processes are in contact with at least two principal neuron somata (filled arrows), but also establish contact to a blood vessel (hollow arrow). Single focal plane, scale bar 10 µm.

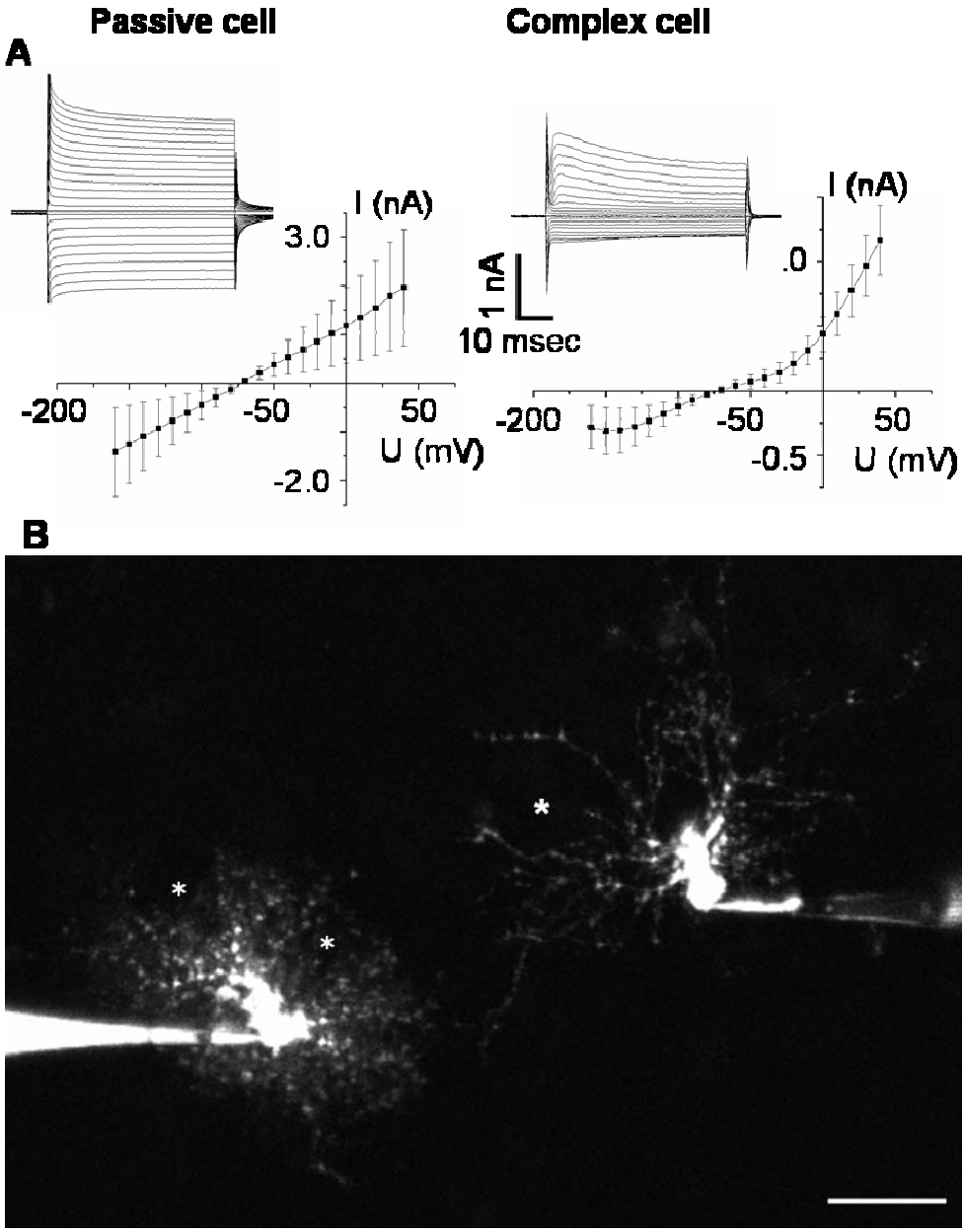

Figure 13. Two distinct types of glial cells in the MNTB
(A) Current profile and current-voltage (IV) relation of the two glial cell types. Left: Average current-voltage (IV) plot obtained from 25 passive cells. Inset: Representative current responses from a passive cell evoked by voltage steps. Membrane currents were evoked by 50 ms voltage steps ranging from –160 to +40 mV from a holding potential of –70 mV. Right: Average IV plot obtained from 25 complex glial cells. Inset: Representative current responses from a complex glial cell evoked by the same voltage steps as applied to the passive cells. Data are the mean ± S.E.M.
(B) Morphology of passive and complex glial cells. Two Photon laser scanning microscopy image of a double recording of a passive (left) and a complex glial cell (right) in the MNTB of the same brainstem slice filled with Lucifer Yellow via the patch pipettes, taken few minutes after disrupting the patch. Note the morphological difference between the two cells, especially apparent in process length as well as thickness. The somata of principal neurons in contact with the glial cells are marked with asterisks. The somata of the neurons in contact with the passive glial cell (left) are partially covered with astrocytic processes (right asterisk). The image is an overlay of thirty consecutive confocal sections taken 1 µm apart. Scale bar 20 µm.

3.2. Cellular composition of the MNTB

To characterize the cellular composition of the MNTB, a series of immunohistochemical stainings was performed in GFAP-eGFP transgenic mice. As shown in Figure 14, most of the cells expressing eGFP are labelled for GFAP. However, some cells (asterisk in Figure 14B, C) showed no eGFP expression but were detected by the anti-GFAP antibody.

To distinguish other macro- and microglial cell types as well as neurons, stainings for NeuN, a neuronal marker (Mullen et al., 1992), MOG, the myelin oligodendroglial glycoprotein to visualize oligodendrocytes (Scolding et al., 1989) and Iba1, a microglial marker (Ito et al., 1998) as well as the proteoglykan NG2, a marker for oligodendrocyte precursor cells, presumably representing complex glial cells (Schools et al., 2003) were performed. The NeuN staining showed clear signals in the big somata of the MNTB brain region (Figure 14 F). An overlay with the eGFP expression could never be observed, confirming a non glial staining. The MOG antibody labeled the fiber bundels crossing the MNTB (Figure 14G), as expected for this highly myelinated fiber tract. The staining against Iba1, the microglial marker, showed the presence of microglial cells in the MNTB and no overlay with eGFP fluorescence. In contrast, some cells positive for NG2 showed a partial overlap with eGFP fluorescence (Figure 14D). This is in line with previous findings (Matthias et. al. 2003) in the hippocampus, namely low GFAP expression in some NG2 positive cells.

Taken together these results indicate that neurons as well as all expected macro- and microglial cell types are present in the MNTB and that they are evenly distributed in this brain region.

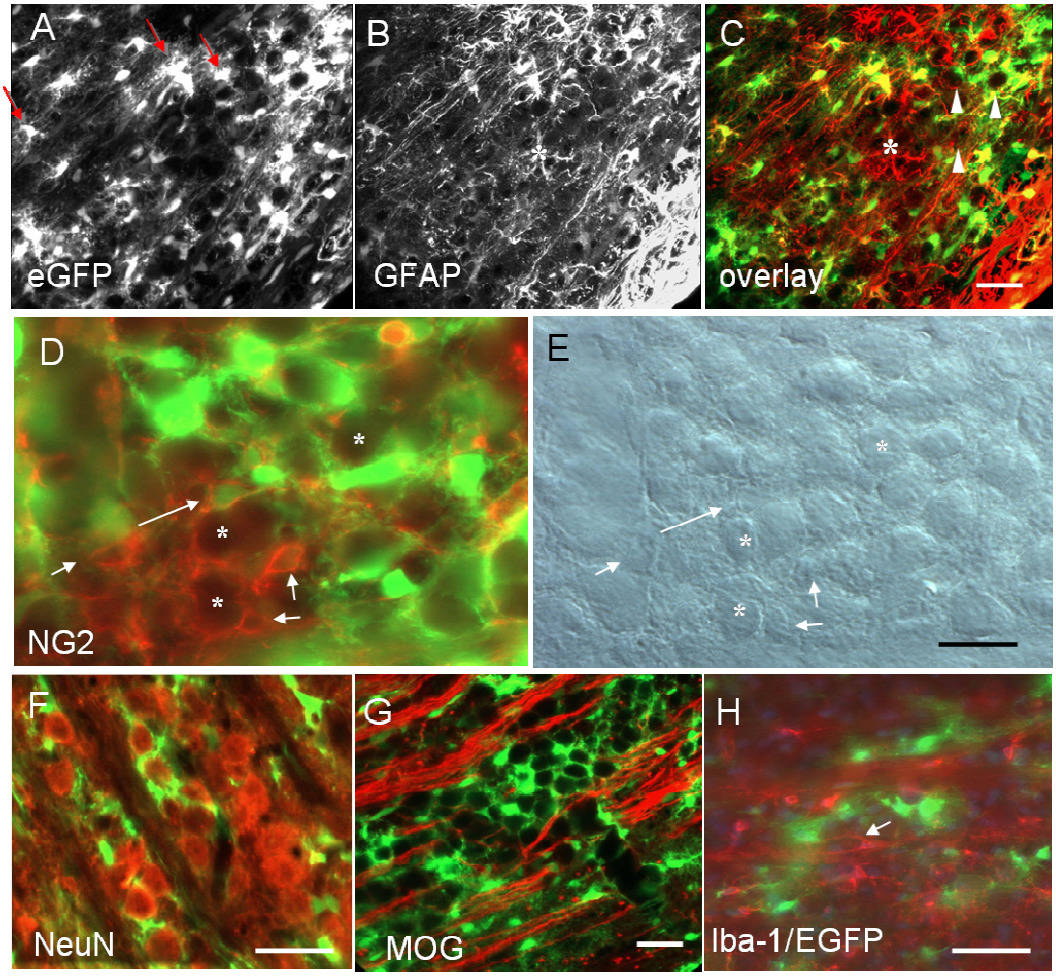

Figure 14. Cellular composition of the MNTB
(A) eGFP fluorescence from the MNTB area of a GFAP-eGFP transgenic mouse. Astrocytes are marked with arrows.
(B) Immunolabeling of the same area shown in (A) with GFAP antibodies. Secondary antibodies coupled with Alexa 594. Note the labeled cell in the middle of the picture (asterisk), showing no eGFP expression in (A).
(C) Overlay of (A) and (B) shows that most eGFP positive cells (green) are also labeled for GFAP (yellow), although there is no complete overlap (asterisk indicates a GFAP positive cell (red), which is negative for eGFP). Usually the eGFP signal is more pronounced in the cell body while GFAP labelling is more prominent in processes. The principal neurons appear as hollow dark circles (white arrowheads). Note that the amount of GFAP is much higher in close vicinity to the meninges (lower right corner). Scale bar, 20 µm, refers to (A), (B) and (C).
(D) Immunolabeling for NG2 in the MNTB of a GFAP-eGFP transgenic mouse. Some cells show NG2 expression but no overlap with eGFP expression (small arrows), whereas some cells show an overlap (long arrow). In this case the eGFP expression level is smaller as comapred to the other highly eGFP fluorescent cells, which show no overlay with the NG2 labeled cells. The principal neurons appear as hollow dark circles (asterisks).
(E) Same area as in (D) under Nomarski DIC optics. Note the difference in soma size of the cells labelled with arrows (glial cells) and asterisks (neurons). Scale bar 20 µm, refers to (D) and (E).
(F) Immunolabeling for NeuN in the MNTB of a GFAP-eGFP transgenic mouse. Only the biggest somata show NeuN staining, no overlay with eGFP expression is visible. Scale bar 50 µm.
(G) Immunolabeling for MOG in the MNTB of a GFAP-eGFP transgenic mouse. Note the parallel orientation of the stained myelinated fiber bundels crossing the MNTB area. No overlay with eGFP expression is visible. Scale bar 20 µm.
(H) Immunolabeling for Iba1 in the MNTB of a GFAP-eGFP transgenic mouse. An even distribution of stained cells with small somata (arrow) was observed. No overlay with eGFP expression is visible. Scale bar 20 µm.

3.3. Molecular identity of the glial cells

Labelling with GFAP antibodies revealed that most eGFP positive cells in the MNTB area were also labelled for GFAP (Figure 14A-C) identifying these cells as astrocytes.

However, to better study the morphology of a single passive cell in a GFAP-eGFP transgenic mouse brainstem slice, Alexa 594 was injected via the patch micropipette. Figure 15 (left) shows clear overlay of the eGFP and the Alexa signal. The current pattern identified this cell unequivocally as passive glial cell (data not shown), confirming the previous results. When recording non-fluorescent cells with a complex current pattern as shown in Figure 13A (right) and filling them with Alexa 594 in a GFAP-eGFP transgenic mouse, it became evident that no overlay with the eGFP-fluorescent signal could be observed (Figure 15, middle).

To better identify the complex glial cells and to verify them as the population stained positive for NG2 (Figure 14D) patched cells were identified and stained post-recording. After recording membrane currents from complex glial cells in wildtype NMRI mice and dialyzing the cells with a solution containing 0.1 % LY, slices were fixed and labelled with a monoclonal antiAN2 antibody, the mouse homologue for the rat NG2 proteoglycan. All cells showing the complex current pattern were positive for AN2 (n = 7; Figure 15 right). This is in line with previous findings in the hippocampus (Matthias et al., 2003), cerebellum (Lin et al., 2005) and corpus callosum (Kukley et al., 2007; Ziskin et al., 2007).

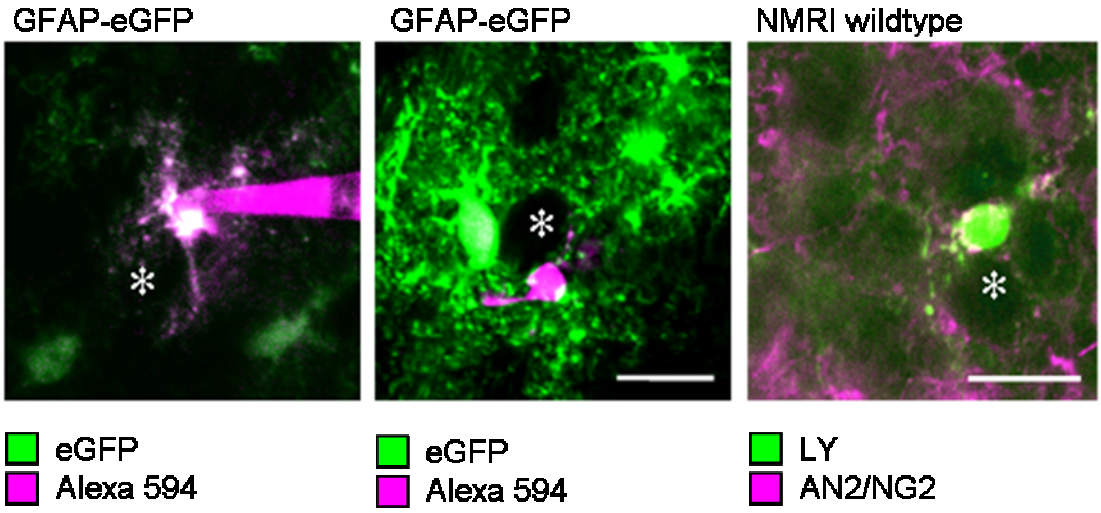

Figure 15. Identification of passive and complex glial cells
A passive and a complex glial cell (middle, right) were injected with Alexa 594 via the patch pipette and identified based on their membrane currents in the MNTB in an GFAP-eGFP transgenic mouse (left, middle) or NMRI wild-type mouse (right). The left and middle images are overlays of five consecutive confocal sections taken 1 µm apart, the right image is a single confocal section. The images are the overlays of eGFP (green) and Alexa594 emission (magenta, left, middle). In the passive cell a clear overlay is visible, whereas no overlay is visible in the complex glial cell. Complex glial cells express the AN2 (mouse homologue of the rat NG2) proteoglycan (right). The image is the overlay of lucifer yellow (green) and AN2 inmunostaining (Cy3, magenta). The complex glial cell was filled with lucifer yellow through the patch pipette, fixed postrecording and proceded for immunostaining with AN2 antibody (see methods). The asterisk indicates a principal neuron in close contact with the recorded cell. Scale bar, 20 µm, refers to all pictures.

3.4. Complex glial cells do not show dye-coupling while passive cells form a syncytium

To determine the extent of gap junctional coupling among passive and complex glial cells, LY and biocytin were injected into both cell types. Directly following the recording, LY fluorescence was determined by two-photon laser scanning microscopy (Figure 13B). Subsequently cells were fixed and further processed to determine the extent of dye spread via the biocytin labelling. In cells with a passive current profile a network of biocytin-positive cells was observed (Figure 16, left). On average, a cluster of 19.5 ± 5.9 cells occupied an area of about 0.017 ± 0.004 mm² (n = 9) indicating that the passive astrocytes are coupled via gap junctions. In contrast, dye-coupling was never observed in complex glial cells, where the dye remained solely within the intracellulary filled cell (n = 32, Figure 16, right). Only in one case dye-transfer into a single neighbouring cell was observed (data not

shown). The results in the mouse MNTB support the idea that passive cells are electrically coupled via gap junctions while complex cells are not (Wallraff et al., 2004; Schools et al., 2006).

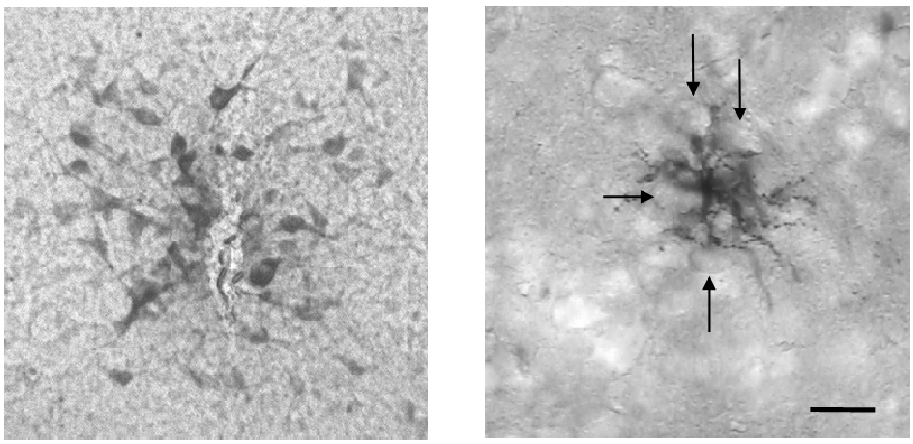

Figure 16. Gap junctional coupling
Section of the MNTB under phase contrast optics, showing biocytin injected glial cells labelled with DAB reaction. On the left, a passive cell was filled, and the dye spread to a number of neighboring cells. on the right, a complex cell was filled and the biocytin did not spread into neighbouring cells indicating no gap junctional coupling in the complex glial cell. Note also that the processes of the complex glial cell contact neuronal somata (arrows). Scale bar, 20 µm, refers to both pictures**.**

3.5. Passive glial cells express glutamate transporters and receptors, complex glial cells express only glutamate receptors

To test for the expression of functional AMPA/KAR, kainic acid (KA, 0.5 mM, 50 s) was applied to the bath while recording membrane currents at a holding potential of –70 mV. KA elicited small inward currents in passive (79 ± 20 pA; n = 9) and a significantly larger currents in complex cells (456 ± 132 pA; n = 8; Figure 17). Co-application of KA and the AMPA-KAR antagonist CNQX (50 µM) reduced the KA induced current to 20% (16 ± 4 pA; n = 5) and 6% (27 ± 7 pA; n = 7) in passive and complex cells, respectively (Figure 17).

To test for the presence of functional glutamate transporters, D-Aspartate (D-Asp, 0.5 mM, 50 s) was bath-applied. In passive cells, D-Asp elicited an inward current (132 ± 29 pA; n = 6) while no response was detected in complex cells (n = 6, Figure 17). Co-application of D-Asp and the non-selective blocker of excitatory amino acid

transporters DL-threo-β-benzyloxyaspartic acid (TBOA, 100 µM) reduced the D-Asp induced current to 58% (77 ± 22 pA; n = 6) in the passive cells (Figure 17). These results in the mouse MNTB as those in the mouse hippocampus (Matthias, et al., 2003), support the idea that passive cells express glutamate transporters while complex cells do not.

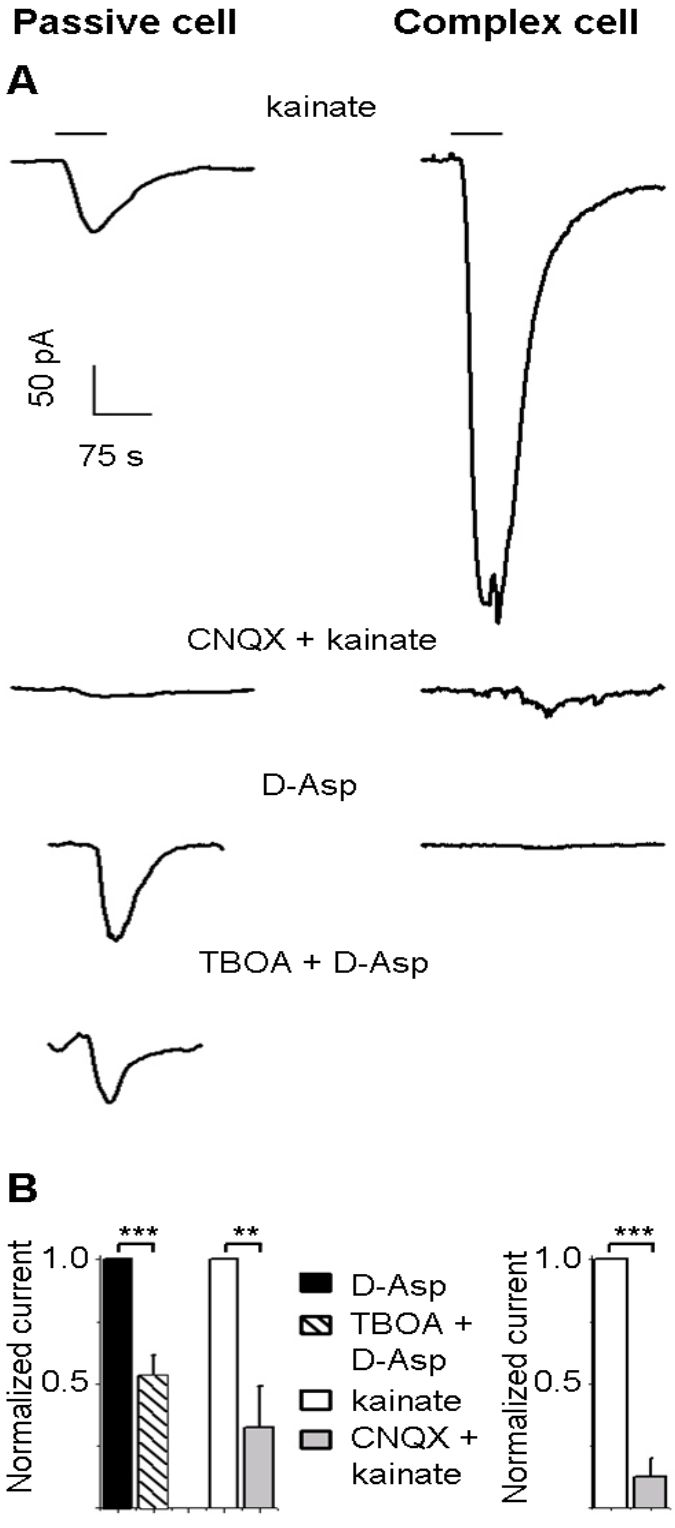

Figure 17. Response to KA and D-Asp
(A) Bath application of KA (0.5 mM) induced inward currents in both, passive (left) and complex cells (right). Note the difference in amplitude between passive and complex cells. The response was blocked when CNQX (50 µM) was pre-incubated and co-applied with KA (0.5 mM). D-Asp (0.5 mM) elicited an inward current in passive but not in complex cells. The response in the passive cell was reduced when TBOA (100 µM) was pre-incubated and co-applied with D-Asp (0.5 mM). The application bars on the top correspond to all applications.
(B) Summary of the effect of CNQX on kainate and of TBOA on D-Asp currents. The amplitudes of kainate and D-Asp currents were normalized showing the relative reduction induced by CNQX (passive n = 5; complex n = 7) and TBOA (passive n = 6). Data are the mean ± S.E.M. Asterisks represent significant differences, (**) $p < 0.01$ and (***) $p < 0.001$.

3.6. Complex glial cells express functional AMPA receptors

To further verify the presence of the AMPA subtype of glutamate receptors in complex glial cells kainic acid (KA) was applied, an agonist of both AMPAR and KAR. Bath application of KA (0.5 mM, 50 s) elicited a response of 347 ± 231 pA in n = 5 cells recorded (Figure 18). This response was increased to 180 % of the control (627 ± 129 pA; n = 5) upon coapplication of cyclothiazide (CTZ), a blocker of AMPAR desenitization (Figure 18). After preincubation of the slice in 100 µM GIKY 52466, a selective antagonist of the AMPAR, the KA response was decreased to 26 % of the control (90 ± 58 pA; n = 5; Figure 18). This indicates that the complex glial cell express the AMPA subtype of ionotropic glutamate receptors as previously shown in the hippocampus (Matthias et al., 2003).

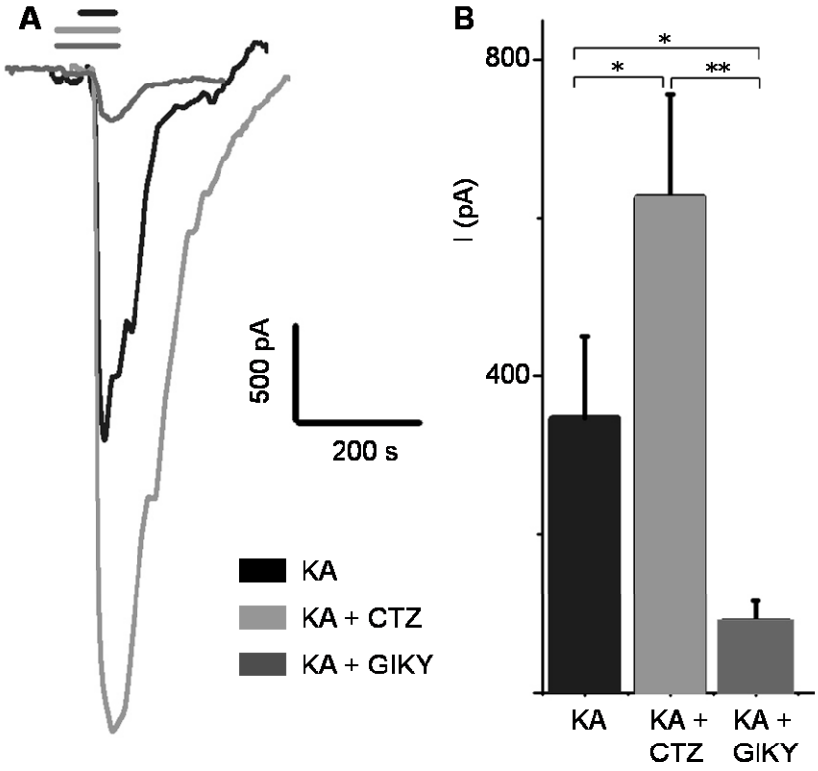

Figure 18. Responses to KA in complex glial cells are AMPA-receptor-mediated
(A) Bath application of KA (0.5 mM) produced an inward current that was potentiated after pre-incubation with CTZ (100 µM). The response was blocked when GIKY 52466 (100 µM) was pre-incubated and co-applied with KA (0.5 mM).
(B) Summary of the effect of CTZ and GIKY 52466 on KA elicited currents (n = 5). Data are the mean ± S.E.M. Asterisks represent significant differences, (*) $p < 0.05$ and (**) $p < 0.01$.

3.7. GFAP-eGFP positive astrocytes, the passive cells, contact pre- and postsynaptic elements

The GFAP-eGFP transgenic mice were also used to identify astrocytic compartments at the electron microscopic (EM) level using antibodies against eGFP (Nolte et al., 2001; Jabs et al., 2005). All electron microscopy studies were performed in collaboration with Dr. Tatjyana Pivneva from the Bogomoletz Institute of Physiology in Kiev, Ukraine. Pre-embedding immunohistochemistry for eGFP was carried out and ultrathin sections (10 µm) were inspected for labelled astrocytic processes at the ultrastructural level. Labelled processes were frequently found in close proximity to the CoH terminal and were found to directly contact the pre- and postsynaptic membrane (Figure 19A). Most importantly, fine astrocytic processes were located at the apposition zone of the finger-like stalks of the CoH and the principal neurons (Figure 19B, D). Furthermore, fine astrocytic processes were also frequently observed in close vicinity to active zones, the sites of transmitter release and to puncta adherentia, desmosome-like structures which connect and stabilize the pre- and postsynaptic membrane (Figure 19C; see also (Sätzler et al., 2002; Hoffpauir et al., 2006; Rollenhagen and Lübke, 2006)). However, no synaptic-like structures between the neuronal elements and the eGFP-labeled processes were observed.

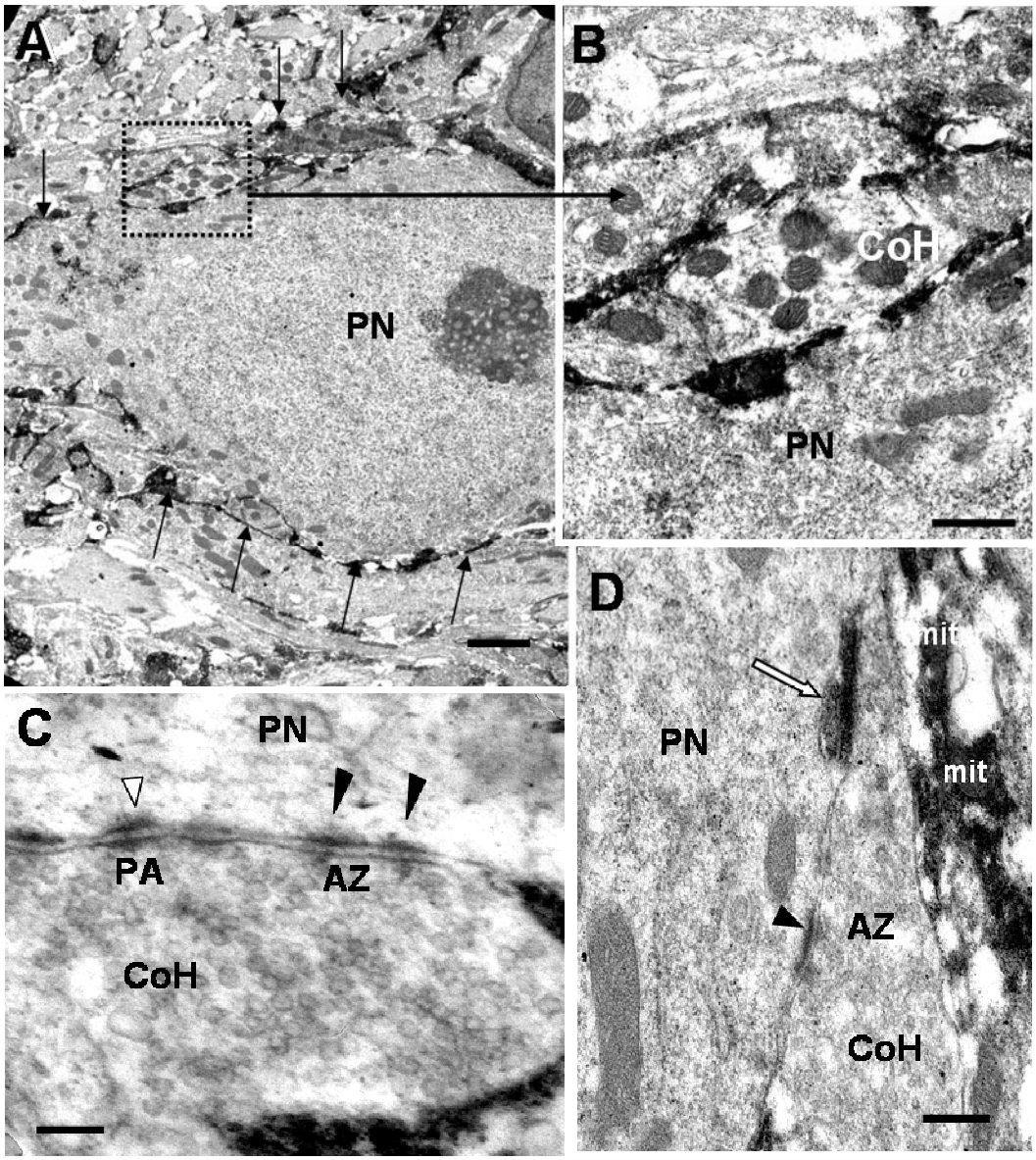

Figure 19. Immunhistological and ultrastructural analysis of eGFP-positive passive astrocytes in the MNTB area

(A-D) Immunoelectronmicroscopic analysis of eGFP positive astrocytes: slices were immunolabeled by anti-GFP-antibodies and visualized by HRP-reaction.

(A) Overview of a MNTB principal neuron (PN) surrounded by black processes of astrocytes (arrows).

(B) Magnified image of outlined area in (A). Astrocytes extend their fine processes between the fingers of the calyx of Held (CoH) and the principal neuron (PN).

(C, D) Further examples that show how astrocytic processes interdigitate between the fingers of the calyx and principal neuron (PN). Black arrowheads indicate active zones (AZ) between a principal neuron and a CoH. Puncta adherentia (PA; white arrowhead) are shown in (C). The astrocytic compartments in close vicinity to the CoH contain mitochondria (mit, in (D). Note the close apposition of the labeled glial process (white arrow) to the active zone. Scale bars, (A) = 2 µm; (B, C and D) = 0.2 µm.

3.8. Complex glial cells form synapse-like contacts with the CoH

The morphology of complex glial cells was studied after biocytin injection and processing for subsequent electron microscopic analysis (Figure 20). Consecutive ultrathin sections of biocytin-labelled complex glial cells (n = 7) were examined. Somata and fine processes of labelled complex glial cells were found in close proximity to the CoH terminal (Figure 20A, C). Processes of complex glial cells were frequently observed to contact both, the presynaptic terminal and the postsynaptic principal neuron (Figure 20A, C). Presynaptic elements were sometimes ensheated by fine glial processes (Figure 20B). In contrast to passive cells (data not shown), synapse-like contact sites between processes of the complex glial cell and the CoH were detected (Figure 20B, D, E). In addition, an accumulation of synaptic vesicles was frequently observed at the glial contact site. In some of the presynaptic structures so-called docked vesicles were visible at the presynaptic densities (Figure 20D, E). A cleft-like structure containing electron opaque material could also be detected. Due to the strong labelling of the glial cell by biocytin, it was, however, not possible to identify a postsynaptic density. The length of synaptic-like junctions was 0.05 - 0.3 µm, but varied substantially from synapse to synapse as described for the cerebellar climbing fiber innervation of NG2–expressing glia (Lin et al., 2005). Taken together, these findings strongly imply that the complex glial cells establish synapse-like contacts with the presynapse, the CoH. This type of synaptic contacts was never observed between elements of complex glial cells and the postsynapse, the principal neurons in the MNTB".

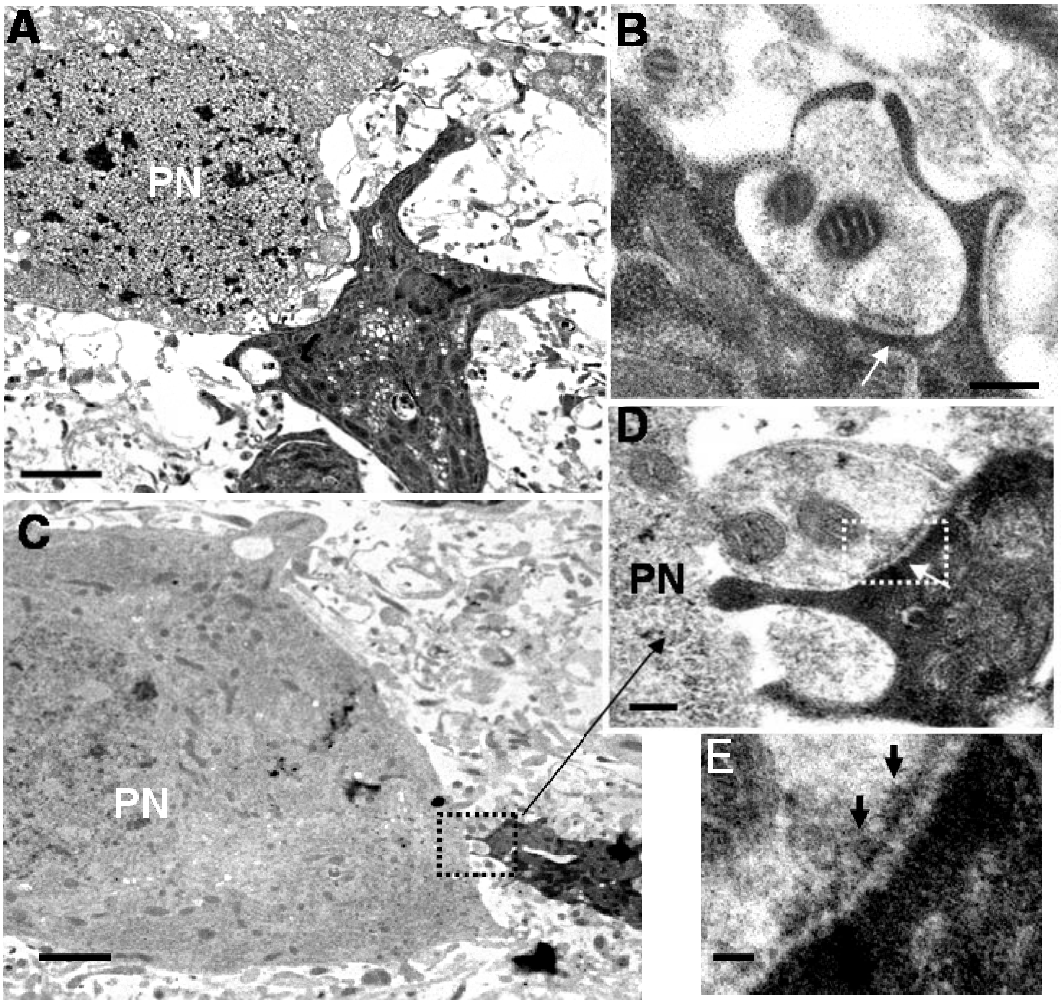

Figure 20. Ultrastructural evidence for synaptic junctions between CoH and complex glial cells
(A) Complex glial cell (dark profile) in close vicinity to a principal neuron (PN)
(B) Example of a synaptic-like junction (arrow) between a finger of a CoH and a process of a biocytin-labelled complex glial cell as shown in (A).
(C) A labelled process of a complex glial cell is in contact with the CoH.
(D) Higher magnification of the area delineated by dashed rectangles in (C) shows a synaptic junction (arrow). Presynaptic areas contain small clear vesicles.
(E) Consecutive section at higher magnification; vesicles appear as docked to the pre-synaptic membrane (arrows). Note a cleft-like structure contains electron opaque material. (C, D and E) were obtained from a different complex glial cell. Scale bars, (A and C) = 2 µm. (B and D) = 0.2 µm, (E) = 0.1 µm.

3.9. Stimulation of the midline fibers triggers synaptic-like currents in complex glial cells

To test whether the synapse-like structures observed at the ultrastructural level have a functional correlate, membrane currents in complex glial cells and neighbouring principal neurons were recorded during electrical stimulation of the

midline fibers (pulse legth 100 µs, 1, 10 and 100 Hz, 0.1 – 1 mA, see also methods, figure 10). As described above, the cells were identified based on their current profile and morphology (Figure 13A, B). At 1 and 10 Hz stimulation frequency, inward currents were evoked which averaged to 20.8 ± 4.0 pA in the complex glial cells (range 10.4 – 155.0 pA, n = 14; Figure 21A). The response of principal neurons was significantly larger when using the same stimulation protocol (2.2 ± 1.4 nA, range 1.3 – 6.3 nA; decay time constant = 5.4 ± 4.5 ms; n = 5; Figure 21D). The decay time constant was faster in glial cells (1.2 ± 1.0 ms; n = 14). Since the CoH synapse is glutamatergic, CNQX (20 µM) + APV (50 µM), blockers of the AMPA-KARs and NMDARs, respectively, were bath-applied to prove the glutamatergic origin of the current response. The current response of the glial cells was reversibly blocked (n = 7; Figure 21B, C). The response was also completely abolished when TTX (1 µM) was added to the bath solution (n = 7; Figure 21B, C).

At 10 and 100 Hz stimulation frequency, the current responses of the complex glial cells showed a pronounced failure rate of 39 ± 18 and 52 ± 22 %, respectively (Figure 22). This was in contrast to neuronal responses which are known for their ability to cope with high stimulation frequencies up to several hundred Hz without showing failures ((Wu and Kelly, 1993) data not shown).

Stimulation of the afferent fibers crossing the midline of the brainstem slice (midline stimulation) with a train of stimuli in aCSF containing 2 mM Ca^{2+} reveals a form of postsynaptic depression in the principal neuron of the MNTB (Schneggenburger et al., 2002). The mechanisms are mainly considered to be presynaptic and include a change in the action potential wave form, inactivation of presynaptic calcium currents and vesicle pool depletion (for review see (Schneggenburger et al., 2002)). When afferent fibers were stimulated with 20 pulses at a frequency of 10 Hz, a depression of ePSCs could be observed in complex glial cells. It was, however, not possible to reliably analyse the depression at higher stimulation frequencies, due to the above mentioned high failure rate at this stimulation frequencies. At 10 Hz, the depression amounted 31.8 % of the amplitude of the last response (20^{th} stimulus), when compared to the first.

The results clearly indicate that the complex glial cells in the MNTB receive synaptic glutamatergic input from the calyx of Held.

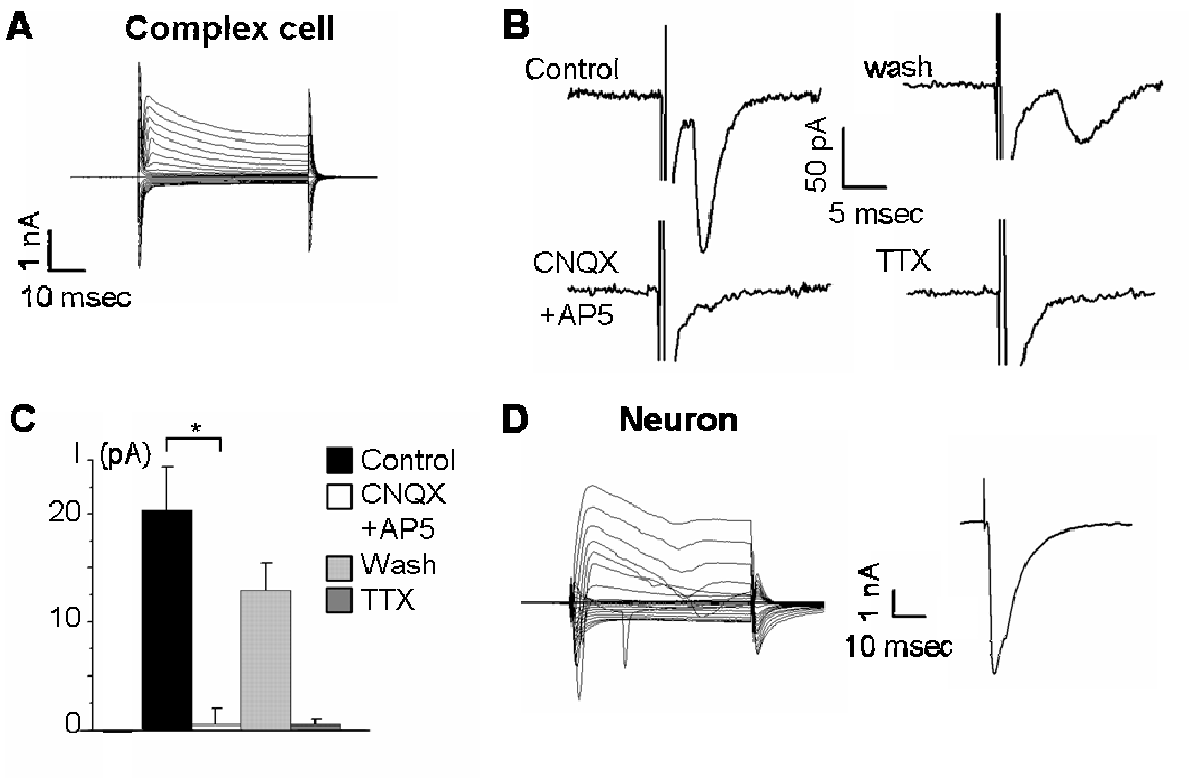

Figure 21. Evoked postsynaptic currents in complex glial cells and neurons
(A) Current profile of a complex glial cell, showing representative current responses evoked by voltage steps. Membrane currents were evoked by 50 ms voltage steps ranging from –160 to +40 mV from a holding potential of –70 mV.
(B) Example traces showing midline stimulation-induced responses of a complex glial cell (stimulus intensity 100 µA). Top left row shows control conditions. Bottom left row: application of CNQX (20 µM) and AP5 (50 µM) to block AMPA-KAR and NMDAR, respectively, reversibely inhibited the postsynaptic current. Top right row: After ten minutes of wash the postsynaptic current partially recovered in the complex glial cell. Bottom right row: TTX (1 µM) abolished the current response.
(C) Summary of current responses to midline stimulation corresponding to the 4 experiments shown in B (n = 7). Data are the mean ± S.E.M. Asterisk represents significant difference, (*) $p < 0.05$.
(D) Left: Current response from a principal neuron evoked by step voltages (50 ms, 10 mV increment) from –160 to +40 mV from a holding potential of –70 mV. Right: Current response of the principal neuron shown on the left to midline stimulation with same parameters as applied to glial cells (100 µA).

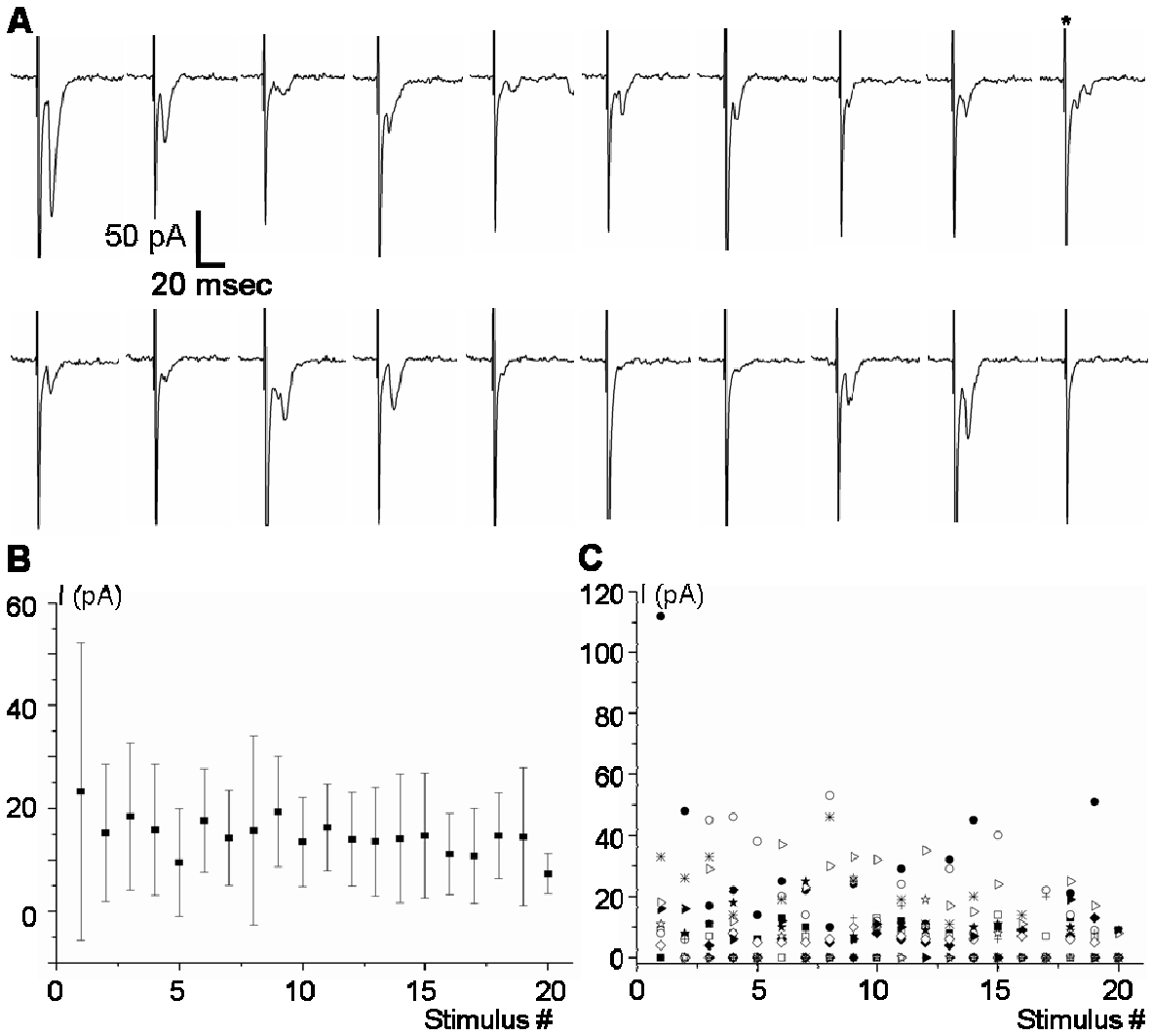

Figure 22. Failure rate and depression of evoked postsynaptic currents recorded from a complex glial cell
(A) Afferent fibers crossing the midline of the brainstem slice were stimulated with intensities between 100 µA and 1 mA and evoked postsynaptic responses were recorded from comlex glial cells in the MNTB. The vertical lines are stimulation artefacts (example in the top row, right, marked with an asterisk). Note the difference in ePSC amplitude and the failures of transmission.
(B) Depression of ePSC amplitudes in complex glial cells. After an initial response of 23.3 ± 28.9 pA the amplitude steadily declines to 31.8 % of the initial value (7.4 ± 3.9 pA, n = 14).
(C) Failure rate in complex glial cells upon 10 Hz midline stimulation. Every symbol in the graph refers to one recording. Symbols at 0 pA refer to failures of transmission (n = 14).

3.10. Repetitive midline stimulation triggers a slow inward current in the passive cells

Midline stimulation triggered only small currents (12 ± 6 pA; n = 16) in passive cells, with a fast decay time (0.72 ms ± 0.70 ms; n = 16) independent from the stimulation frequency (Figure 23B). These responses were blocked by TTX (1 µM) (Figure 23B

and C), but were neither affected by CNQX (20 µM) + APV (50 µM), blockers of the AMPA-KAR and NMDAR, respectively (Figure 23B and C), nor by antagonists of GABA or glycine receptors and glutamate transporters (data not shown). These currents are assumed to be due to the fiber volley similar as described in the cerebellum (Bellamy and Ogden, 2005).

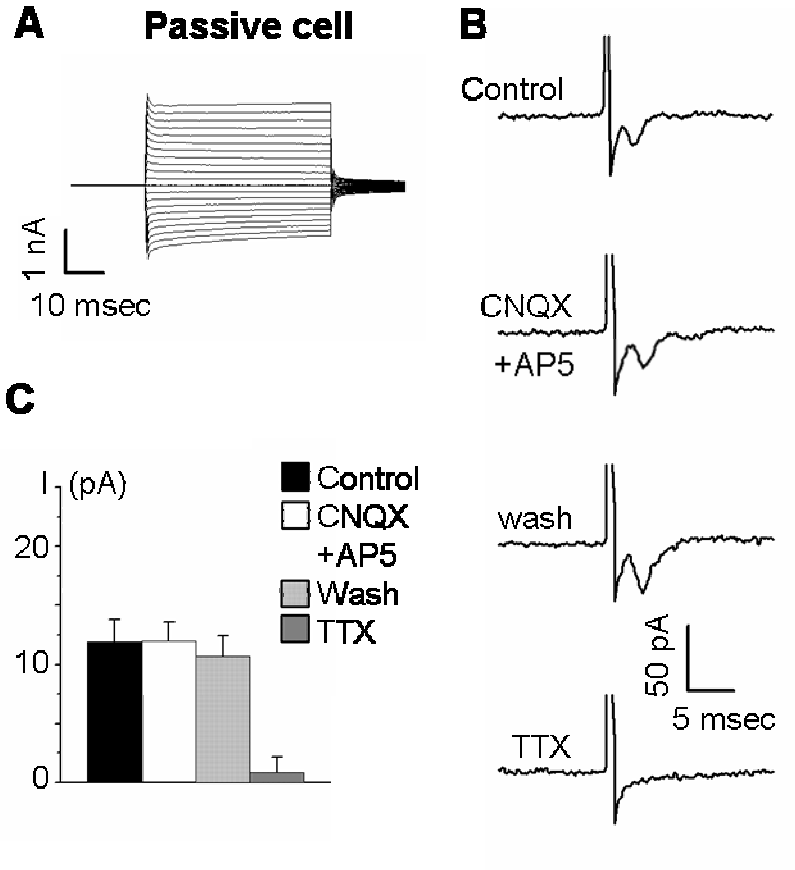

Figure 23. Midline stimulation does not elicit evoked postsynaptic currents in passive glial cells
(A) Current profile of a passive glial cell, showing representative current responses evoked by voltage steps. Membrane currents were evoked by 50 ms voltage steps ranging from –160 to +40 mV from a holding potential of –70 mV.
(B) Example traces showing midline stimulation-induced fiber volleys recorded from a passive glial cell (stimulus intensity 100 µA). Top row shows control conditions. Second row: application of CNQX (20 µM) and AP5 (50 µM) to block AMPA-KAR and NMDAR, respectively, does not influence the response. Third row: After ten minutes of wash the response is still unchanged. Bottom row: TTX (1 µM) abolished the current response.
(C) Summary of current responses to midline stimulation corresponding to the 4 experiments shown in B (n = 7). Data are the mean ± S.E.M.

However, when repetitive stimulation was applied a slow inward current was observed. With a 1 Hz stimulation, this current slowly increased during the stimulation time to 14.6 ± 10.6 pA and decayed within 6.2 ± 2.7 s after the last

stimulus (Figure 24A). With a 10 Hz stimulation, the current further increased to 41.4 ± 39.1 pA and decayed with a time constant of 10.8 ± 7.0 s, while with a 100 Hz stimulation it increased to 51.9 ± 53.7 pA and decayed with a time constant of 11.8 ± 6.1 ms (Figure 24A). The slow inward current was not affected by CNQX (20 µM), but blocked by TTX (1 µM, n = 11, Figure 25B). Application of TBOA (200 µM) increased the slow inward current being most prominent at 100 Hz (112.1 ± 31.7 pA; Figure 24B and C). This increase was blocked by CNQX (20 µM) to 36.7 ± 6.7 pA (Figure 24B and C). The CNQX-sensitive current had a decay time of 20.22 ± 7.11 s thus, slower than the inward current recorded in the absence of TBOA (Figure 24C). Under CNQX blockade the decay time of the slow inward current under TBOA (200 µM) was 10.3 ± 6.1 s.

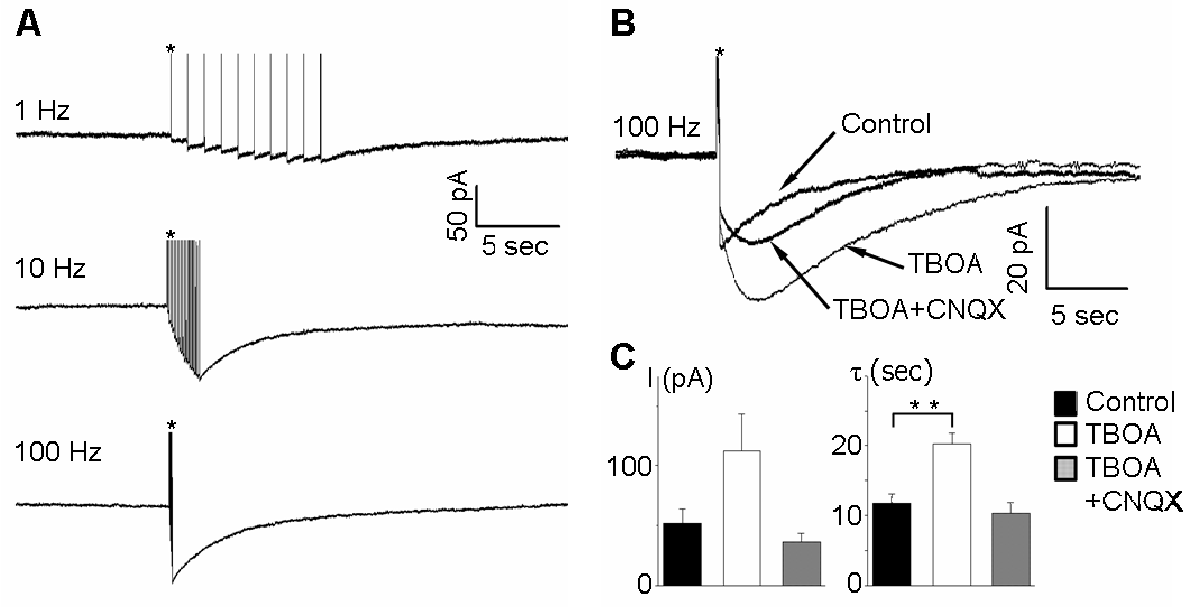

Figure 24. Tetanic stimulation reveals slow inward currents in the passive cells
(A) Currents recorded from passive glial cells in response to midline stimulation with ten pulses at 1 Hz (top), 20 pulses at 10 Hz (middle) and 20 pulses at 100 Hz (bottom). Stimulation artefacts are marked with asterisks.
(B) Currents recorded in response to midline stimulation with 20 pulses at 100 Hz. Overlay of three consecutive records from the same cell. Inhibition of glutamate transporters with TBOA (200 µM) results in an increase of the current as compared to control. Application of TBOA (200 µM) and CNQX (20 µM) results in a reduction of the current to almost control value. Stimulation artefact is marked with an asterisk.
(C) Summary of the current amplitudes and the decay times of the current induced by 20 pulses at 100 Hz under control conditions, under TBOA and under TBOA together with CNQX (n = 21). Data are the mean ± S.E.M. Asterisks represent significant difference, (**) p = 0,002.

In contrast to the situation in passive cells, repetitive stimulation under control conditions or glutamate transporter blockade did not trigger slow inward currents in complex cells (n = 14, Figure 25A) The only obvious effect under glutamate transporter blockade was that the complex cell sometimes showed some sPSCs after the last stimulation pulse, presumably due to some residuing glutamate left in the synaptic zone. A significant effect of the TBOA application on amplitude or kinetics of complex cell excitatory PSCs could not be observed (data not shown). This is line with the findings from Renden and coworkers (Renden et al., 2005), showing no effect of transporter blockage on amplitude and kinetics of evoked EPSCs when recorded from MNTB principal neurons, but describing the function of the glutamate transporters in the MNTB as a barrier for regulating the activity of calyceal metabotropic glutamate receptors.

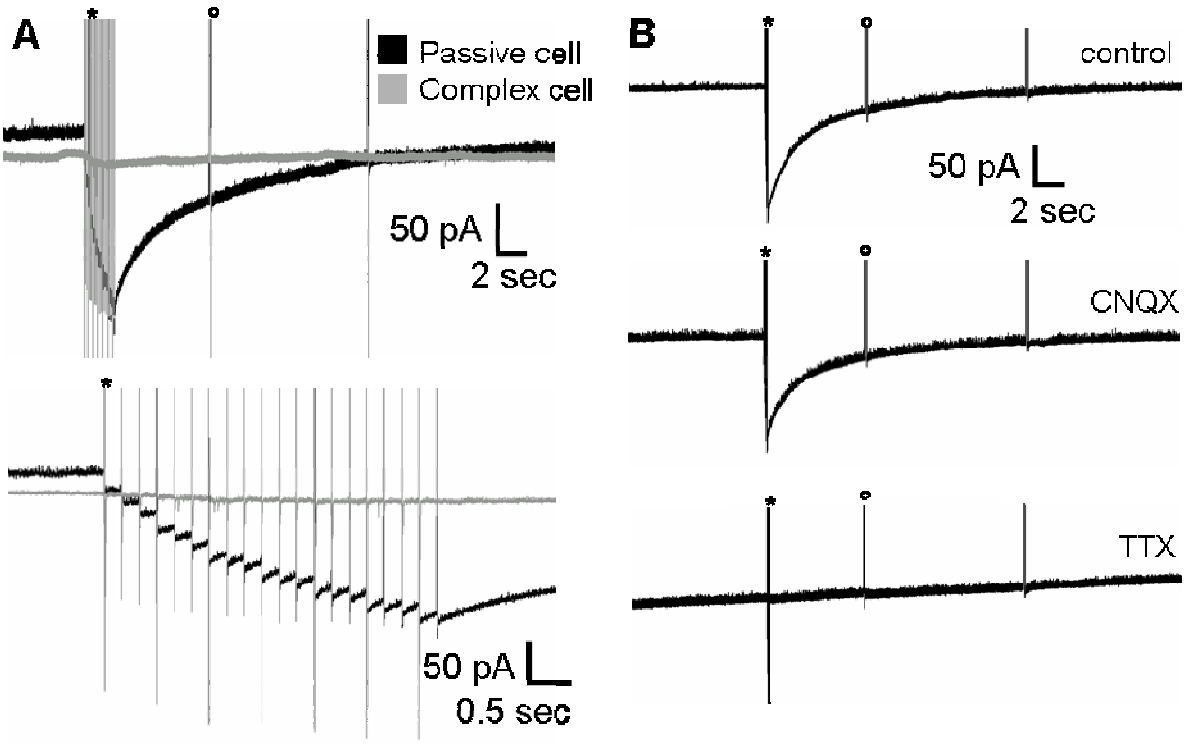

Figure 25. Slow inward current is visible in passive but not complex glial cells, insensitive to CNQX but dependent on neuronal activity
(A) Upper panel: double recording of a complex (gray trace) and a passive glial cell (black trace) during tetanic stimulation of the midline (10 Hz, 100 µA) under control conditions. The passive glial cell shows a slow inward current of prominent amplitude, while the complex glial cell shows ePSCs but no slow inward current. The vertical lines that accompany the slow inward current are stimulation artefacts (asterisks). The vertical lines that accompany the recovery are current responses to 10 mV pulses applied via the patch pipette (example marked with a small circle) to track eventual changes of the input resistance R_s (see methods). Lower panel: magnification of the same recording as in the upper panel. Note the step-like summation of the slow inward current in the passive glial cell. The vertical lines are stimulation artefacts.
(B) Upper panel: representative example trace of a slow inward current recorded from passive glial cells at 100 Hz midline stimulation under control conditions. The current has an amplitude of 134 pA.
Middle panel: preincubation of the slice for 2 min in 20 µM CNQX had no significant impact on the slow inward current. The amplitude is 128 pA. The vertical lines that accompany the slow inward current are stimulation artefacts (asterisks). The vertical lines that accompany the recovery are current responses to 10 mV pulses applied via the patch pipette (examples marked with small circles) to track eventual changes of the input resistance R_s (see methods).
Lower panel: preincubation of the slice for 2 min in 1 µM TTX abolishes the slow inward current.

3.11. Midline stimulation triggers a Ca^{2+} response in astrocytes

To test whether passive glial cells would sense the activity of the calyx, and since the passive glial cells did not show postsynaptic current responses to midline stimulation, the Ca^{2+} activity in passive glial cells was recorded while the midline was stimulated (see methods, Figure 10). The slices were loaded with 10 µM Fluo 4-AM,

which is preferentially taken up by passive glial cells (Dallwig and Deitmer, 2002). A stimulation with 40 pulses at 10 Hz triggered a $[Ca^{2+}]_i$ increase in a subset of cells within the visual field (average 1.35 ± 0.30 F/F_0, n = 5 slices, Figure 26A). A second stimulation triggered a similar response (n = 5). These responses were blocked (average 1.05 ± 0.16 F/F_0, n = 5, Figure 26B) when neuronal activity was blocked by a 2 min pre-incubation of the slice with 1 µM tetrodotoxin in Ca^{2+} free conditions to block both action potential propagation and transmitter release. These results indicate that Ca^{2+} responses in passive glial cells are mediated by the activity of neurons.

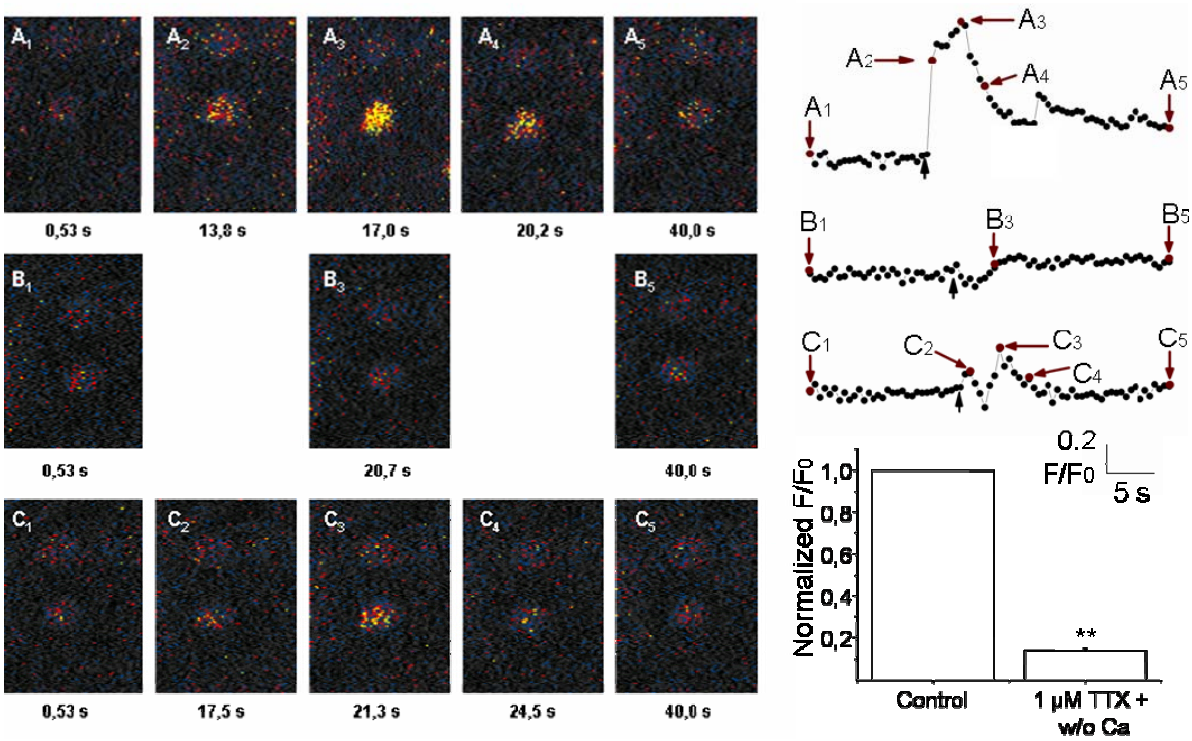

Figure 26. Stimulation of the midline evokes calcium responses in the MNTB astrocytes
Calcium transients in astrocytes recorded in the MNTB. Cells were bulk loaded with Fluo-4 to show $[Ca^{2+}]_i$ increases (F/F_0). Black arrows (right) indicate the stimulation period.
(A) Under control conditions the astrocytes shows a response of 1.35 ± 0.30 F/F_0 (n = 5). The corresponding Ca^{2+}-trace is shown on the right. A_1-A_5 show Ca^{2+}-increases recorded at time points indicated with dark red filled circles and arrows labelled with the letters and numbers (right) referring to the pictures on the left.
(B) 1 µm TTX and zero Ca^{2+} in the aCSF abolish the Ca^{2+} increase, indicating the neuronal origin of the evoked Ca^{2+} response (n = 5).
(C) After ten minutes of wash with normal aCSF the Ca^{2+}-signal partially recovers to 1.11 F/F_0. ** indicates significant difference from control, $p < 0.01$, n = 5.

Since the calyx of Held is a glutamatergic synapse, 50 µM CNQX was bath applied to block AMPA/KAR and to prove the origin of the midline stimulus evoked Ca^{2+} response. After a preincubation of 2 min the same stimulation protocoll was applied as mentioned before. CNQX reduced the peak of the control response (1.54 ± 0.38 F/F_0, n = 19, Figure 27A) to 77 % of control values (1.19 ± 0.24 F/F_0, n = 19, Figure 27B). Ten minutes of wash with aCSF recovered the respone to 95 % (1.47 ± 0.18 F/F_0, n = 19, Figure 27C).

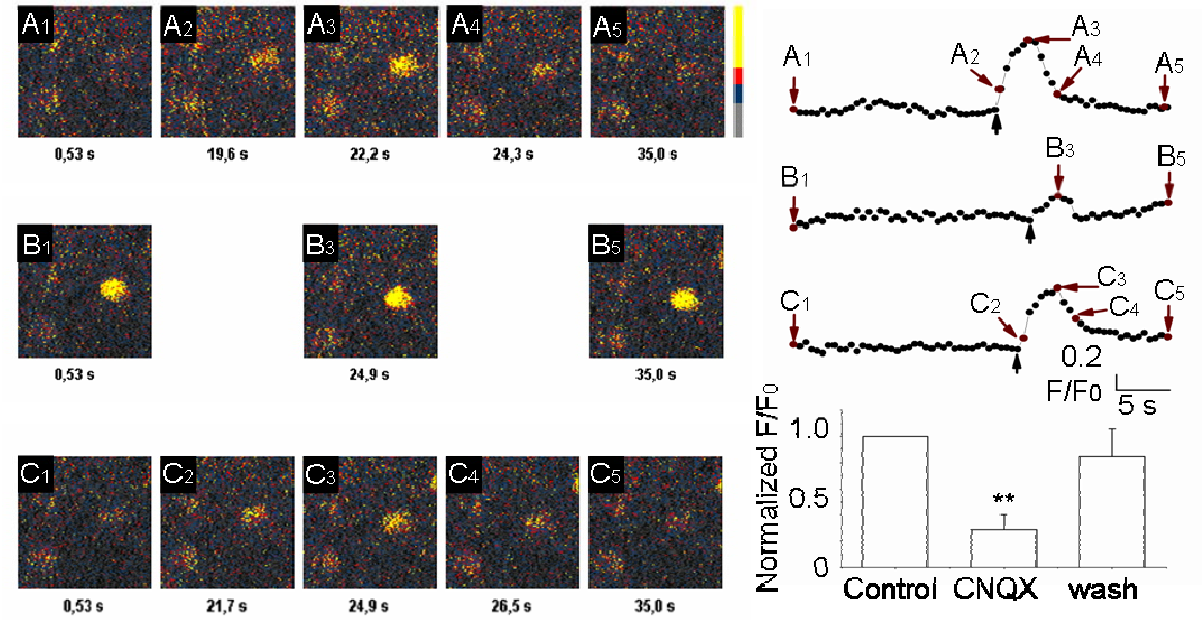

Figure 27. Midline stimualtion evoked calcium responses in MNTB astrocytes are partially mediated by glutamate
Calcium trace recorded in the MNTB. Cells were bulk loaded with Fluo-4 to show $[Ca^{2+}]_i$ increases (dF/F_0). Black arrows indicates the stimulation period (right).
(A) Under control conditions the astrocyte shows a peak response of 1.54 F/F_0. The recorded Ca^{2+}-trace is shown on the right side. A_1-A_5 show Ca^{2+}-increases recorded at timepoints indicated with dark red filled circles and arrows labelled with the letters and number referring to the pictures on the left.
(B) 10 µm CNQX in the aCSF reduce the Ca^{2+} increase to 77 % (1.19 F/F_0), indicating calyceal origin.
(C) After ten minutes of wash with normal aCSF the Ca^{2+}-signal recovers to 95 % (1.47 F/F_0). ** indicates sigificant difference from control, $p < 0.01$. n=13

In order to further investigate the origin of the response another set of experiments was performed to test the influence of inhibitory input to the MNTB onto the Ca^{2+} responses of astrocytes. In order to block GABAergic and glycinergic transmission 100 µM gabazine and 5 µM strychnine were applied 2 minutes before and during the stimulation. The Ca^{2+} response was reduced to 90 % of control values (n = 5, data not shown).

The results, taken together, indicate that the astrocytes of the MNTB do show Ca^{2+} responses to afferent fiber stimulation. The responses are to three quarters mediated by glutamate, when the peak of response was normalized to control, which further indicates a calyceal origin. On the other hand 10 % of the response is mediated via inhibtory transmitters, indicating an additional, though weak, inhibitory input.

3.12. Spontaneous post-synaptic currents can be recorded in complex glial cells

Spontaneous post-synaptic currents (sPSCs) are known to be rare in principal neurons of the MNTB (Barnes-Davies and Forsythe, 1995) and the basal frequency was reported to be as low as 0.05 Hz (Kimura et al., 2003). In the preparation used in this study, a frequency of 0.16 Hz (± 0.11 Hz; n = 20) could be observed in principal neurons (Figure 28A). To test for the presence of spontaneous activity in complex glial cells a series of experiments was performed recording spontaneous activity. In complex glial cells, spontaneous currents were also observed with a low frequency (0.11 ± 0.11 Hz; Figure 28A; n = 28). The spontaneous responses had a mean amplitude of 19 (± 12 pA; n = 616 events in 20 cells) in the neurons and 9.3 (± 4.4 pA; n = 308 events in 28 cells) in the complex glial cells (Figure 28C, 29). Spontaneous currents in the passive glial cells of the MNTB could never be observed, confirming the results achieved with electron microscopy that passive glial cells do not form synaptic contacts with the CoH (n = 20, > 3000 s observation time). Since the basal activity was too low, especially in the complex glial cell, to be reliably analysed, experiments were performed under 4-aminopyridine (100 µM, 4-AP). This K^+ channel blocker enhances neurotransmitter release by depolarising neurons and can be used to enhance spontaneous transmitter release (Flores-Hernandez et al., 1994).

To test for the impact of 4-AP on membrane currents in complex glial cells and the postsynaptic neuron, the membrane was clamped with 50 ms voltage pulses from –

160 to +70 mV in 10 mV steps (see methods, Figure 11). 4-AP (100 µM) reduced the peak current at +70 mV in complex glial cells by 32 %, from 2.18 ± 0.57 to 1.48 ± 0.48 nA (n = 10; data not shown) and neurons by 21 %, from 2.57 ± 0.91 to 2.03 ± 0.81 nA (n = 11; data not shown).

Indeed, application of 4-AP increased the frequency of spontaneous currents to 5.14 Hz (± 4.96 Hz; n = 15) in neurons and to 1.37 (± 2.21 Hz; n = 26) in complex glial cells (Figure 28A). 4-AP also increased the mean amplitude of the sPSCs to 53.4 ± 56.9 pA (n = 8434 events in 15 cells) and 12.1 ± 6.1 pA (n = 2756 events in 25 cells) in the neuron and complex glial cell, respectively (Figure 28). The amplitude histogram of the spontaneous currents showed a peak of 9 pA and 25 pA for glial cells and neurons, respectively (pooled data from 16 neurons and 26 complex cells, Figure 28). From Figure 28, it is evident that the majority of events in glial cells are within the amplitude range of about 10 pA while in neurons a significant number of events with higher amplitudes occurred (see also Figure 31). TTX (1 µM) almost completely abolished the spontaneous events stimulated by 4-AP in the complex glial cells (from 1.38 ± 1.10 Hz to 0.01 ± 0.01 Hz; n = 5), indicating that they were due to action potential firing in the presynaptic neuron.

The results, taken together, indicate clearly that complex glial cells in the MNTB, as principal neurons, receive action potential mediated spontaneous activity mediated by the CoH.

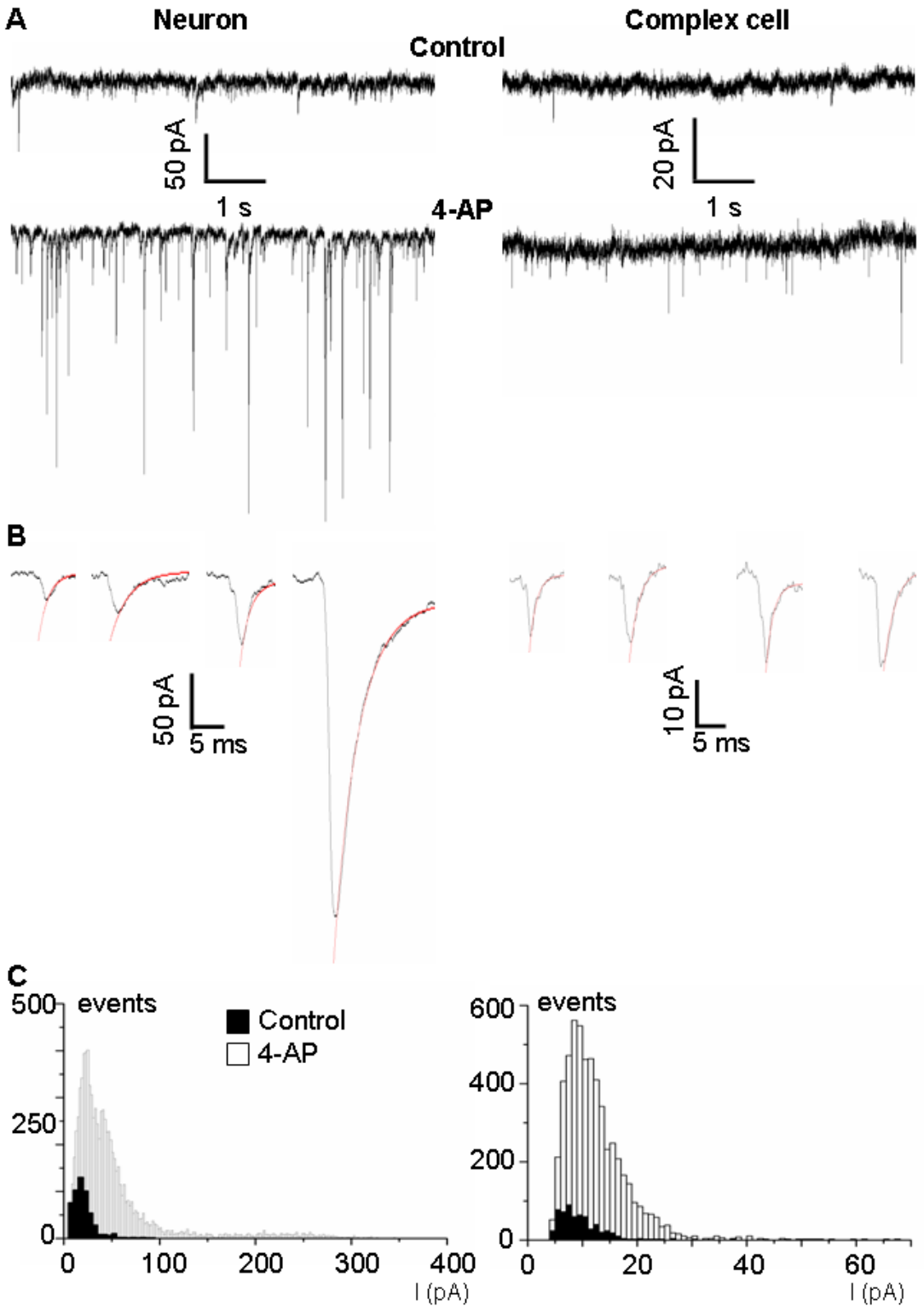

Figure 28. Spontaneous postsynaptic currents in complex glial cells and principal neurons of the MNTB

(A) Top row: Spontaneous postsynaptic currents (sPSCs) recorded from a neuron and a complex glial cell under control conditions. Middle row: Bath application of 4-AP (100 µM) increased the sPSCs frequency in both cells. For neuronal recordings, we added strychnine (1 µM), gabazine (10 µM), D-APV (50 µM). Note the amplitude difference in neuron and complex glial cell.
(B) Single spontaneous events shown with higher time resolution fitted to a monoexponential.
(C) Histograms of the amplitudes of sPSCs recorded under control conditions (black columns) or 4-AP (white columns) of 16 neurons and 26 complex cells, respectively.

3.13. Spontaneous post-synaptic currents in complex glial cells are mediated by AMPA receptors

In principal neurons, 46 % of the activity remained when CNQX was applied and spontaneous activity were recorded and the internal solution A (see methods) was used (n = 5), indicating that neurons receive inputs additional to the CoH. Therefore, a cocktail of antagonists (strychnine (1 µM), gabazine (10 µM), D-APV (50 µM) and MK-801 (10 µM)) to block glycinergic, GABAergic and NMDAR-mediated glutamatergic activity, respectively, were used in combination with internal solution B (see methods) to isolate AMPA-KAR mediated currents and to compare them with those recorded in complex glial cells (data not shown). The decay time of sPSCs in neurons under these conditions was 3.0 ± 1.66 ms (n = 237 events), thus, similar to the ones obtained in the complex glial cells (1.88 ± 1.83 ms (n = 2119 events). When CNQX was added to the cocktail only rarly sPSCs were observed in principal neurons (from 1.77 ± 1.4 to 0.06 ± 0.04 Hz; n = 6). Thus, the kinetics of AMPA-mediated sPSC are similar in neurons and glial cells (see also Figure 30).

To test for the receptor mediating the spontaneous postsynaptic events in the presence of 4-AP, the non-NMDAR antagonist CNQX (25 µM) and the AMPA specific antagonist GIKY 52466 (100 µM) or CTZ (100 µM), which blocks desensitization of AMPA receptors, were applied. Addition of CNQX almost completely abolished the occurrence of sPSCs (0.09 Hz ± 0.13 Hz; n = 7). Similarly GIKY blocked sPSCs (0.03 ± 0.02 Hz; n = 4, Figure 29). CTZ did not influence the frequency of events (control 2.28 ± 3.92 Hz; n = 5 and with CTZ, 2.37 ± 4.15 Hz; n = 4), but slowed the decay time constant from 1.34 ± 0.66 to 2.74 ± 1.8 (Figure 29A, B). This is also reflected in the decay time constant histogram (Figure 29D, right) and the cumulative fraction plot, which shows that the average decay time constant increases when CTZ is added (Figure 29E, right). The average amplitude of the spontaneous postsynaptic currents was not significantly affected (Figure 29D, E left).

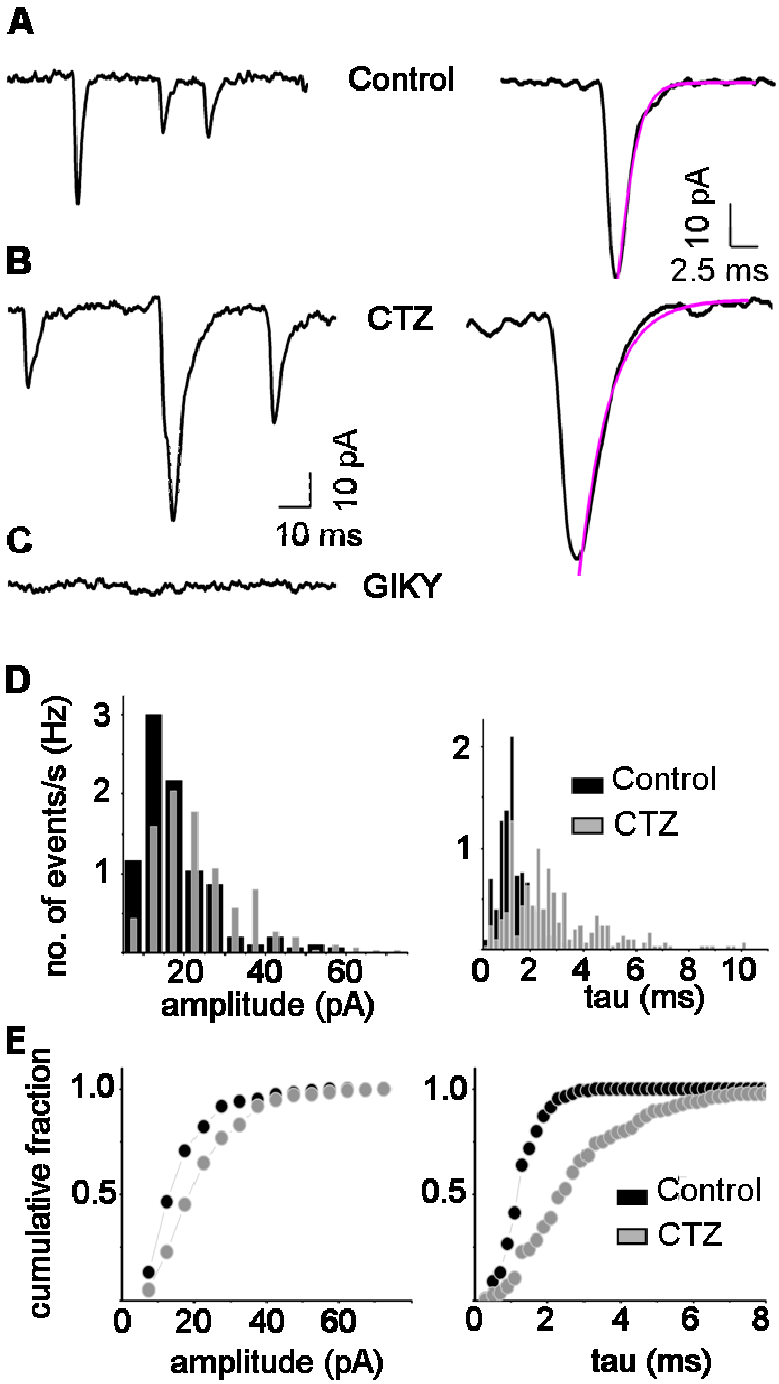

Figure 29. Spontaneous postsynaptic currents recorded in complex glial cells are AMPA receptor-mediated

(A) sPSCs recorded during bath application of 4-AP (100 µM). A single event fitted to a monoexponential is shown with higher time resolution (right).

(B) sPSCs recorded after pre-incubation with CTZ (100 µM) and co-application of 4-AP (100 µM) + CTZ (100 µM). A single event, fitted to a monoexponential, is shown with higher time resolution (right). Note that the time decay constant (tau) under CTZ is slower than that observed with 4-AP alone.

(C) GIKY 52466 blocks the sPSCs completely.

(D) Histograms of amplitude distribution (left) and time decay constants (right) under control conditions and in the presence of CTZ.

(E) Cumulative fraction for amplitude (left) and decay time constants (right).

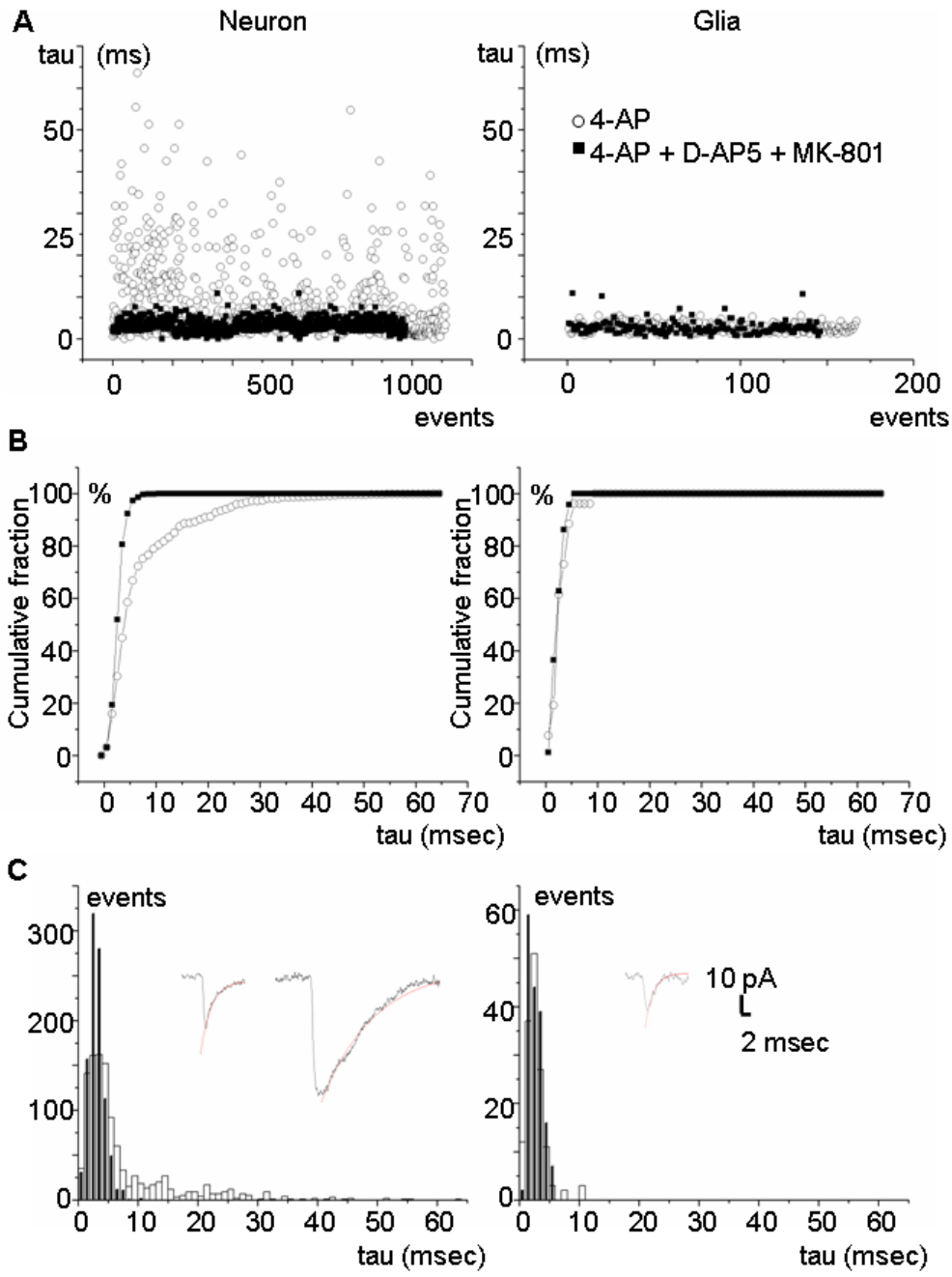

Figure 30. Distribution of decay times of spontaneous postsynaptic currents recorded in a neuron and a complex glial cell

(A) Scatter plot of sPSC decay time constants (tau) obtained from a pair recording of a principal neuron (left) and a complex glial cell (right) under 4-AP (100µM) (open circles) and under 4-AP (100µM) + D-AP5 (50µM) + MK-801 (10µM) (filled circles). Note that the slow (t >10 ms) NMDAR mediated component was only observed in the neuron.

(B) Cumulative fraction plot of the data shown in (A). In the neuron (left) 80% of the sPSCs have a decay time constant of <10 ms. In the complex glial cell (right) no slow NMDAR-mediated sPSCs are visible.

(C) Histogram of the data shown in (A) and (B). Insets: representative examples of sPSCs recorded in neuron (left) and complex glial cell (right), respectively. The neuronal fast event had an amplitude of 27 pA a 10 - 90 rise time of 0.50 ms and a decay time constant of 3.5 ms. The neuronal slow event had an amplitude of 61 pA, a 10 - 90 rise time of 2.00 ms and a decay time constant of 35.0 ms. The glial event has an amplitude of 19 pA, a 10 - 90 rise time of 0.47 ms and a decay time constant of 2.2 ms.

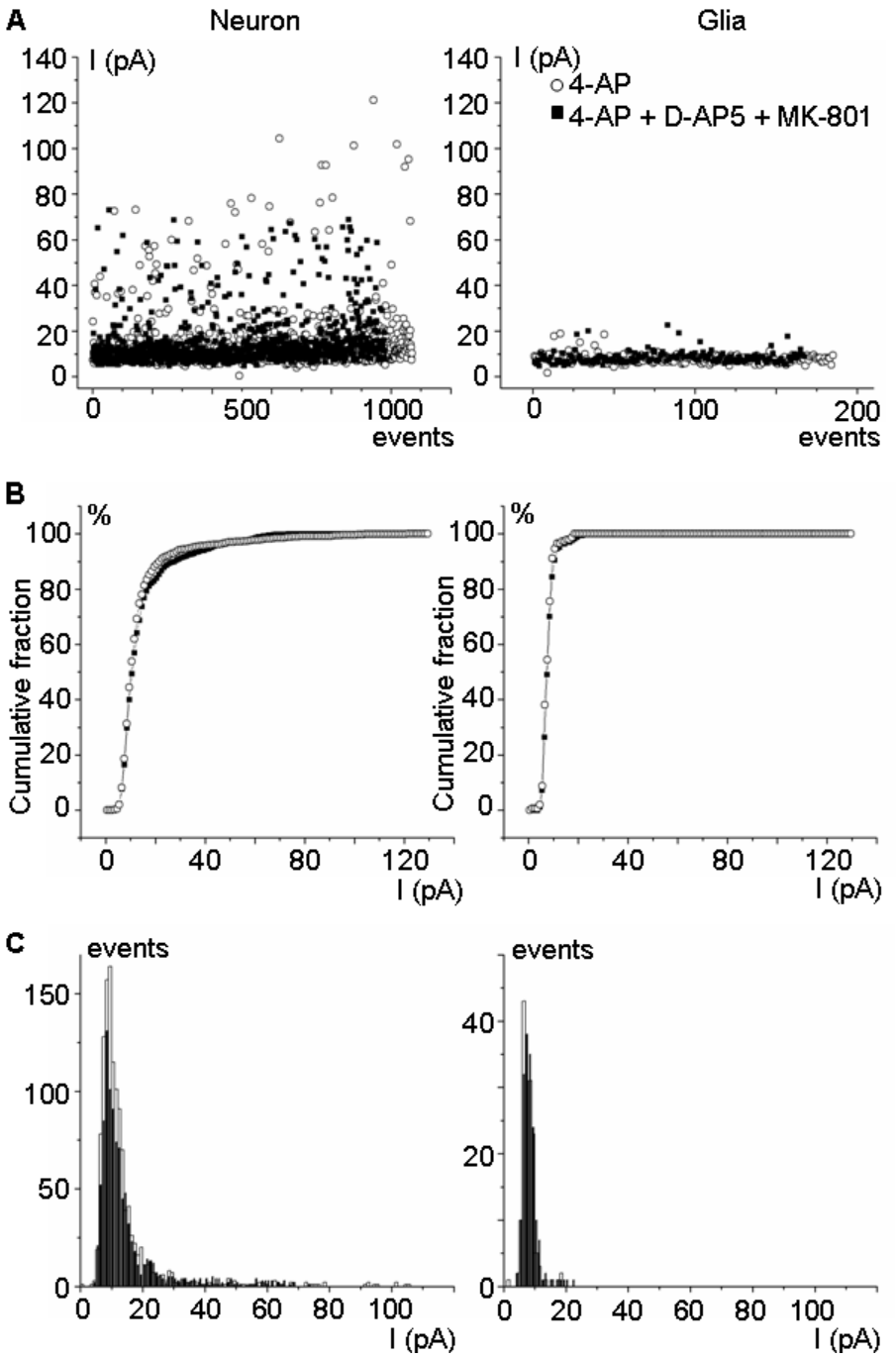

Figure 31. Distribution of amplitudes of spontaneous postsynaptic currents recorded in a neuron and a complex glial cell

(A) Scatter plot of the sPSC amplitudes obtained from a pair recording of a principal neuron (left) and a complex glial cell (right) under 4-AP (100µM) (open circles) and under 4-AP (100µM) + D-AP5 (50µM) + MK-801 (10µM) (filled circles).

(B) Cumulative fraction plot of the data shown in (A). In this neuron (left) 80% of the sPSCs had an amplitude of <30 pA. In this complex glial cell (right) almost all events were within 5 to 10 pA.

(C) Histogram of the data shown in (A) and (B).

3.14. Complex glial cells and principal neurons receive input from the same presynaptic terminal

To directly compare AMPA-receptor mediated sPSCs in neurons and glial cells, sPSCs from closely apposed neurons and complex glial cells were simultaneously recorded in the presence of 4-AP and strychnine (1 µM), gabazine (100 µM), D-APV (50 µM) and MK-801 (10 µM) (Figure 32, see also Figure 30, 31). To determine whether the two cells receive input from the same presynaptic terminal, the time relationship between postsynaptic currents in neurons and complex glial cells was analysed, assuming that sPSCs are synchronized in the principal neuron and the complex glial cell if both are contacted by the same presynaptic terminal (Figure 32A, B and E).

To determine coincident events, the time difference between the peak of a given event in the complex glial cell and the closest event in the neuron was analysed. Plotting these data as a histogram showed a peak of events at 0 ms difference with a scatter of less than ± 2 ms (Figure 32E). When the two current traces were shifted against each other by increasing time steps (step size 1 ms) and analyzed for coincidence, the amount of coincident events decreases abruptly to noise level after more than ± 2 ms shifting (Figure 33) indicating that coincident events occur within a time frame of less than ± 2 ms. Therefore only events within this time window were considered as coincident. In average 4.6 ± 4.6 % (range 0.7 - 13.3%) of the neuronal events and 32.1 ± 24.7 % (range 4.5 – 77.9 %) of the glial events were coincident with glial and neuronal events, respectively (Figure 32D; n = 9). The average frequency of coincident events was 0.38 ± 0.60 Hz (range 0.01 - 1.64 Hz, n = 9). The average frequency of non-coincident events in the complex glial cell was 0.41 ± 0.31 Hz (range 0.16 - 1.15 Hz, n = 9) and 4.8 ± 3.5 Hz (range 1.4 - 12.5 Hz, n = 9) for neurons.

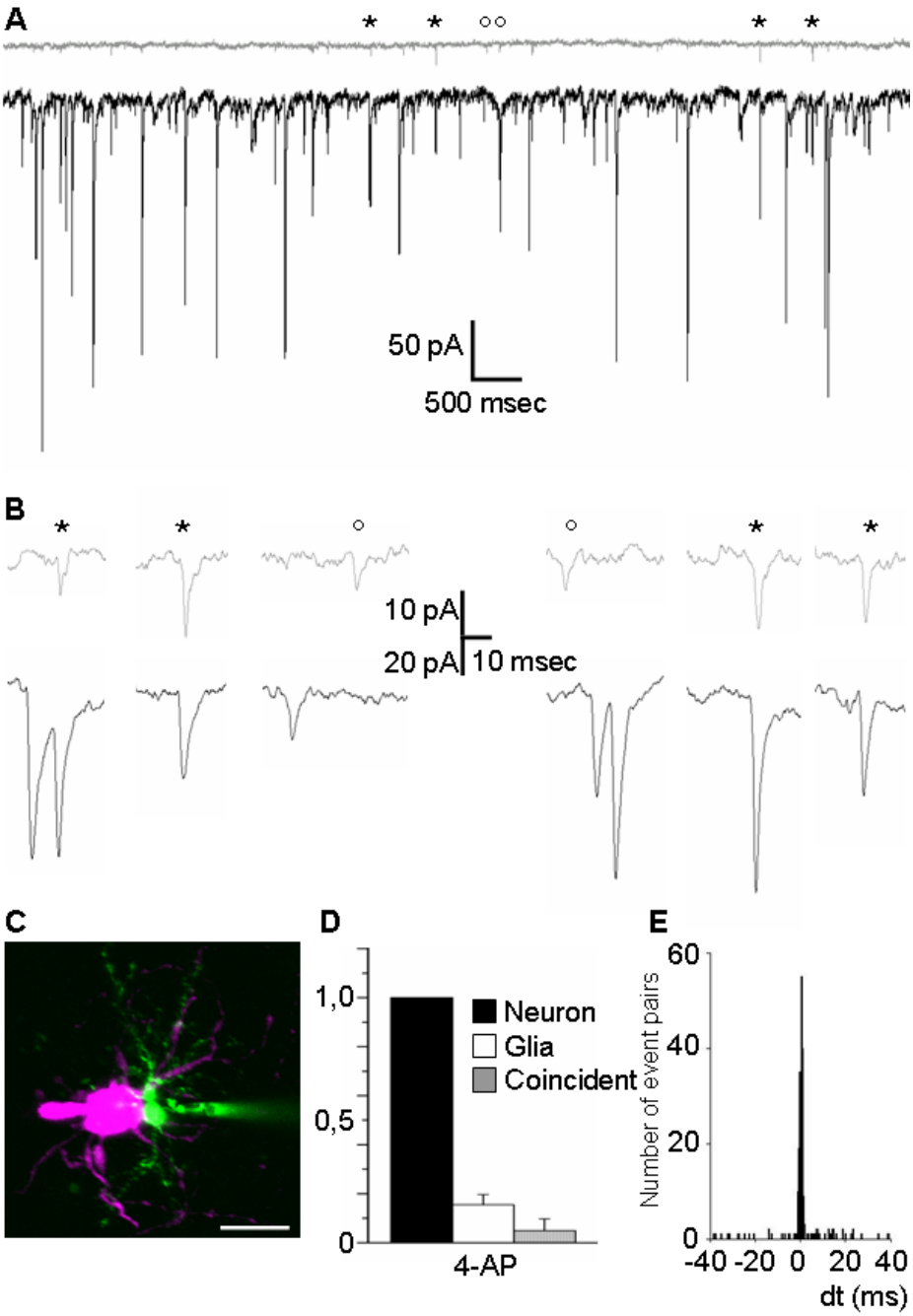

Figure 32. Coincident spontaneous synaptic activity recorded in complex glial cells and neurons

(A) Double whole-cell recording showing the sPSCs in a principal neuron (black) and a closely apposed complex glial cell (gray) elicited by 4-AP (100 µM). The asterisks mark examples of coincident events while the circles mark examples of non-coincident events. Note the frequency difference in neuron and complex glial cell.

(B) Higher time resolution of representative sPSCs marked in A.

(C) Two-Photon laser scanning microscope image of a recorded cell pair showing the neuron in magenta and complex glial cell in green (filled with Alexa 594 and LY, respectively, through the patch pipette). Scale bar = 10 µm.

(D) Summary of events in neurons, glial cells and coincident events. The number of events were normalized to the number of events recorded in neurons (n = 9). Data are the mean ± S.D.M.

(E) Coincidence (latency) histogram of events in glial cells related to neurons. The time difference between events in the two cells is plotted as histogram. The bin width was 0.5 ms. Note the sharp peak around 0 ms.

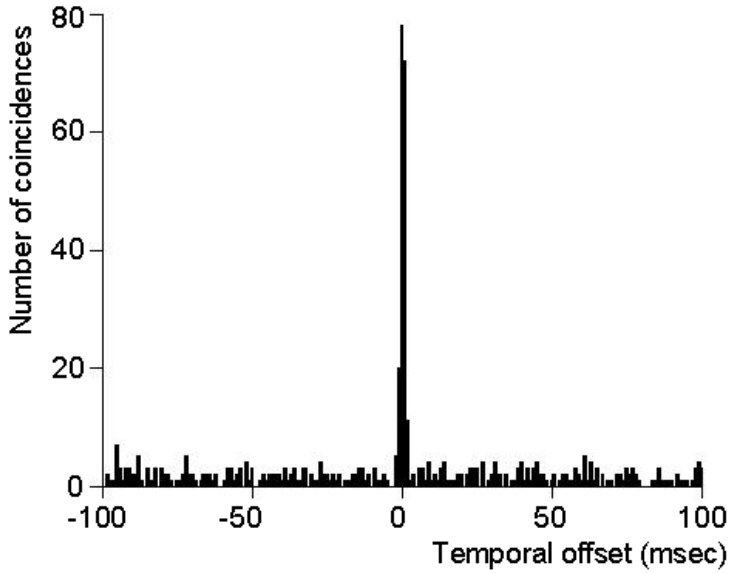

Figure 33. Cross correlation histogram of the coincident events from the experiment shown in Figure 32

Two traces of spontaneous activity recorded simultaneously in a complex glial cell and a principal neuron were time shifted against each other. The bin width was 1 ms. Each column refers to one shifting. Note that the sharp peak disappears as soon as the traces are shifted more than 2 ms in each direction. No other time relation than ± 2 ms is visible.

3.15. Miniature postsynaptic currents

The amplitude histograms of the spontaneous events indicated a peak at 9 pA for glial cells and 25 pA for neurons. To compare the quantal size in glial cells and neurons, miniature spontaneous events were compared. Membrane currents were recorded from cells clamped at -70 mV in the presence of TTX and ruthenium red (Lim et al., 2003). To selectively record the calyceal events, strychnine (1 µM) and gabazine (10 µM) were added to the bath solution, thereby avoiding the reported inhibitory sPSC amplitude increase upon application of ruthenium red. NMDAR were not blocked pharmacologically, since under TTX the spontaneous vesicle release was not able to depolarize the postsynaptic cells enough to release the Mg^{2+} block of the NMDAR. In complex glial cells, the average single event was 12.56 pA (± 6.00; 106 events; n = 7). In neurons, the mean mEPSC amplitude was 16.51 pA (± 3.82; n = 270 events, n = 6). The decay time constant was similar for complex glial cells

(1.64 ± 1.21; 106 events; n = 7) and neurons (1.85 ± 0.59; 270 events, n = 6). The frequency was 0.08 Hz (± 0.06; n = 7) for glial cells and 0.19 Hz (± 0.14, n = 6) for neurons. No influence of ruthenium red on glutamatergic sPSC kinetics and amplitude was observed, as reported by Trudeau and coworkers (Trudeau et al., 1996).

3.16. Complex glial cells receive input from more than one calyx

The morphological features of the complex glial cells indicate that these cells could potentially be in contact with more than one calyx. The data presented in this study show that 2/3 of the spontaneous events of complex glial cells are not matched with a coincident event in the neuron (Figure 31D). These non-coincident events in glial cells could be either due to input from another calyx or calyces, or caused by complete failure of synaptic transmission to the principal neuron. To distinguish between these two possibilities, probability of failure of synaptic transmission from the calyx to the principal neurons was estimated. When events in the neuron are evoked by presynaptic spikes, as done under 4-AP, PSCs can be described as the product of the number of available vesicles (*n*), release probability of each quanta (*p*) and size of the quantal unit *q* (amplitude of mPSCs).

$$I\,(PSC) = n*p*q \text{ (Sakaba et al., 2002).} \qquad (1)$$

The release-site model (Vere-Jones, 1966) is based on the assumption that *N* is the finite number of release sites, determining the maximum number of available vesicles *n*. However, the release site has not necessarily to be equal to the active zone as defined by ultrastructure. The release-site model assumes maximal one docked vesicle per release site, which can be released per stimulus with some release probability. This would change equation (1) to

$$I\,(PSC) = N*p*q \text{ (Vere-Jones, 1966; Katz, 1969).} \qquad (2)$$

If the number of release sites *N*, the quantal amplitude *q,* and the mean amplitude *I* of the postsynaptic current are known, one can estimate the release probability *p* of an individual release site out of the readily releasable pool of vesicles simply from

$$p = I/N*q. \qquad (3)$$

It is well established that a given Calyx is connected to only one postsynaptic neuron (Kuwabara et al., 1991). To obtain an estimate of the quantal amplitude, amplitude of the mEPSCs was determined and a value of 16.5 pA was found, which was similar to the peak of the amplitude histogram of spontaneous postsynaptic activity. The mean 4-AP induced spontaneous postsynaptic current amplitude in neurons was 53.4 pA, indicating that on average 3 release sites were simultaneously activated per neuronal event under 4-AP (53.4 ~ 3 * 16.5). The number of release sites in mice is estimated from under 100 at P5 to around 600 at P12 (Youssoufian et al., 2005). Therefore, 400 release sites for the P8 – P10 mice were assumed, and thus a value of 0.008 for *p* under 4-AP was obtained. The probability of complete failure of synaptic transmission to the neurons can then be calculated as

$$P_f = (1 - p)^N \quad (4)$$

and for the above mentioned value a probability of failure of 0.036, or 3.6 %, was calculated. This indicates that only roughly 4 out of 100 non-coincident events in the glial cells can be explained by a failure in the neuronal response, whereas the majority of non-coincident events in the glial cells cannot, but must be due to input from another calyx. Since about a 2/3 of the events in the glial cell is not synchronized (Figure 32D) it is assumed that one complex glial cell receives (on average) input from three calyces.

.

3.17. Estimation of the number of release sites contacted by complex glial cells

The number of release sites towards the glial cell can be roughly estimated based on the glial failures related to the neuronal activity. Only about 3.6 % of the events in the neurons are coincident with glial events, indicating that the glial failure rate in reference to one Calyx is 96.4 %. The number *N* of release sites can be obtained from the probability of failure P_f and the probability *p* of activation of individual release sites by

$$N = \log P_f / \log(1 - p). \quad (5)$$

Assuming a release probability of 0.008 as for the release sites towards the neuron, an estimate of 4.6 release sites from one calyx towards the glial cell can be assumed. This suggests that neurons contact about 87 times more release sites (400 / 4.6 = 86.96), which is in line with the observed ratio of 106 between the amplitudes of evoked responses to midline stimulation in neurons and glial cells (2200 / 20.8 = 105.77). As one complex cell contacts three calyces on average, it is estimated that each complex cell is in contact with about 14 release sites (3 * 4.6 = 13.8).

4. Discussion

4.1. Identity of the two distinct types of glial cells in the MNTB area

In this study it could be shown that two types of glial cells establish intimate contact with the CoH. One type is the classical astrocyte characterized by high levels of GFAP expression, passive membrane properties, presence of glutamate transporter and extensive gap junctional coupling. The other, termed complex cell in this study, is characterized by very low or non GFAP but AN2/NG2 expression. In contrast to the passive cells, these cells do not form a syncytium and do not show dye-coupling, express no functional glutamate transporters, but glutamate receptors of the AMPA type. A similar cell type has been described in hippocampus, cerebellum and corpus callosum (Bergles et al., 2000; Ge et al., 2006; Jabs et al., 2005; Lin et al., 2005; Ziskin et al., 2007). In the hippocampus, this distinct type of glial cell was characterized by low GFAP promoter activity, observed as a low expression of eGFP, expressed under this promotor (Jabs et al., 2005; Matthias et al., 2003), whereas the complex cells in the MNTB area investigated in this study in most cases did not show any eGFP expression. This difference between complex cells in the hippocampus and those in the MNTB described within this study could be explained by lower levels of (human) GFAP promoter activity in the brainstem. Indeed, GFAP positive cells that did not show green fluorescence could be observed, suggesting a low expression of GFAP only detectable by a GFAP antibody. This observation is consistent with a previous study that showed GFAP mRNA, but no protein expression in NG2+ cells acutely isolated from the hippocampus (Schools et al., 2003). The AN2/NG2 proteoglycan, which has been initially described as an oligodendrocyte progenitor marker in the developing and adult CNS (Niehaus et al., 1999; Nishiyama et al., 1999; Diers-Fenger et al., 2001; Dawson et al., 2003; Lin and Bergles, 2004; Peters, 2004) could also be detected in a small population of cells in the MNTB area (Figure 14D, 15). In this study it could be shown that the complex cells can be compared to the NG2+ cells from other studies. Immunohistochemistry

in GFAP-eGFP transgenic animals revealed that most AN2/NG2-positive cells are either eGFP-negative or, in rare cases, very faintly labelled for eGFP. The AN2/NG2+ positive cells in the MNTB, which are usually located in close vicinity to the principal neurons, are characterized by a rounded soma with several branched processes, as previously described by Matthias et al. (2003) for the hippocampus.

4.2. Identity of other cell types in the MNTB area

In order to test for the presence of other macro- and microglial cells as well as neurons in the MNTB several immunhistochemical stainings were performed. Neither NeuN, a neuronal marker (Mullen et al., 1992), MOG, an oligondendroglial marker (Scolding et al., 1989), nor Iba-1, a marker for microglial cells (Ito et al., 1998) could be detected on eGFP expressing cells in the MNTB of GFAP-eGFP transgenic mice in this study. This proofs that the eGFP-positive cells in the MNTB indeed represent a separate cell population, as described by Nolte and coworkers for other brain regions (Nolte et al., 2001). However it could still be possible that the above mentioned markers show overlay with the marker for oligodendrocyte precursor cells expressed on complex glial cells in this study, namely AN2/NG2. This overlay has been reported for GFAP-expressing cells in the hippocampus (Matthias et al., 2003). In this study it was not tested for overlay of AN2/NG2 and other glial and non-glial markers. However, this was not subject of this work. According to a review from Berry and coworkers (Berry et al., 2002) the expression of NG2 declines as the cells start to differentiate into mature oligodendrocytes and reaches undetectable levels before MOG expression can be detected. Belachew and coworkers reported that the decline of NG2 expression even reached undetectable levels before the expression of NeuN started to be detectable (Belachew et al., 2003). These studies imply that coexpression of AN2/NG2 with NeuN or MOG can be excluded.

However there are publications reporting coexpression of Iba-1 and NG2 on some cells in the mammalian CNS (Yokoyama et al., 2006; Matsumoto et al., 2008). In these publications, though, the authors favour the interpretation that the cells

expressing both markers act as multipotent neural progenitors to replace injured or dead cells in pathologic brains. Since the authors of these studies investigated cells in vitro or in response to pathological insults, it is possible to argue that in the normal brain *in vivo* coexpression of microglial markers and AN2/NG2 does not occur. Since NG2 positive cells have been reported do possess some precursor cell properties and to be able to give rise to neurons, as well as oligodendrocytes and astrocytes *in vitro* as well as *in vivo* (Belachew et al., 2003; Zhu et al., 2008) it could still be possible that the population of AN2/NG2 cells do not form an "own" glial cell type. The controversy about this glial cell type is still ongoing and within this work these open questions could not be elucidated.

4.3. Functional properties of the two distinct types of glial cells in the MNTB area

With respect to functional properties a more homogenous scenario has been observed. A typical voltage dependent K^+ current profile with outward rectification is the signature of the complex glial cells and this feature distinguishes them from mature astrocytes or oligodendrocytes, in grey or white matter (Berger et al., 1991; Jabs et. al., 2005; Matthias et al., 2003). Additionally, complex cells exhibited AMPAR mediated currents and showed no dye coupling or glutamate transporter mediated currents (Borges et al., 1994; Matthias et. al., 2003; Wallraff et al., 2004). Indeed, these criteria characteristic for NG2 positive cells established previously in the hippocampus and cerebellum (Bergles et al., 2000; Ge et al., 2006; Lin et al., 2005; Matthias et al., 2003) and recently in the corpus callosum (Kukley et al., 2007; Ziskin et al., 2007) are in aggreement with the results for complex cells in the MNTB.

4.4. The two types of glial cells establish contacts to the CoH terminal

The ultrastructural analysis demonstrates that fine processes of passive astrocytes enwrap and directly contact the pre-and postsysnaptic components of the CoH

terminal, as previously described for other brain regions such as the cerebellum (Grosche et al., 1999). Furthermore, passive cells extended their fine finger-like processes very close to the active zones, the sites of transmitter-release. These finger-like processes have been shown to express the glutamate transporter GLAST and account for the only available mechanism of glutamate removal (Palmer et al., 2003; Renden et al., 2005). However, no specific contacts that resemble synaptic-like structures could be observed between the CoH and the passive cells.

In contrast, the complex cell receives direct synaptic input from the CoH. The ultrastructural analysis demonstrates that this input is possible because anatomically distinct axo-glial synaptic-like contacts are formed between processes of the complex cell and the CoH. Therefore, this unique type of glial cell represents a postysnaptic element which is integrated into the synaptic circuit of the MNTB. These findings support observations from other brain areas (Bergles et al., 2000; Jabs et al., 2005; Lin et al., 2004b, 2005; Kukley et. al., 2007; Ziskin et al., 2007) and further substantiate the concept that synapse-based information processing is a property not only of neurons, but also of certain glial cells.

4.5. Current response of passive cells to CoH activity

In the passive cells, no spontaneous activity was observed and midline stimulation triggered only a small but fast current response which was not sensitive to CNQX or TBOA. Thus, this response was not mediated by glutamate receptors nor transporters. One might therefore assume that this is not a direct response but due to ephaptic interactions as also described for Bergmann glial cells (Bellamy and Ogden, 2005).

In contrast to astrocytes in the hippocampus or cerebellar Bergmann glial cells (Bergles et al., 1997; Bergles and Jahr, 1997) no glutamate uptake currents correlated with the electrical stimulation of presynaptic fibers could be recorded from passive glial cells in the MNTB in this study. It is possible that the glutamate uptake occurs only at the far tip of thin processes and the resulting current can not be recorded in the soma of the cell. The processes of Bergmann glial cells, however,

show even a higher arborization, and glutamate uptake currents can be reliably recorded. Renden et al. (Renden et al., 2005) reported that GLAST is the predominant glutamate transporter in the MNTB and that it is expressed by astrocytes. In agreement with this study, the experiments presented in this study with D-Asp to activate glutamate transporters exogenously applied demonstrate the functional expression of the glutamate transporter exclusively in passive cells. Nevertheless, according to Renden et al. (2005), the glial transporters are excluded from the synaptic cleft and they are not essential for controlling the postsynaptic response at a given CoH terminal, but rather have a role in limiting diffusion between adjacent CoH terminals. Likewise, interference with glutamate uptake did not affect the evoked postsynaptic current waveform (Renden et al., 2005). On the other hand, the data presented here indicate that, evoked glutamatergic neuronal activity is not directly followed by a rapid glutamate uptake current in astrocytes, in contrast to other brain areas (Bergles et al., 1997; Bergles and Jahr, 1997). However, it could be observed that repetitive stimulation triggers a slow inward current in the passive cells. This current is augmented in the presence of the glutamate uptake blocker TBOA and could be blocked with CNQX. These results support the model where glutamate transporters act as a barrier (Renden et al., 2005).

High frequency stimulation triggered a slow inward current and an additional slow current component by application of the glutamate uptake blocker. A similar current response has been observed in Bergmann glial cells in response to parallel fiber activation. This current was blocked by inhibiting G proteins and it has been speculated that this response could be due to the release of an unknown substance from neurons activating a G-protein-coupled receptor in the glial cells (Bellamy and Ogden, 2005). Likewise, a similar slow inward current was observed in astrocytes from the hippocampus that was blocked by kynurenic acid or treatment with K^+ channel blockers (Ge et al., 2006; Ge and Duan, 2007).

4.6. Ca^{2+}-signals of passive cells in response to CoH activity

On the other hand, even though no glutamate transporter or receptor mediated current could be recorded, passive glial cells showed Ca^{2+}-increases upon stimulation of the afferent fibers. The identity of the cells is suggested to be astrocytic, because of the loading with the AM ester form of Fluo-4, which is known to preferentially load astrocytes (Dallwig and Deitmer, 2002). However, the publication of Dallwig and Deitmer refered to glial cells in the hippocampus, which are not necessarily equal to those from the MNTB. However one can still assume that the majority of the observed responses were from glial cells because of the smaller somata size when compared with neurons. However, the exact nature of the cells that do show Ca^{2+}-responses to midline stimulation could not be proven in this study. The reaction could be shown to be glutamatergic to a great extent, indicating a calyceal origin. However, a small contribution of inhibitory transmission could also be shown by partial blockage of the Ca^{2+}-responses with gabazine and strychnine, blockers of GABA and glycine receptors, respectively, which hints to an inhibitory signalling to MNTB astrocytes. Unfortunately, however, up to now there is no publication available identifying the origin of inhibitory transmission in the MNTB. Since the principal neuron is an inhibitory interneuron, it is though possible, that the astrocytes somehow sense the activity of the postsynaptic neuron. On the other hand it could also be possible that the Ca^{2+}-responses was a secondary one and not due toligand binding but rather to potassium release from the postsynapse after synaptiuc transmission. But this is unlikely due to the time course of the response, which was to fast for this secondary type of response. However the experiments as performed in this study can not rule out this possibility completely. Taken together these results indicate that MNTB passive glial cells do detect neuronal transmission in the auditory brainstem, even though the exact mechanisms of interaction still needs to be clarified.

4.7. Response of complex cells to CoH activity, triggered by midline stimulation

The CoH is a giant glutamatergic terminal where evoked postsynaptic neuronal responses are mediated by a a fast AMPA/KAR (τ < 2 ms) or a slow NMDAR (τ > 50 ms) EPSC (Forsythe and Barnes-Davies, 1993; Joshi and Wang, 2002). In the complex glial cells, evoked responses with a sensitivity to ionotropic glutamate receptor antagonists and a decay time of tau = 1.2 ms could be recorded. This indicates that the response of the postsynaptic glial cell is most probably also mediated by AMPA/KAR. The glutamatergic response of the GluR cell in the hippocampus or the NG2+ cells in corpus callosum and cerebellum also rely on AMPAR-mediated signalling (Jabs et al., 2005; Lin et al., 2005; Kukley et al., 2007; Ziskin et al., 2007) suggesting a common glial expression of this receptor in complex cells across different brain regions.

Likewise, since postsynaptic currents in the complex glial cells could be recorded with stimulation intensities as low as 100 µA applied via a bipolar stimulation electrode, thereby avoiding a depolarization of the whole specimen between the stimulation electrode and the bath chamber ground electrode, as would have been in monopolar stimulation, it can be concluded that the response is indeed initiated and transmitted by transmitter release at the CoH. It has been shown that stimulation of non-calyceal excitatory inputs requires significantly higher stimulation intensities when the stimulation electrode was positioned on the midline of the slice and the recording site was > 300 µm away from the stimulation site (Hamann et al., 2003). This indicates that the evoked activity recorded from complex glial cells in the MNTB in this study does indeed stem from calyceal inputs, and not, as one might have expected from other, non-calyceal excitatory inputs.

Since the CoH shows high fidelity and high frequency synaptic transmission, the analysis of the latency of the postsynaptic response in the principal neuron in reference to the stimulus artefact, the “jitter”, became a tool to prove the calyceal origin of the recorded response. When evoked PSCs were recorded from principal neurons in the MNTB the jitter remained very constant (< 1ms in P13 – 15 rats and

P14 – 17 mice (Hamann et al., 2003)) due to the axo-somatic architecture of the CoH and the contact of only a single calyx to a given postsynaptic neuron. The analysis of this jitter of the postsynaptic response (Fedchyshyn and Wang, 2007) could not be performed in complex glial cells, since this cell type contacts more than one synapse with different cellular regions, such as the soma and the processes, which made a jitter analysis inappropriate. However, the 100-fold larger responses in the principal neuron further indicates that the postsynaptic neuron is contacted by the CoH since non-calyceal inputs elicit currents of < 300 pA (Hamann et al., 2003). The CoH is known to evoke giant responses up to 15 nA in mature animals under conditions of high release probability (for review, see (Schneggenburger and Forsythe, 2006)). The principal neuron, however, contacts many more release sites than the complex cell, due to the axo-somatic architecture of this synapse.

4.8. Response of complex cells to CoH activity, triggered by application of 4-AP

To compare the amplitude and frequency of responses in neurons and complex glial cells, sPSCs were studied. By applying 4-AP, a simultaneous and significant increase in the probability of spontaneous activity in the principal neuron and the complex glial cell was observed. One might assume that these events were elicited by spontaneous action potentials, since their activity was blocked by TTX. A similar effect of TTX was observed with ATPγS-evoked facilitation of sPSCs in principal neurons from the rat MNTB (Watano et al., 2004). In contrast, CNQX did not completely block the sPSCs in neurons in this study, but this effect was only accomplished after blocking NMDA, glycine and GABA receptors. sPSCs mediated by glycine and GABA receptors have previously been described in MNTB principal neurons (Lim et al., 2003). In contrast, in complex cells investigated in this study the sPSCs elicited with 4-AP were blocked by CNQX or GYKI indicating that the events were only AMPAR mediated. The kinetics and pharmacological profile of these responses in principal neurons and complex cells were similar to those reported for principal neurons in the rat MNTB (blocked by CNQX and with a decay time constant

≤ 3 ms, (Watano et al., 2004)). This is in marked contrast to the hippocampus where the GluR cells, which are comparable to the complex cells from this study, receive additional GABAergic input (Jabs et al., 2005). Thus, the complex cell in the MNTB is only wired to the glutamatergic CoH despite its ability to respond to bath application of ATP, glycine and GABA (not shown).

4.9. Estimation of the number of calyces and their release sites contacted by complex glial cells

In this study the release site model as initially proposed by Vere-Jones in 1966 (Vere-Jones, 1966) was used to determine quantal parameters and the number of calyces and their release sites contacting complex glial cells in the MNTB. With this model some assumptions go along. 1.) A finite number of release sites. 2.) Maximally one docked vesicle per release site. However, it can be possible that the number of release sites is infinite. The model then allows unlimited supply of vesicles to the releasable pool from a reserve pool. This model is called vesicle-state model and has been used to explain exocytosis at chromaffin cells (Heinemann et al., 1993). The release-site model and the vesicle-state model predict different synaptic responses under certain conditions. For example if the vesicle-state model is correct and refilling of vesicles is Ca^{2+}-dependent, a transient overfilling of the synaptic vesicle pool can occur during recovery from synaptic depression (Weis et al., 1999), but no such overfilling is possible for a release-site model. Several publications could not show experimental evidence for overfilling at the calyx of Held (von Gersdorff et al., 1997; Wang and Kaczmarek, 1998; Weis et al., 1999; Wu and Borst, 1999; Sakaba and Neher, 2001) although the refilling process was shown to be dependent on Ca^{2+} (Wang and Kaczmarek, 1998; Sakaba and Neher, 2001). Based on these facts the release-site model was applied in this study.

According to the equation presented in the release-site model, it is necessary to know q and N to get an estimate of p. In this study q was determined from spontaneous miniature EPSCs, yielding a value of 16 pA for neurons. This is in line with values achieved form different groups in mice as well as in rats (Meyer et al.,

2001; Youssoufian et al., 2005). However, a difference in amplitude in comparison to the complex cells was found, which had a *q* of 12 pA, most probably due to a different amount of receptors in the postsynaptic membrane. If the quantal size *q* is known, then *p* can only be estimated after the number of release sites *N* has been determined. According to the release-site model only one vesicle is docked and released per release site. This equals the number of release sites *N* and the number of available vesicles *n*. The total number of vesicles released during a train of high frequency stimuli can represent the readily releasable pool size provided that the pool is completely depleted and is not replenished. This means that *N* can be estimated by depleting the releasable pool with a series of stimuli. Unfortunately the complex glial cells were not able to follow stimulation frequencies of 10 Hz, which are comparatively low for this synapse and though not able to deplete the vesicle pool. However, the literature gives a good estimate for *N* over the first two weeks of postnatal development as determined from recordings from the postsynaptic neuron. Therefore *N* was extrapolated from the values achieved by Youssoufian and co-workers from mice between P5 and P12 (Youssoufian et al., 2005). The achieved value of *N* = 400 has still to be experimentally proven from recordings from principal neurons in the P8 – P10 NMRI mice used in this study. However, with these values it was possible to calculate the release probability under 4-AP. The achieved value of 0.008 is low when compared with the value of 0.34 as calculated for the midline stimulated evoked responses. On the other hand it is not surprising that 100 µM 4-AP are not able to stimulate the presynapse to the same extent as 100 µA applied via a bipolar stimulation electrode directly placed on the afferent fibre tract. This also explains why the spontaneous events under 4-AP are not of the same size as the ones recorded after midline stimulation. However the events recorded under 4-AP can still be assumed to be action potential mediated since they were abolished with TTX. If the smaller size of the spontaneous events under 4-AP would be explained by a non-calyceal origin, then a calyx-mediated event would be of remarkable bigger amplitude. However, in far more than 20 neurons as well as glial cells, with recording times of at least 300 s per cell, no giant 4-AP-evoked spontaneous event could be recorded. It is unlikely that all cells recorded were not contacted by a functional

calyx, leaving it extremely unlikely that the achieved values under 4-AP originate from non-calyceal inputs.

In this study the calculation of quantal parameters for a glial cell was performed for the first time at the calyx of Held giant synapse. The first publication in which *p* has been calculated for a NG2 positive cell receiving input from unmyelinated axons in mouse corpus callosum (Kukley et al., 2007) yielded a value for *p* of 0.09, which is in line with the values achieved in this study. With *p* it was possible to calculate for the first time the number of neuronal release sites contacted by a given complex glial cell.

4.10. Complex glial cells can integrate the activity of few calyces

In Bergmann glial cells, the microdomains are structural units which enwrap a defined set of synapses from parallel fibres onto Purkinje neurons. Stimulation of parallel fibres results in an increase in intracellular Ca^{2+} in small compartments of Bergmann glial cells which have the size of the structural microdomain. It has been hypothesized that these units might serve to synchronize defined ensembles of synapses assuming that there is a feedback signal from the activated microdomain to the synapses (Grosche et al., 1999; Grosche et al., 2002). An ensemble of synapses is defined by the structure of the microdomain and a given microdomain contains hundred(s) of synapses. There are several molecules which are released from glial cells and influence synaptic activity. Glutamate release from astrocytes has been shown to modulate synaptic activity (Parpura et al., 1994; Araque et al., 1998; Jourdain et al., 2007), D-serine released from astrocytes can modulate NMDA receptors (Schell et al., 1995; Oliet and Mothet, 2006), and ATP released from hippocampal astrocytes mediates heterosynaptic depression in the hippocampus (Serrano et al., 2006). In the MNTB, astrocytes and the complex cells are in close contact with several calyces. On the basis of the investigations performed in this study evidence could be found that the complex cells receive input from on average three calyces. For passive cells it could be shown morphologically that they contact also more than one calyx with their processes. Whether this is a principle also in

other brain areas and on other synapses remains to be shown. However, it indicates that complex cells have the capacity to integrate the information from a small ensemble of synapses. This might be a way of how glial cells could synchronize or influence the activity of defined groups of MNTB neurons.

4.11. Final conclusions

Figure 34 summarizes the findings in a schematic way. The complex cell contacts a small number of synapses with different regions (soma and different number of processes). The passive cell also contacts a small number of synapses with its soma and processes, also establishing contact to blood vessels.

The role of the two distinct glial cell types investigated in this study for the function of the calyx of Held giant synapse in the MNTB and the possible ways by which they might be able to influence it transmission remains to be elucidated in another set of experiments.

As a final conclusion one can state that for the first time it could be shown that two morphologically and physiologically distinct macroglial cell types contact one given synapse at the same time, sensing their activity with completely different mechanisms. The one, the passive cell, contacts the CoH synapse non-synaptically, responding to its activity with Ca^{2+}-signals and to high frequency activity under transporter blockage with a slow inward current, whereas the other, the complex cell, establishes synaptic contacts, receiving coordinated synaptic input from the CoH along with the principal neuron.

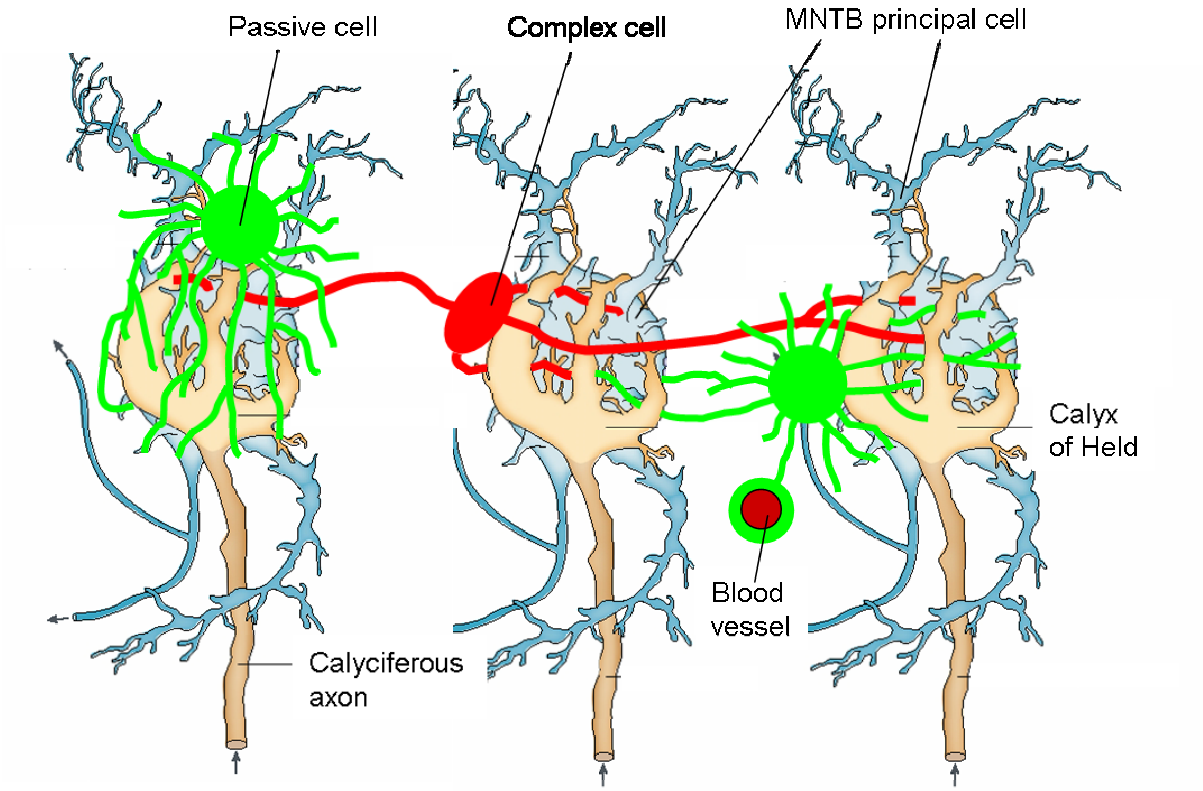

Figure 34. Schematic drawing of the actual connection of passive and complex glial cells with the CoH synapse as proposed in this study
Each calyx of Held (beige) contacts one principal neuron (blue). A given complex cell (magenta) contacts one CoH synapse with its soma and a given number of processes, as well as two other CoH synapses with varying number of processes, establishing synaptic contacts and integrating the activity of on average three synapses. The situation for the passive cells (green) is different. These cells also contact one CoH synapse with their soma and also others with their processes. In contrast to the complex cells the passive cells have more but shorter processes, with which they can either totally enwrap a single CoH synapse (left), or contact more CoH synapses and also blood vessels (right) reaching there processes over the calyceal arms as well as under them, separating the active zones from another and sense the activity of the synapse, responding with Ca^{2+}-signals. Modified from (von Gersdorff and Borst, 2002)

5. Summary

The calyx of Held is a giant presynaptic terminal forming an axo-somatic contact to the principal neuron in the medial nucleus of the trapezoid body. In the last few years this preparation has been used to study mechanisms of synaptic transmission and plasticity since both, pre- and postsynaptic elements are accessible to physiological recording and manipulation. In the present study, the glial elements associated with the calyx synapse were studied by using acute slices of the brain stem of young (P8-P10) mice. Two morphologically distinct types of cells in close association with the calyx synapse were found, one characterized by passive membrane currents and expression of the astrocytic marker glial fibrillary acidic protein (GFAP, passive cells), the other by voltage gated currents and expression of the proteoglycan NG2 (complex cell). Upon electrical stimulation of the afferent fibres crossing the midline of the brainstem slice, postsynaptic responses could be elicited in the complex cell that were sensitive to CNQX, an antagonist of AMPA/kainate type glutamate receptors (AMPA/KAR). In contrast to this, passive cells did not show a postsynaptic current response to midline stimulation, but responded with an increase in $[Ca^{2+}]_i$ that depended on AMPA/KAR. High frequency stimulation under glutamate transporter blockage elicited a slow inward current in passive cells, which was sensitive to CNQX, whereas no such current could be observed in complex cells.

The cells were also studied on the ultrastructural level and synaptic-like structures between the calyx and complex cells could be found. In contrast to this no such structures could be identified between the calyx and passive cells.

In addition double whole cell recordings of spontaneous activity from principal neurons of the MNTB and closely apposed complex cells were performed. It could be found that about a third of the glial events were synchronized with the neuron. By determining mEPSCs the quantal size of neuronal and glial responses could be estimated, namely 16 and 12 pA. Based on these data, it could be concluded that one complex glial cell integrates, in average, input from three calyces, but contacts much less release sites than the principal neuron.

6. References

Angulo MC, Kozlov AS, Charpak S, Audinat E. 2004. Glutamate released from glial cells synchronizes neuronal activity in the hippocampus. J.Neurosci. 24:6920-6927.

Araque A, Parpura V, Sanzgiri RP, Haydon PG. 1998. Glutamate-dependent astrocyte modulation of synaptic transmission between cultured hippocampal neurons. Eur.J.Neurosci. 10:2129-2142.

Araque A, Parpura V, Sanzgiri RP, Haydon PG. 1999. Tripartite synapses: glia, the unacknowledged partner. Trends Neurosci. 22:208-215.

Barnes-Davies M, Forsythe ID. 1995. Pre- and postsynaptic glutamate receptors at a giant excitatory synapse in rat auditory brainstem slices. J.Physiol 488 (Pt 2):387-406.

Belachew S, Chittajallu R, Aguirre AA, Yuan X, Kirby M, Anderson S, Gallo V. 2003. Postnatal NG2 proteoglycan-expressing progenitor cells are intrinsically multipotent and generate functional neurons. J Cell Biol 161:169-186.

Bellamy TC, Ogden D. 2005. Short-term plasticity of Bergmann glial cell extrasynaptic currents during parallel fiber stimulation in rat cerebellum. Glia 52:325-335.

Bergles DE, Dzubay JA, Jahr CE. 1997. Glutamate transporter currents in bergmann glial cells follow the time course of extrasynaptic glutamate. Proc.Natl.Acad.Sci.U.S.A 94:14821-14825.

Bergles DE, Jahr CE. 1997. Synaptic activation of glutamate transporters in hippocampal astrocytes. Neuron 19:1297-1308.

Bergles DE, Jahr CE. 1998. Glial contribution to glutamate uptake at Schaffer collateral-commissural synapses in the hippocampus. J.Neurosci. 18:7709-7716.

Bergles DE, Roberts JD, Somogyi P, Jahr CE. 2000. Glutamatergic synapses on oligodendrocyte precursor cells in the hippocampus. Nature 405:187-191.

Berry M, Hubbard P, Butt AM. 2002. Cytology and lineage of NG2-positive glia. J Neurocytol 31:457-467.

Brockhaus J, Deitmer JW. 2002. Long-lasting modulation of synaptic input to Purkinje neurons by Bergmann glia stimulation in rat brain slices. J.Physiol 545:581-593.

Butt AM, Kiff J, Hubbard P, Berry M. 2002. Synantocytes: new functions for novel NG2 expressing glia. J Neurocytol 31:551-565.

D'Ambrosio R, Wenzel J, Schwartzkroin PA, McKhann GM, Janigro D. 1998. Functional specialization and topographic segregation of hippocampal astrocytes. J.Neurosci. 18:4425-4438.

Dallwig R, Deitmer JW. 2002. Cell-type specific calcium responses in acute rat hippocampal slices. J.Neurosci.Methods 116:77-87.

Dani JW, Chernjavsky A, Smith SJ. 1992. Neuronal activity triggers calcium waves in hippocampal astrocyte networks. Neuron 8:429-440.

Dawson MR, Polito A, Levine JM, Reynolds R. 2003. NG2-expressing glial progenitor cells: an abundant and widespread population of cycling cells in the adult rat CNS. Mol Cell Neurosci 24:476-488.

Diers-Fenger M, Kirchhoff F, Kettenmann H, Levine JM, Trotter J. 2001. AN2/NG2 protein-expressing glial progenitor cells in the murine CNS:

isolation, differentiation, and association with radial glia. Glia 34:213-228.

Elezgarai I, Bilbao A, Mateos JM, Azkue JJ, Benitez R, Osorio A, Diez J, Puente N, Donate-Oliver F, Grandes P. 2001. Group II metabotropic glutamate receptors are differentially expressed in the medial nucleus of the trapezoid body in the developing and adult rat. Neuroscience 104:487-498.

Fedchyshyn M, Wang L. 2007. Activity-dependent changes in temporal components of neurotransmission at the juvenile mouse calyx of Held synapse. J Physiol 581.2:581-602.

Fellin T, Pascual O, Gobbo S, Pozzan T, Haydon PG, Carmignoto G. 2004. Neuronal synchrony mediated by astrocytic glutamate through activation of extrasynaptic NMDA receptors. Neuron 43:729-743.

Flores-Hernandez J, Galarraga E, Pineda JC, Bargas J. 1994. Patterns of excitatory and inhibitory synaptic transmission in the rat neostriatum as revealed by 4-AP. J Neurophysiol 72:2246-2256.

Forsythe ID. 1994. Direct patch recording from identified presynaptic terminals mediating glutamatergic EPSCs in the rat CNS, in vitro. J.Physiol 479 (Pt 3):381-387.

Forsythe ID, Barnes-Davies M. 1993. The binaural auditory pathway: excitatory amino acid receptors mediate dual timecourse excitatory postsynaptic currents in the rat medial nucleus of the trapezoid body. Proc.Biol.Sci. 251:151-157.

Franklin K, Paxinos G. 1997. The Mouse Brain in Stereotaxic Coordinates. Academic Press Ltd, London.

Grosche J, Matyash V, Möller T, Verkhratsky A, Reichenbach A, Kettenmann H. 1999. Microdomains for neuron-glia interaction: parallel fiber signaling to Bergmann glial cells. Nat.Neurosci. 2:139-143.

Hamann M, Billups B, Forsythe ID. 2003. Non-calyceal excitatory inputs mediate low fidelity synaptic transmission in rat auditory brainstem slices. Eur.J.Neurosci. 18:2899-2902.

Hamill OP, Marty A, Neher E, Sakmann B, Sigworth FJ. 1981. Improved patch-clamp techniques for high-resolution current recording from cells and cell-free membrane patches. Pflugers Arch 391:85-100.

Heinemann C, von Ruden L, Chow RH, Neher E. 1993. A two-step model of secretion control in neuroendocrine cells. Pflugers Arch 424:105-112.

Held H. 1893. Die zentrale Gehörleitung. Arch Anat Physiol Anat Abtheil 17:201-248.

Held H. 1903. Über den Bau der Neuroglia und über die Wand der Lymphgefässe in Haut und Schleimhaut. Des XXVIII Bandes der Abhandlungen der mathematisch-physischen Klasse der Königl. Sächsischen Gesellschaft der Wissenschaften IV:202-318.

Hoffpauir BK, Grimes JL, Mathers PH, Spirou GA. 2006. Synaptogenesis of the calyx of Held: rapid onset of function and one-to-one morphological innervation. J Neurosci 26:5511-5523.

Ito D, Imai Y, Ohsawa K, Nakajima K, Fukuuchi Y, Kohsaka S. 1998. Microglia-specific localisation of a novel calcium binding protein, Iba1. Brain Res Mol Brain Res 57:1-9.

Jabs R, Pivneva T, Huttmann K, Wyczynski A, Nolte C, Kettenmann H, Steinhäuser C. 2005. Synaptic transmission onto hippocampal glial cells with hGFAP promoter activity. J.Cell Sci. 118:3791-3803.

Joshi I, Wang LY. 2002. Developmental profiles of glutamate receptors and synaptic transmission at a single synapse in the mouse auditory brainstem. J.Physiol 540:861-873.

Jourdain P, Bergersen LH, Bhaukaurally K, Bezzi P, Santello M, Domercq M, Matute C, Tonello F, Gundersen V, Volterra A. 2007. Glutamate exocytosis from astrocytes controls synaptic strength. Nat Neurosci 10:331-339.

Kandel E. 1995. Neurowissenschaften, Eine Einführung. Spektrum Akademischer Verlag, Heidelberg, Oxford.

Kandler K, Friauf E. 1993. Pre- and postnatal development of efferent connections of the cochlear nucleus in the rat. J.Comp Neurol. 328:161-184.

Kang J, Jiang L, Goldman SA, Nedergaard M. 1998. Astrocyte-mediated potentiation of inhibitory synaptic transmission. Nat.Neurosci. 1:683-692.

Katz B. 1969. The Release of Neural Transmitter Substances. Liverpool University Press, Liverpool, UK.

Kettenmann H, Ransom B. 2005. Neuroglia. Oxford University Press second edition.

Koike-Tani M, Saitoh N, Takahashi T. 2005. Mechanisms underlying developmental speeding in AMPA-EPSC decay time at the calyx of Held. J.Neurosci. 25:199-207.

Korogod N. 2006. Mechanisms of posttetanic potentiation and its possible role in maturation of the calyx of Held synapse. PhD thesis, Max-Planck Institut für biophysikalische Chemie, Göttingen, Germany.

Kukley M, Capetillo-Zarate E, Dietrich D. 2007. Vesicular glutamate release from axons in white matter. Nat Neurosci 10:311-320.

Kulik A, Haentzsch A, Luckermann M, Reichelt W, Ballanyi K. 1999. Neuron-glia signaling via alpha(1) adrenoceptor-mediated Ca(2+) release in Bergmann glial cells in situ. J Neurosci 19:8401-8408.

Kuwabara N, DiCaprio RA, Zook JM. 1991. Afferents to the medial nucleus of the trapezoid body and their collateral projections. J.Comp Neurol. 314:684-706.

Levine JM, Nishiyama A. 1996. The NG2 chondroitin sulfate proteoglycan: a multifunctional proteoglycan associated with immature cells. Perspect Dev Neurobiol 3:245-259.

Lin SC, Bergles DE. 2004. Synaptic signaling between GABAergic interneurons and oligodendrocyte precursor cells in the hippocampus. Nat Neurosci 7:24-32.

Lin SC, Bergles DE. 2004. Synaptic signaling between neurons and glia. Glia 47:290-298.

Lin SC, Huck JH, Roberts JD, Macklin WB, Somogyi P, Bergles DE. 2005. Climbing fiber innervation of NG2-expressing glia in the mammalian cerebellum. Neuron 46:773-785.

Matsumoto H, Kumon Y, Watanabe H, Ohnishi T, Shudou M, Chuai M, Imai Y, Takahashi H, Tanaka J. 2008. Accumulation of macrophage-like cells expressing NG2 proteoglycan and Iba1 in ischemic core of rat brain after transient middle cerebral artery occlusion. J Cereb Blood Flow Metab 28:149-163.

Matthias K, Kirchhoff F, Seifert G, Huttmann K, Matyash M, Kettenmann H, Steinhäuser C. 2003. Segregated expression of AMPA-type glutamate

receptors and glutamate transporters defines distinct astrocyte populations in the mouse hippocampus. J.Neurosci. 23:1750-1758.

Matyash V, Filippov V, Mohrhagen K, Kettenmann H. 2001. Nitric oxide signals parallel fiber activity to Bergmann glial cells in the mouse cerebellar slice. Mol.Cell Neurosci. 18:664-670.

Meyer AC, Neher E, Schneggenburger R. 2001. Estimation of quantal size and number of functional active zones at the calyx of held synapse by nonstationary EPSC variance analysis. J.Neurosci. 21:7889-7900.

Montana V, Malarkey EB, Verderio C, Matteoli M, Parpura V. 2006. Vesicular transmitter release from astrocytes. Glia 54:700-715.

Mullen RJ, Buck CR, Smith AM. 1992. NeuN, a neuronal specific nuclear protein in vertebrates. Development 116:201-211.

Newman EA. 2005. Calcium increases in retinal glial cells evoked by light-induced neuronal activity. J.Neurosci. 25:5502-5510.

Niehaus A, Stegmuller J, Diers-Fenger M, Trotter J. 1999. Cell-surface glycoprotein of oligodendrocyte progenitors involved in migration. J Neurosci 19:4948-4961.

Nishiyama A, Chang A, Trapp BD. 1999. NG2+ glial cells: a novel glial cell population in the adult brain. J Neuropathol Exp Neurol 58:1113-1124.

Nolte C, Matyash M, Pivneva T, Schipke CG, Ohlemeyer C, Hanisch UK, Kirchhoff F, Kettenmann H. 2001. GFAP promoter-controlled EGFP-expressing transgenic mice: a tool to visualize astrocytes and astrogliosis in living brain tissue. Glia 33:72-86.

Oliet SH, Mothet JP. 2006. Molecular determinants of D-serine-mediated gliotransmission: from release to function. Glia 54:726-737.

Oliet SH, Piet R, Poulain DA. 2001. Control of glutamate clearance and synaptic efficacy by glial coverage of neurons. Science 292:923-926.

Oliet SH, Piet R, Poulain DA, Theodosis DT. 2004. Glial modulation of synaptic transmission: Insights from the supraoptic nucleus of the hypothalamus. Glia 47:258-267.

Parpura V, Basarsky TA, Liu F, Jeftinija K, Jeftinija S, Haydon PG. 1994. Glutamate-mediated astrocyte-neuron signalling. Nature 369:744-747.

Paukert M, Bergles DE. 2006. Synaptic communication between neurons and NG2+ cells. Curr.Opin.Neurobiol. 16:515-521.

Perea G, Araque A. 2005. Properties of synaptically evoked astrocyte calcium signal reveal synaptic information processing by astrocytes. J Neurosci 25:2192-2203.

Peters A. 2004. A fourth type of neuroglial cell in the adult central nervous system. J Neurocytol 33:345-357.

Porter JT, McCarthy KD. 1996. Hippocampal astrocytes in situ respond to glutamate released from synaptic terminals. J Neurosci 16:5073-5081.

Porter JT, McCarthy KD. 1997. Astrocytic neurotransmitter receptors in situ and in vivo. Prog Neurobiol 51:439-455.

Renden R, Taschenberger H, Puente N, Rusakov DA, Duvoisin R, Wang LY, Lehre KP, von Gersdorff H. 2005. Glutamate transporter studies reveal the pruning of metabotropic glutamate receptors and absence of AMPA receptor desensitization at mature calyx of held synapses. J.Neurosci. 25:8482-8497.

Rollenhagen A, Lübke JH. 2006. The morphology of excitatory central synapses: from structure to function. Cell Tissue Res 326:221-237.

Sakaba T, Neher E. 2001. Calmodulin mediates rapid recruitment of fast-releasing synaptic vesicles at a calyx-type synapse. Neuron 32:1119-1131.

Sakaba T, Schneggenburger R, Neher E. 2002. Estimation of quantal parameters at the calyx of Held synapse. Neurosci Res 44:343-356.

Sätzler K, Sohl LF, Bollmann JH, Borst JG, Frotscher M, Sakmann B, Lübke JH. 2002. Three-dimensional reconstruction of a calyx of Held and its postsynaptic principal neuron in the medial nucleus of the trapezoid body. J.Neurosci. 22:10567-10579.

Schell MJ, Molliver ME, Snyder SH. 1995. D-serine, an endogenous synaptic modulator: localization to astrocytes and glutamate-stimulated release. Proc.Natl.Acad.Sci.U.S.A 92:3948-3952.

Schneggenburger R, Forsythe ID. 2006. The calyx of Held. Cell Tissue Res. 326:311-337.

Schneggenburger R, Meyer AC, Neher E. 1999. Released fraction and total size of a pool of immediately available transmitter quanta at a calyx synapse. Neuron 23:399-409.

Schneggenburger R, Sakaba T, Neher E. 2002. Vesicle pools and short-term synaptic depression: lessons from a large synapse. Trends Neurosci. 25:206-212.

Schools GP, Zhou M, Kimelberg HK. 2003. Electrophysiologically "complex" glial cells freshly isolated from the hippocampus are immunopositive for the chondroitin sulfate proteoglycan NG2. J.Neurosci.Res. 73:765-777.

Schools GP, Zhou M, Kimelberg HK. 2006. Development of gap junctions in hippocampal astrocytes: evidence that whole cell electrophysiological

phenotype is an intrinsic property of the individual cell. J Neurophysiol 96:1383-1392.

Scolding NJ, Frith S, Linington C, Morgan BP, Campbell AK, Compston DA. 1989. Myelin-oligodendrocyte glycoprotein (MOG) is a surface marker of oligodendrocyte maturation. J Neuroimmunol 22:169-176.

Serrano A, Haddjeri N, Lacaille JC, Robitaille R. 2006. GABAergic network activation of glial cells underlies hippocampal heterosynaptic depression. J.Neurosci. 26:5370-5382.

Spacek J. 1985. Three-dimensional analysis of dendritic spines. II. Spine apparatus and other cytoplasmic components. Anat Embryol (Berl) 171:235-243.

Steinhäuser C, Berger T, Frotscher M, Kettenmann H. 1992. Heterogeneity in the Membrane Current Pattern of Identified Glial Cells in the Hippocampal Slice. Eur.J.Neurosci. 4:472-484.

Südhof TC. 2004. The synaptic vesicle cycle. Annu Rev Neurosci 27:509-547.

Trudeau LE, Doyle RT, Emery DG, Haydon PG. 1996. Calcium-independent activation of the secretory apparatus by ruthenium red in hippocampal neurons: a new tool to assess modulation of presynaptic function. J Neurosci 16:46-54.

Turecek R, Trussell LO. 2000. Control of synaptic depression by glutamate transporters. J.Neurosci. 20:2054-2063.

Ventura R, Harris KM. 1999. Three-dimensional relationships between hippocampal synapses and astrocytes. J Neurosci 19:6897-6906.

Vere-Jones D. 1966. Simple stochastic models for the release of quanta of transmitter from a nerve terminal. Aust. J. Statist. 8:53-63.

Virchow R. 1858. Die Cellularpathologie und ihre Begründung auf physiologischer und pathologischer Gewebelehre. Berlin:Verlag von August Hirschwald.

Volterra A, Magistretti P, Haydon P. 2002. The Tripartite Synapse: Glia in Synaptic Transmission. Oxford University Press, USA.

von Gersdorff H, Borst JG. 2002. Short-term plasticity at the calyx of held. Nat.Rev.Neurosci. 3:53-64.

von Gersdorff H, Schneggenburger R, Weis S, Neher E. 1997. Presynaptic depression at a calyx synapse: the small contribution of metabotropic glutamate receptors. J.Neurosci. 17:8137-8146.

Wallraff A, Odermatt B, Willecke K, Steinhäuser C. 2004. Distinct types of astroglial cells in the hippocampus differ in gap junction coupling. Glia 48:36-43.

Wang LY, Kaczmarek LK. 1998. High-frequency firing helps replenish the readily releasable pool of synaptic vesicles. Nature 394:384-388.

Watano T, Calvert JA, Vial C, Forsythe ID, Evans RJ. 2004. P2X receptor subtype-specific modulation of excitatory and inhibitory synaptic inputs in the rat brainstem. J.Physiol 558:745-757.

Weis S, Schneggenburger R, Neher E. 1999. Properties of a model of Ca(++)-dependent vesicle pool dynamics and short term synaptic depression. Biophys J 77:2418-2429.

Wu LG, Borst JG. 1999. The reduced release probability of releasable vesicles during recovery from short-term synaptic depression. Neuron 23:821-832.

Wu SH, Kelly JB. 1993. Response of neurons in the lateral superior olive and medial nucleus of the trapezoid body to repetitive stimulation:

intracellular and extracellular recordings from mouse brain slice. Hear.Res. 68:189-201.

Xu-Friedman MA, Harris KM, Regehr WG. 2001. Three-dimensional comparison of ultrastructural characteristics at depressing and facilitating synapses onto cerebellar Purkinje cells. J Neurosci 21:6666-6672.

Yokoyama A, Sakamoto A, Kameda K, Imai Y, Tanaka J. 2006. NG2 proteoglycan-expressing microglia as multipotent neural progenitors in normal and pathologic brains. Glia 53:754-768.

Youssoufian M, Oleskevich S, Walmsley B. 2005. Development of a robust central auditory synapse in congenital deafness. J.Neurophysiol. 94:3168-3180.

Zhu X, Bergles DE, Nishiyama A. 2008. NG2 cells generate both oligodendrocytes and gray matter astrocytes. Development 135:145-157.

Ziskin JL, Nishiyama A, Rubio M, Fukaya M, Bergles DE. 2007. Vesicular release of glutamate from unmyelinated axons in white matter. Nat.Neurosci. 10:321-330.

Acknowledgements

I would like to thank my supervisor Prof. Dr. Helmut Kettenmann for giving me the opportunity to work on this particular subject in his laboratory. I am grateful for the support and advice. Thanks go also to my colleague Dr. Daniel Reyes-Haro for the co-operation on this project and to Rainer Kröber for excellent technical support.

I also wish to thank Dr. Tatjyana Pivneva and Dr. Roland Schaette for the fruitful collaboration. Especially I want to thank Dr. Tatjyana Pivneva and Dr. Christiane Nolte for their help with the immunhistochemistry and for all the help with the overall lab work, for every nice word and for the wonderful work atmosphere.

Supporting in correcting the manuscript for this thesis thousand special thanks go to Dr. René Jüttner, Dr. Carola Schipke and Dr. Christiane Nolte. I will not forget this.

For the wonderful atmosphere in the lab and for support in the darkest moments of desperation I thank the FSS members Dr. Joo-Hee Wälzlein and Giselle Cheung as well as all the other lab members. That was a group!

And last but not least I want to thank my friends and family.
Thanks to my closest friends Peer Bergholter, Svenja Kettenbeil and my Mufti Olga Kirilow for their patience, their friendship and love. This is true friendship!
Additional thanks go to Mufti for help with Figure 8. Photoshop sucks.
Thanks to my parents and my sister for their endless love and support.
And of course exceeding thanks go to my love Melanie Benna and Sean Benna for supporting me patiently and loving me in all this stress.

This work was supported by a grant of the German Research Association DFG (Schwerpunktprogramm 1172 „Die Bedeutung der Neuroglia für Bildung, Funktion und Plastizität von Synapsen“).

Curriculum vitae

Mein Lebenslauf wird aus Datenschutzgründen in der elektronischern Form meiner Arbeit nicht mit veröffentlicht.

List of Publication

1. **Jochen Müller**, Daniel Reyes-Haro, Tatjyana Pivneva, Christiane Nolte, Roland Schaette, Joachim Lübke and Helmut Kettenmann. *Glial cells and principal neurons of the medial nucleus of the trapezoid body receive coordinated synaptic input from the calyx of Held*. (Submitted)

2. **Jochen Müller**, Daniel Reyes-Haro, Tatjyana Pivneva, Christiane Nolte and Helmut Kettenmann. *Astrocytes in the medial nucleus of the trapezoid body interact with the calyx of Held*. (Manuscript in preparation)

Meetings with Poster Presentations

1. 09/2005, MDC PhD retreat, Straußberg, Germany.

2. 10-11/2005, Berlin Brain Days, Berlin, Germany.

3. 09/2006, annual meeting of the priority program 1172 of the DFG “The role of neuroglia for the formation, function and plasticity of synapses”, Bonn, Germany.

4. 09/2006, MDC PhD retreat, Motzen, Germany.

5. 10-11/2006, Berlin Brain Days, Berlin, Germany.

6. 09/2007, 8th European Meeting on Glial Cell Function in Health and Disease, London, Great Britain.

7. 09/2007, annual meeting of the priority program 1172 of the DFG “The role of neuroglia for the formation, function and plasticity of synapses”, Bad Dürckheim, Germany.

8. 11/2007, Berlin Brain Days, Berlin, Germany.

9. 03/2008, 1st European Synapse Meeting, Bordeaux, France.

Eidesstattliche Erklärung

Ich versichere an Eides statt, dass ich die vorliegende Dissertation

Two glial cell types make structural and functional contact to the calyx of Held in the mouse medial nucleus of the trapezoid body

Selbst und ohne unzulässige Hilfe Dritter verfasst habe, dass sie auch in Teilen keine Kopie anderer Arbeiten darstellt und die benutzten Hilfsmittel sowie die Literatur vollständig angegeben sind.

Berlin, den 29.02.2008

_____

Jochen Müller